The FIAT transcriptional repressor as a drug target for bone regeneration

Caitlin Anderson

Department of Human Genetics

McGill University, Montreal, Canada

May 2024

A thesis submitted to McGill University in partial fulfillment of the requirements of the degree of

Doctor of Philosophy

ABSTRACT

There are currently several therapies available to treat low bone mass disease that either stimulate osteoblastic bone formation (anabolic) or inhibit osteoclast resorption (anti-resorptive). Many of these therapies come with drawbacks that ranges from constrained therapeutic regimes to more serious risks of myocardial infarction, stroke, and cardiovascular death. There thus remains a need for new osteoanabolic drugs, with different mechanisms of action, leading to more effective and safer treatments to stimulate bone formation in patients with low bone mass. Our long-standing research on the transcriptional repressor FIAT (Factor Inhibiting ATF4-mediated Transcription) has characterized it as a valid target for drug development. FIAT interacts with the osteoanabolic Activating Transcription Factor 4 (ATF4) to prevent its binding to cognate response elements and thus, as its acronym implies, inhibit ATF4-mediated transcription. *FIAT* transgenic mice are osteopenic, while *Fiat*-deficient mice show a reciprocal high bone mass phenotype, supporting the selection of FIAT as a drug development target. Using a high throughput screen targeting this interaction, we have identified C73 (structure withheld at behest of counsel pending patent filing), a small molecule compound targeting FIAT, that has potential as a novel first-in-class osteoanabolic drug. Cultured osteoblasts treated with C73 throughout differentiation exhibit an increase in mineralization and differentiation when assessed via alizarin red staining and gene expression monitoring. Using Chromatin Immunoprecipitation (ChIP) we show an increase in ATF4 binding to the OSE1 canonical binding region upstream of the osteocalcin gene promoter after osteoblasts are treated with C73. GST-pulldown assays suggest specificity of C73 for the ATF4-FIAT interaction, by modulating this interaction but having no effect on ATF4 binding to other partners. The dose ranging and safety testing show C73 is well tolerated in mice through intraperitoneal injections or oral gavage over many weeks of intervention. We could rescue the low bone mass phenotype of the *FIAT* transgenic mouse model through both modes of administration, regardless of sex. In a classic bone loss model of ovariectomized mice, which recapitulates the low bone mass associated with post-menopausal osteoporosis, treatment with C73 was shown to prevent the bone loss in an early intervention model, and rescue bone loss after it had occurred. Collectively, this study is the first to report a first-in-class compound targeting the ATF4-FIAT interaction that can modulate osteoblastogenesis and bone mass accrual.

RÉSUMÉ

Il existe actuellement plusieurs thérapies disponibles pour traiter les maladies métaboliques osseuses comportant une perte de masse osseuse. Ces thérapies peuvent être divisées en deux catégories : celles qui stimulent la formation osseuse ostéoblastique (anabolique) ou celles qui inhibent la résorption ostéoclastique (anti-résorptive). La plupart de ces thérapies présentent des inconvénients allant de régimes thérapeutiques contraignants jusqu'à des risques plus graves tel que : infarctus du myocarde, accident vasculaire cérébral ou décès cardiovasculaire. Il existe donc un besoin pour de nouveaux médicaments ostéoanaboliques, avec différents mécanismes d'action, conduisant à des traitements plus efficaces et plus sûrs pour stimuler la formation osseuse chez les patients ayant une faible masse osseuse. Nos recherches sur le répresseur transcriptionnel FIAT (*Factor Inhibiting ATF4-mediated Transcription*) l'ont caractérisé comme une cible valable pour le développement de médicaments. FIAT intéragit avec le facteur de transcription ostéoanabolique ATF4 (*Activating Transcription Factor* 4) pour l'empêcher de se lier aux éléments de réponse correspondants et inhiber la transcription médiée par ATF4. Des souris transgéniques surexprimant la séquence *FIAT* humaine sont ostéopéniques, tandis que des souris déficientes pour le gène *Fiat* présentent un phénotype réciproque de masse osseuse élevée, ce qui supporte la sélection de FIAT comme cible pour le développement d'un médicament. En utilisant un criblage à haut débit visant l'interaction FIAT/ATF4, nous avons identifié C73 (structure non divulguée à la demande de nos avocats, en attente de dépôt de brevet), une petite molécule ciblant FIAT, qui a le potentiel d'être un nouveau médicament ostéoanabolique de nouvelle génération. Des ostéoblastes cultivés traités avec C73 tout au long de la différenciation présentent une augmentation de la minéralisation et de la différenciation, évaluée par coloration au rouge d'alizarine et la mesure de l'expression génique. Le traitement d'ostéoblastes avec C73 augmente la liaison d'ATF4 à sa séquence cible en amont du promoteur du gène cible ostéocalcine. Des tests d'interaction protéiques révèlent la spécificté de C73 pour le dimère FIAT/ATF4 sans affecter la liaison d'ATF4 avec ses autres partenaires. C73 est bien toléré chez les souris lorsqu'administré par injections intrapéritonéales ou par gavage pendant plusieurs semaines d'intervention. Le traitement avec C73 corrige le phénotype de faible masse osseuse du modèle de souris transgénique *FIAT*, peu importe le mode d'administration. Dans un modèle classique de perte osseuse de souris ovariectomisées, qui récapitule la faible masse osseuse associée à l'ostéoporose post-ménopausale, le traitement par le C73 s'est révélé capable

de prévenir la perte osseuse dans un modèle d'intervention précoce, et de corriger la perte osseuse une fois qu'elle s'est produite. Collectivement, cette étude est la première à identifier un composé de première génération ciblant l'interaction ATF4/FIAT pouvant moduler l'ostéoblastogenèse et l'accumulation de masse osseuse.

Table of Contents

LIST OF ABBREVIATIONS

α-MEM	Minimum Essential Medium α
µA	microampere
µCT	microtomography or micro computed tomography
µm	Micron, micrometer
ALPL	Alkaline phosphatase
AP-1	Activator protein 1
AST	aspartate aminotransferase
ATF2	Activating transcription factor 2
ATF3	Activating transcription factor 3
ATF4	Activating transcription factor 4
BGLAP	bone gamma-carboxyglutamate protein, osteocalcin
BRET	bioluminescence resonance energy transfer
BSA	Bovine serum albumin
BSP	Bone sialoprotein
BUN urea	Blood urea nitrogen
BV	Bone volume
BV/TV	Bone volume/tissue volume
BW	Body Weight
bZIP	Basic domain leucine zipper
C/EBPß	CCAAT enhancer-binding protein beta

C/EBPα	CCAAT enhancer-binding protein alpha
C73	Compound 73
CBC	complete blood count
cDNA	complementary DNA
ChIP	Chromatin Immunoprecipitation
CHOP	C/EBP homologous protein
CLogP	Calculated Log P
CMARC	Comparative Medicine and Animal Resources Center
CMV	Cytomegalovirus
Col1α1	Collagen, type I, α 1
Col1α2	Collagen, type I, α 2
CRE	cAMP responsive element
CREM	cAMP responsive element modulator
Ct.Ar/Tt.Ar	cortical area/total area percentage
Ct.Th	Cortical Thickness
DDIT3	DNA damage inducible transcript 3, CHOP
DLX5	Distal-Less Homeo box 5
DMEM	Dulbecco's Modified Eagle's Medium
DMP1	Dentin Matrix Protein 1
DMSO	Dimethylsulfoxide
DNA	Deoxyribonucleic acid
E11/gp38	podoplanin

EDTA	Ethylenediaminetetraacetic acid
ELISA	Enzyme-linked immunosorbent assay
ER	Endoplasmic Reticulum
FBS	Fetal bovine serum
FDA	U.S Food and Drug administration
FGF23	Fibroblast growth factor 23
FIAT	Factor inhibiting ATF4-mediated transcription
FOSB	FosB Proto-Oncogene, AP-1 transcription factor subunit
cFOS	Fos proto-oncogene, AP-1 transcription factor subunit
FP	fluorescence polarization
FRET	fluorescence resonance energy transfer
G418	*Geneticin*
GAPDH	Glyceraldehyde-3-phosphate dehydrogenase
GPCR	G protein-coupled receptor
GST	glutathione S-transferase
HFD	High Fat Diet
ICER	inducible cAMP early repressor
IgG	Immunoglobulin G
IP	intraperitoneal
J	Joule
cJUN	Jun proto-oncogene
kDa	Kilodaltons

KO	Knockout
kV	kilovolt
LC-MS	Liquid chromatography–mass spectrometry
Luc	Luciferase gene
MAX	MYC Associated Factor X
M-CSF	Macrophage colony-stimulating factor
MEF3	mitochondrial editing factor 3
MEPE	Matrix extracellular phosphoglycoprotein
mm	millimeter
MMP9	Matrix metalloproteinase 9
MyoD	Myogenic Differentiation 1
mRNA	messenger RNA
MSC	mesenchymal stem cells
MTT	3-(4,5-dimethylthiazol-2-yl)-2,5-diphenyltetrazolium bromide
MYC	MYC Proto-Oncogene, basic domain Helix-Loop-Helix Transcription Factor
N	Newton
NACA	Nascent polypeptide Associated Complex and coregulator alpha
NFkb	Nuclear factor kappa-light-chain-enhancer of activated B cells
NMR	Nuclear magnetic resonance spectroscopy
OPG	Osteoprotegerin
OSE1	osteoblast specific element 1
OSE2	osteoblast specific element 2

OSX	Osterix
OVX	Ovariectomized
PBS	Phosphate-buffered saline
PCR	polymerase chain reaction
PHEX	Phosphate regulating endopeptidase homolog X-linked
PKPD	pharmacokinetic/pharmacodynamic
PMSF	phenylmethylsulfonyl fluoride
PPI	protein-protein interaction
PTH	Parathyroid Hormone
PTHrP	parathyroid hormone-related protein
PVDF	Polyvinylidene fluoride
qPCR	Quantitative polymerase chain reaction
RANK	Receptor activator of nuclear factor-kB
RANKL	Receptor activator of nuclear factor-kB ligand
RI-MUHC	Research Institute - McGill University Health Centre
RIPA	Radio-Immunoprecipitation Assay
RNA	Ribonucleic acid
ROI	Region of interest
RPM	revolutions per minute
RSK2	ribosomal S6 kinase 2
RT-PCR	Reverse transcription polymerase chain reaction
RUNX1	Runt-related transcription factor 1

RUNX2	Runt-related transcription factor 2
RUNX3	Runt-related transcription factor 3
SATB2	Special AT-rich sequence binding protein 2
SDS	Sodium dodecyl sulfate
siRNA	Small interfering RNA
Sost	Sclerostin
SOX9	SRY-Box Transcription Factor 9
Sp1	Sp1 Transcription Factor
Sp3	Sp3 Transcription Factor
Sp4	Sp4 Transcription Factor
Sp7	Sp7 Transcription Factor, Osterix
Spp1	Secreted Phosphoprotein 1
STD	saturation transfer difference
Tb.N	Trabecular Number
Tb.Sp	Trabecular Seperation
Tb.Th	Trabecular Thickness
TBST	tris-buffered saline & tween 20
TE	Tris-EDTA buffer
TNFRSF11b	TNF Receptor Superfamily Member 11b, OPG
TNFSF11	TNF Superfamily Member 11, RANKL
TRAP	Tartrate resistant acid phosphatase
TV	Tissue Volume

TXLNA	Taxilin Alpha
TXLNB	Taxilin beta
TXLNG	Taxilin Gamma
WT	Wild Type

LIST OF FIGURES

LIST OF TABLES

ACKNOWLEDGEMENTS

I would like to express my gratitude to my supervisor Dr. René St-Arnaud for his mentorship throughout my PhD. Thank you for taking a chance on me and giving me the opportunity to grow into the scientist I am today. I appreciate your guidance and willingness to let me explore a plethora of techniques throughout my studies, opportunities I would not have gotten elsewhere.

I would like to extend my gratitude to my supervisory committee members, Dr. Pierre Moffatt, and Dr. John H. White, for not only sharing their knowledge and useful feedback over the years, but giving me grace as I navigated a field I had little experience in. Every committee meeting was a delight full of scientific insight that was invaluable to the success of my project.

St-Arnaud's research group was instrumental in my success as a scientist. The warmth and community I felt within the laboratory fostered many long scientific discussions that helped me throughout my studies. I am extremely grateful to have learned techniques and explored philosophies from each member of the lab. My sincerest thanks goes to Dr. Martin Pellicelli who I perceive as a mentor both on and off the bench. Without his countless hours spent in the lab working side by side, I would not have learned the bulk of the techniques I know today. I have the utmost gratitude for Alice Arabian who kept both the lab and myself in check. Every day was a great day when Alice was in the lab. A warm thanks to Dr. William Addison and Dr. Hadla Hariri who always indulged me in deep scientific debate and passed onto me their expertise in the bone biology field. I am forever grateful for allowing me to pick their brains. More recently, Dr. Omar Al Rifai has given me support and humored me in scientific banter. He has been a great source of knowledge and insight throughout the writing process.

The research community at the Shriners has been equally as influential in my studies as the relationships built within my laboratory. The biggest thanks to the animal facility technicians Mia Esser, Louise Marineau and Alexandria Norquay. Working alongside this team has been the biggest pleasure during my studies and they are the unsung heroes behind many of my scientific successes.

A thank you to Mark Lepik for his talented graphic design work. My appreciation also goes out to all the talented researchers on the floor who were always willing to take the time for me especially Lisa Lamplugh, Marie-Hélène Gaumond, Dr. Hadil Al-Jallad, Dr. Josephine T. Tauer, and Dr. Kerstin Tiedemann.

Finally, I would like to thank the people in my life outside of academics. My friends have been great in giving me a space away from science and disconnect from the struggles of research. I would like to thank my parents who never extinguished my flame of curiosity and allowed me the freedom to pursue my interests in higher education. To my big brother Ian, who was the first scientist in the family, a cheerleader in my life and my trusted confidant throughout my studies. Lastly, thank you to my husband, Winston, who has been integral to my success. His kindness, support and love gave me the opportunity to pursue my interests to the fullest extent, which is something I will forever be grateful for.

CONTRIBUTIONS TO ORIGINAL KNOWLEDGE

The report presented here describes a novel, first in class compound, that targets the ATF4-FIAT interaction leading to meaningful impact on bone mass accrual.

Chapter III describes the process in which a large library of compounds was screened to identify compounds that can modulate the binding between ATF4 and FIAT. The screen identified eight compounds that could modulate the interaction. *In vitro* work discerning the effects of these compounds on osteoblast differentiation and mineralization identified a lead compound (C73), which excelled in both aspects and would be the focus of downstream efforts. **Chapter IV** characterizes the mechanism of action of the compounds. We are the first to characterize a compound that can disrupt the ATF4-FIAT interaction without impacting the interaction of ATF4 with other bZIP partners. Furthermore, we show that treatment with C73 can increase the binding of ATF4 to the OSE1 site upstream of the Osteocalcin promoter.

The studies conducted in **chapters V** and **VI** follow the next steps in a classical drug discovery pipeline. The work in **chapter V** exhibits the safety, tolerance and pharmacokinetic-pharmacodynamic properties of the lead compound, C73. Using the low bone mass, *FIAT*-transgenic mouse model (generated in our lab), the results of **chapter VI** support our preferred hypothesis that C73 disrupts the ATF4-FIAT interaction leading to an increase in bone mass. We show C73 is effective in restoring bone mass in the *FIAT*-transgenic mice to levels comparable to wild-type littermates. The fact that similar effects are obtained whether the compound is administered through intraperitoneal injections or oral gavage adds credence to notion C73 could eventually make it to market as a viable therapeutic for osteoporosis. The ovariectomy studies conducted in **chapter VII** demonstrate the multifaceted attributes of C73 in a post-menopausal bone loss model, as it can be administered as either a preventative or restorative therapeutic.

Altogether, our findings characterize an orally effective, novel compound that has the potential to be brought to market to treat low bone mass.

FORMAT OF THE THESIS

The thesis is written in the traditional format and consists of ten chapters.

Chapter I is the introduction, which is comprised of a review of literature pertinent to this thesis. It also contains the rationale, hypothesis, and objectives of the thesis.

Chapter II details the materials and methods relevant to this thesis.

Chapters III, **IV**, **V**, **VI** and **VII** summarizes the research findings and the results of the study.

Chapter III focuses on the results of the high throughput screen, including the effects of the identified compounds on osteoblast mineralization and differentiation *in vitro.*

Chapter IV focuses on the results from *in vitro* studies exploring the effect of the lead compound on the ATF4-FIAT interaction and other ATF4 bZIP family members.

Chapter V focuses on the safety, tolerance, and pharmacokinetics-pharmacodynamics of the lead compound *in vivo*. It also encompasses the effect of the lead compound on a long-term steady state study.

Chapter VI focuses on the efficacy of the lead compound to rescue to low bone mass phenotype of the *FIAT*-transgenic mouse model.

Chapter VII focuses on the efficacy of the lead compound to prevent and rescue ovariectomy-induced bone loss.

Chapter VIII is a discussion of all the results presented in the preceeding chapters and explores future experiments that could build upon the data presented. Chapter IX is the conclusion of the thesis. Chapter X catalogues the references used in this thesis.

CONTRIBUTION OF AUTHORS

Caitlin Anderson and Dr. René St-Arnaud designed the study. Caitlin Anderson generated the data. Caitlin Anderson and Dr. René St-Arnaud participated in data analysis and interpretation. Dr. René St-Arnaud obtained the funding. Caitlin Anderson wrote the initial draft of the thesis and Dr. René St-Arnaud edited the final version of the thesis.

Chapter I: INTRODUCTION

1.1. Bone Tissue

The skeleton is the structural framework of a vertebrate organism. It consists of bones, tendons, and cartilage. Along with providing shape, the skeleton supports and protects vital organs. Movement can be achieved through the attachment of connective tissues and muscles to the skeleton [1]. Although commonly thought of as a simple rigid structure, the skeleton, and the bones that comprise it, are associated with multiple functions within the body. The bone extracellular matrix is comprised of minerals, type I collagen fiber, noncollagenous proteins, water and lipids, all of which contribute to the mechanical and metabolic functions of bone [2]. Bones are comprised of minerals and are the largest reservoir of calcium and phosphate, making bone tissue critical in mineral homeostasis [3]. The cavities of bone are filled with red bone marrow, the primary site of hematopoiesis [4]. Bone has also been characterized more recently as an endocrine organ as bone derived factors regulate both local bone metabolism and global energy homeostasis [5].

Skeletal development separates vertebrates from invertebrates. During embryonic development the skeleton arises from three mesenchymal cell lineages: cranial neural crest cells, somites, and the lateral plate mesoderm [6]. From the cranial neural crest cells, the flat bones of the skull, clavicle and cranial bones arise [7]. Somites form the remainder of the axial skeleton while the long bones form from the plate mesoderm [8]. Although these three derivatives are responsible for the spatial allocation of the skeleton the process in which the mesenchymal tissue precursor is transformed into bone is split between intramembranous and endochondral bone formation.

Intramembranous ossification uses the direct conversion of mesenchyme into bone. This process occurs in the neural crest derived mesenchymal cells, in which these cells proliferate and differentiate directly into osteoblasts. Bones formed through this process include flat bones of the skull, the mandible, and the clavicles. Endochondral ossification differs from intramembranous by the need for an intermediary step between the mesenchymal cells and osteoblasts. In this process the mesenchymal cells differentiate into chondrocytes to form a cartilage template which

will be replaced by newly deposited bone. Endochondral ossification is the process in which long bones and all other bones are formed [7].

1.2. Bone Cells

Bone is comprised of three cell types: osteoblast, osteocytes, and osteoclasts (Figure 1). Osteoblasts are derived from mesenchymal stem cells (MSCs), multipotent cells that can differentiate into chondrocytes, osteoblasts, myoblasts, and adipocytes [9]. Lineage commitment of MSCs is tightly controlled by molecular signaling and transcription factors. For osteogenic differentiation, Runt-related transcription factor 2 (RUNX2) and osterix (OSX/SP7) are necessary for the lineage commitment of MSC to osteoblast [10, 11]. Osteoblasts are the bone forming cells of the skeleton and line the bone surface. In their preosteoblastic proliferation state, cells increase expression of fibronectin, type 1 collagen (COL1A1 and COL1A2) and osteopontin [9]. As these cells differentiate from preosteoblasts to osteoblasts they continue the high expression levels of type 1 collagen and begin expressing alkaline phosphatase (ALP), a classical bone differentiation maker. This stage begins the maturation of the extracellular matrix. In the final stage of differentiation, termed mature osteoblast, cells express osteocalcin (BGLAP) promoting the mineralization of the extracellular matrix [12]. Mature osteoblasts are either recruited to the bone surface or undergo apoptosis. A subset of mature osteoblasts undergoes terminal differentiation into osteocytes but the mechanism behind this decision remains unclear [13].

Osteocytes are derived from bone-forming osteoblasts that are trapped in the bone matrix and take on a dendritic-like shape. Each osteocyte resides within its own fluid-filled cavity known as a “lacunae” and can interact with other bone cell types through tunnel-like networks within the bone microenvironment called canaliculi. The canaliculi permeate the entire bone tissue allowing osteocytes to interact with osteoblasts, osteoclasts, and other osteocytes [14]. Osteocytes can modulate bone formation and resorption through the production of sclerostin. Sclerostin, encoded by the *SOST* gene, inhibits bone formation, and stimulates osteoclast function [15]. Osteocytes express a set of unique markers different from their osteoblastic precursor such as: E11/gp38, Dentin Matrix Protein 1 (DMP1), matrix extracellular phosphoglycoprotein (MEPE), fibroblast growth factor 23 (FGF23) and phosphate-regulating neutral endopeptidase on the chromosome X (PHEX) [16].

Osteoclasts are responsible for bone resorption in the skeleton. Mature osteoclasts are large, multinucleated cells that derive from hematopoietic stem cells. Originating as mononuclear macrophages, osteoclastic precursors cells are stimulated by the macrophage colony-stimulating factor (M-CSF) for continued survival, proliferation and initializing differentiation of hematopoietic stems cells into osteoclastic precursor cells [17]. Differentiation into mature osteoclasts is regulated by the receptor activator of nuclear factor-κB ligand (RANKL) [18]. In response to both M-CSF and RANKL, osteoclast precursor cells originating from the bone marrow or circulation, migrate to resorption sites. After attaching to the bone matrix surface, cells differentiate into mature, multinucleated osteoclasts, and form a sealed acidic zone. Within this sealed zone, the osteoclast produces various enzymes that dissolve both the inorganic calcium and phosphorus mineralized matrix or the organic components of the extracellular matrix [19]. In addition to their unique morphology, differentiation markers of osteoclasts include cathepsin K, tartate-resistant acid phosphatase (TRAP), matrix metalloproteinase 9 (MMP9) and Receptor Activator of nuclear factor kappa-B (RANK) [20].

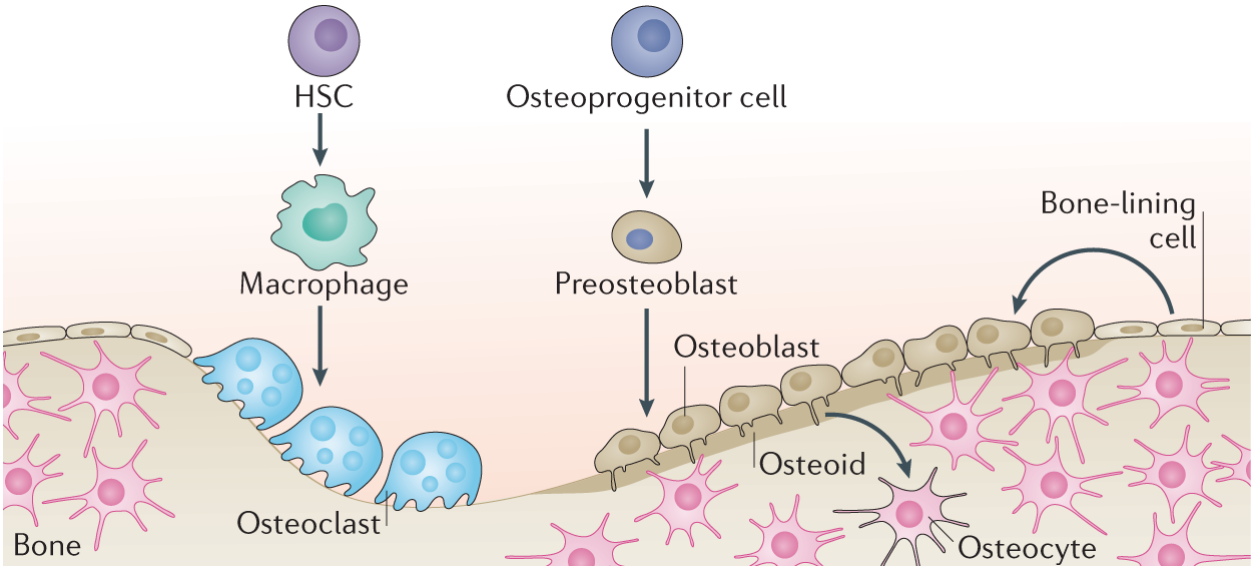

Figure 1. Bone Homeostasis and cell types

Schematic overview of bone homeostasis and cell types. Osteoclasts and osteoblasts lineages arise from different stem cells. Osteoclasts derive from hematopoietic stem cells, committing to differentiation through progression into a macrophage and eventual mature osteoclasts. Osteoclasts are responsible for bone resorption. Osteoblasts derive from mesenchymal stem cells and commit to the osteoblastic lineage through the signaling of transcription factors differentiating the stem cell into an osteoprogenitor cell. The osteoprogenitor cell is further differentiated into a preosteoblast and eventual mature osteoblast. Osteoblasts are responsible for bone formation. Osteocytes are mature osteoblasts that are trapped in the bone matrix and take on a dendritic-like shape. Osteocytes can regulate osteoblast and osteoclasts and are capable of mechanosensing. (Reproduced by permission from Springer Nature: Nature Reviews Molecular Cell Biology, Mechanism of bone development and repair, Salhorta et al. 2020).

1.3. Bone Remodeling

Like other tissues, bone undergoes continuous cycles of remodeling and regeneration. In response to damage, the bone absorbs the damaged area and replaces it with new bone. The three major types of bone cells involved in bone remodeling are osteoblasts, osteoclasts, and osteocytes.

Osteocytes produce many factors that can affect both resorption and formation. Osteocytes can respond to mechanical loading and microdamage as they are mechanosensing cells [21]. Upon sensing this damage, the osteocytes produce ligands, such as RANKL, that cross the bone-lining cell monolayer or the capillaries that are infiltrating the damaged area. These ligands then stimulate the recruitment and differentiation of osteoclast precursor cells [22]. As the levels of M-CSF and RANKL increase, the osteoclast precursor cells attach to the resorptive site and differentiate into mature osteoclasts beginning resorption. As osteoclasts attach and differentiate, osteoprogenitor cells are also being recruited to the damaged area. In tandem with resorption, the recruited osteoprogenitor cells are differentiating into mature osteoblasts [23]. As the damaged bone matrix is being absorbed by the osteoclasts, the osteoblasts begin osteoid synthesis, laying down new bone in the freshly excavated area. As resorption slows and eventually ceases, that osteoid synthesis continues and finally mineralization occurs concluding the bone remodeling event. At the end of bone remodeling there is no net change in bone mass [24].

As shown in bone remodeling, the intricate communication between the three bone cell types is critical for bone repair and bone mass homeostasis. Should the balance between resorption and formation be disrupted two skeletal pathologies can arise. A balance favoring osteoblasts can lead to aberrant bone formation or osteopetrosis. Reciprocally, a balance towards osteoclasts can lead to bone loss or osteoporosis. Maintaining the coupling between osteoblasts and osteoclasts is crucial, should the pairing become uncoupled skeletal pathologies such as osteoporosis or osteopetrosis will arise [25].

1.4. Osteoporosis & Current Therapies

When bone homeostasis becomes dysregulated and the rate of resorption outpaces that of bone building, bone loss can occur. In a human population bone loss occurs as a person ages, leading to a change in the microarchitecture of the bone tissue and ultimately to an increase in fracture risk. The rate of age-related bone loss is accelerated in post-menopausal women. The clinical terms for bone loss are osteopenia, a mild presentation of bone loss, or the more severe presentation, osteoporosis. To note, there are other factors that can lead to secondary osteoporosis such as: hyperthyroidism, prolonged use of glucocorticoids, poor nutrition, and low mobility [26]. With the decrease in bone mineral density, the structural integrity of the skeleton is degraded, increasing the risk of fracture [27]. Osteoporotic fractures then lead to a decrease in the quality of life increasing the risk of morbidity, mortality, and disability [28].

Since the primary risk facture for osteoporosis is age, diagnosis and intervention are crucial to managing low bone mass and decreasing fracture risks. In a clinical setting, a dual energy X-ray absorptiometry (DEXA) test is used to calculate the bone mineral density (BMD) of a patient [29]. With this information, clinicians can assign a BMD T-score with known diagnostic thresholds for osteopenia or osteoporosis. The risk of fracture is inversely correlated to the BMD score [30]. If a patient has a low BMD T-Score they are at a higher risk of fracture. Although the hip and vertebra are the most common sites of fractures, any skeletal site has an increased risk of fracture since osteoporosis is systemic. Once low bone mass has been observed, a patient is prescribed a pharmacological treatment regime depending on the severity of the disease state.

There are two classes of pharmacological treatment for osteoporosis. The first class of drugs is antiresorptive. This class targets osteoclasts, inhibiting their function thereby reducing bone resorption [31]. The main family of antiresorptive drugs are the bisphosphonates. The recommended dosage regime for bisphosphonates is orally daily or weekly, or a yearly intravenous infusion [32]. Other antiresorptive therapies include estrogen replacement therapy, and an anti-RANKL antibody. The recommended length of use for antiresorptive treatment can range from 5 - 10 years and is subject to change as more long term monitoring studies are being completed [33-35].

The second class is anabolic therapy. This class of drug stimulates bone formation by targeting osteoblasts [31]. There are currently 3 approved osteoanabolic drugs: Teriparatide (Forteo), a recombinant molecule comprising the N-terminal fragment of human parathyroid hormone (PTH); Abaloparatide (Tymlos), a 34 amino acid synthetic analog of parathyroid hormone-related protein (PTHrP) (not approved for use in Canada); and Romosozumab (Evenity), a humanized monoclonal antibody that targets sclerostin, an inhibitor of bone formation [36-38]. Teriparatide and Abaloparatide act by stimulating osteoblast activity, recruitment and favoring bone formation during bone remodeling.

Generally, bisphosphonates will be the first line of treatment prescribed to a patient due to the low treatment cost and the high adherence rates. Patients will be monitored bi-yearly to assess the tolerability of the bisphosphonate and if the disease state has progressed. If a follow up DEXA shows a continued decline in the bone mineral density after initial bisphosphonate use, then another anti-resorptive therapy will be prescribed. If the patient presents with a severe BMD T-score, the initial treatment regime might be an anabolic reagent, to which access is currently limited by the high cost of treatment [30].

While all treatments, no matter the class, are efficacious, there are limitations. Long term bisphosphonate treatment is associated with a rare but severe side effect of osteonecrosis of the jaw in which there is substantial bone death within the jaw compartment. As well, atypical femoral fractures have been noted in extended use of bisphosphonates, in which a fracture occurs in the femur under normal stress or load [39]. Teriparatide and Abaloparatide must be administered by daily subcutaneous injections, which significantly impacts patient compliance [40]. Abaloparatide has a health authorities-imposed time limit of a maximum of 2 years of use due to the limited therapeutic window [41]. Romosozumab is administered subcutaneously, once a month for 12 months. After 1 year the bone stimulating activity of the anti-sclerostin antibody wanes. Moreover, despite FDA approval, Romosozumab carries a black box warning concerning potential risk of myocardial infarction, stroke, and cardiovascular death [42].

There thus remains a need for new osteoanabolic drugs, with different mechanisms of action, leading to more effective and safer treatments to stimulate bone formation in patients with low bone mass.

The first step in drug development is the identification of a valid, druggable target. We have focused on the transcriptional control of osteoblast differentiation to identify such a target. The next section reviews the key transcription factors regulating osteoblastogenesis.

1.5. Transcriptional regulation of osteoblast differentiation

The differentiation of mesenchymal stem cells to osteoblasts can be divided into three stages of increasing differentiation: osteoprogenitor, preosteoblast and osteoblast (Figure 2). It is the expression of the transcription factor SOX9 that signals the mesenchymal stem cell to differentiate into an osteoprogenitor [43]. At this point the osteoprogenitor can continue to differentiate into either a chondrocyte or an osteoblast. Continued expression of SOX9 will guide the progenitor cell into the chondrocyte lineage, where it will produce a cartilaginous matrix comprised of collagen and proteoglycans. It is the subsequent expression of RUNX2 in which the osteoprogenitor commits to a preosteoblast [10]. The continued expression of RUNX2 and the expression of osterix (OSX/SP7) is critical for the continuing differentiation of the preosteoblast into an immature osteoblast [11]. Lastly, activating transcription factor 4 (ATF4) regulates the differentiation of the osteoblast to maturation [44].

RUNX2 is a member of the Runx family which consists of RUNX1, RUNX2, and RUNX3. The family is identified by the ability to bind to DNA through the RUNT domain that each protein possesses [45]. RUNX2 is the master regulator of osteoblastogenesis. It initiates the lineage commitment of mesenchymal stem cells into osteoprogenitors. The expression levels of RUNX2 increase as the osteoprogenitor further differentiates into a preosteoblast and achieves peak expression levels in immature osteoblasts [46]. Through its ability to bind to various gene promoters, RUNX2 regulates osteoprogenitor proliferation, commitment to the osteoblastic lineage and bone matrix deposition. RUNX2 knockout mice (*Runx2*$^{-/-}$) lack normal osteoblasts and have low expression levels of bone matrix protein genes including osteopontin (*Spp1*), bone sialoprotein 2 (*Bsp*) and osteocalcin (*Bglap*) [47].

Osterix is also referred to as Sp7 due to the homology of its zinc finger DNA binding domain with Sp1, Sp3, and Sp4. It is required for the differentiation of immature osteoblasts into mature osteoblasts [48]. *Osx* null mice are embryonic lethal as there is no bone formation and a

lack of expression of osteoblast genes such as *Sparc*, and *Spp1* [11]. In a conditional osteoblast-specific knockout of *Osx* using *Col1a1*-Cre, a similar bone phenotype with delayed osteoblast maturation is observed [49]. When *Osx* expression is depleted postnatally, bone formation is perturbed leading to an absence of trabecular bone and porous cortical bone [50].

In addition to regulating osteoblast differentiation, *Runx2* and *Osx* can regulate each other. RUNX2 is an upstream regulator of *Osx* expression, as it is normally expressed in the osteoblasts of $Osx^{-/-}$ mice. OSX along with DLX5 and myocyte enhancer factor 2 (MEF2) control the activation of the *Runx2* enhancer in osteoblasts. It is the expression of RUNX2 that promotes the differentiation of the osteoprogenitor into preosteoblast and the subsequent expression of OSX that continues differentiation into an immature osteoblast [51].

Activating transcription factor 4 (ATF4) is a member of the ATF/CREB family of transcription factors that are characterized by the presence of a basic domain for DNA binding and a leucine zipper interaction domain (bZip) for homo- or hetero-dimerization. ATF4 protein is primarily expressed in osteoblasts, as the protein is degraded in almost all other cell types [52]. ATF4 is required for the differentiation of an immature osteoblast into a mature osteoblast. Along with RUNX2, ATF4 binds to the osteoblast specific element (OSE1) in the promoter region of *Bglap*, regulating osteocalcin expression [53]. Other osteoblastic genes such as *Bsp* and *Osx* are regulated through ATF4 expression [54]. ATF4 expression in osteoblasts can regulate osteoclast differentiation and bone resorption through its binding to the *Rankl* promoter [55]. ATF4 enhances amino acid uptake facilitating proper protein synthesis of type 1 collagen. ATF4 knockout mice exhibit a low bone mass phenotype due to the delay in osteoblast differentiation and subsequent delayed bone formation [56].

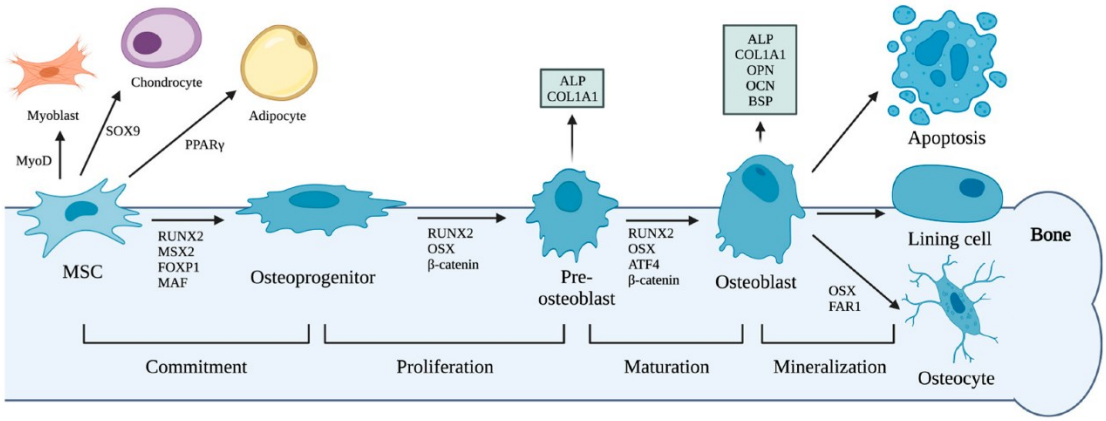

Figure 2. Differentiation of osteoblast lineage cells

Mesenchymal stem cells (MSC) can differentiate into many cell types such as myoblasts, chondrocytes, adipocytes, and osteoblasts. Sox9 signals the MSC cell to begin differentiation into an osteoprogenitor cell. Further signaling by RUNX2 commits the osteoprogenitor cell into a preosteoblast. RUNX2 regulates osteoprogenitor proliferation, commitment to the osteoblastic lineage and bone matrix deposition. Throughout the differentiation of a preosteoblast to an immature osteoblast, OSX levels rise. ATF4 signaling further differentiates the immature osteoblast into a mature osteoblast. Mature osteoblasts can then further differentiate in osteocytes, become bone lining cells, or undergo apoptosis. (Open access article from MDPI: International Journal of Molecular Sciences, The Mechanotransduction Signaling Pathways in the Regulation of Osteogenesis, Liu et al. 2023) [57].

1.6. Regulators of ATF4 function

ATF4 is ubiquitously expressed but the protein is only enriched in osteoblasts. Through post translational modifications, ATF4 is ubiquitinated and marked for proteasomal degradation in most other cell types [52]. Only in situations of endoplasmic reticulum stress or unfolded protein response system is ATF4 proteasomal degradation halted, and the protein allowed to accumulate [58]. Further regulations of ATF4 post translationally influence the functions of ATF4 in osteoblastogenesis.

Phosphorylation of ATF4 by RSK2 is required for osteoblast differentiation and function. Osteoblasts derived from *Rsk2*$^{-/-}$ mice exhibit decreased ATF4 phosphorylation and subsequently a decrease in the expression of ATF4 target genes. Additionally, through post translational modification, RSK2 and ATF4 regulate the synthesis of type 1 collagen protein. Mutations in *RSK2* are causal for the genetic disease Coffin-Lowry Syndrome, and patients are reported to have skeletal abnormalities including short stature, delayed bone formation, and low bone mass. It is believed the dysregulation of RSK2 phosphorylation of ATF4 leads to the loss of downstream ATF4 mediated transcription in osteoblasts and causes the skeletal abnormalities found in Coffin-Lowry Syndrome patients [56] .

ATF4 function is also regulated through various binding partners via the bZip motif. This protein motif consists of heptad repeats of leucine residues which align along one face of an alpha helix. When aligned in parallel, the hydrophobic faces of two complementary helices form a coiled coil. Leucine zipper dimerization serves to juxtapose adjacent regions of each of the dimer's partners that are rich in basic amino acid residues and that serve as the DNA binding domain of the dimer [59]. ATF4 can form homodimers but can also heterodimerize with ATF or AP-1 family members and subsequently bind to the consensus cAMP responsive element (CRE) binding site [60].

In bone, ATF4 can homodimerize or heterodimerize with C/EBPβ (CCAAT/Enhancer-binding protein beta) on the OSE1 site in the osteocalcin promoter. When in a heterodimer with C/EBPβ, the interaction between Runx2 and ATF4, on their respective binding sites OSE2 and OSE1, is enhanced resulting in an increase in osteocalcin expression [61]. ATF4 also binds with SATB2 which also stabilizes the Runx2/ATF4 interaction in the osteocalcin promoter [62].

Binding partners can also inhibit ATF4 function. Vimentin is a type III intermediate filament protein and is expressed in a cell type- and development stage-specific manner. It is often expressed in undifferentiated and proliferative mesenchymal stem cells. Vimentin can localize to the nucleus and interact with ATF4 through a putative leucine zipper. The interaction between the two prevents ATF4 from binding to its cognate response element inhibiting the transcription of ATF4 targets such as *Bsp* and Osteocalcin (*Bglap*). Knockdown of vimentin expression using siRNA induces Osteocalcin expression in immature osteoblasts. Throughout osteoblast differentiation the expression levels of vimentin decrease while ATF4 levels increase. It is suggested that it is the reduction in vimentin in immature osteoblasts that facilitates the differentiation into mature osteoblasts [63].

ICER (inducible cAMP early repressor) is another inhibiting partner of ATF4. It is a member of the CREM (cAMP responsive element modulator) family of basic leucine transcription factors that act as a negative regulator of gene transcription. ICER expression can be induced by treatment with parathyroid hormone in osteoblasts. Transgenic mice that overexpressed ICER in osteoblast specific cells had a smaller body size with reduced trabecular bone volume and bone formation. MSCs derived from these mice exhibited reduced osteoblast differentiation. It was shown that ICER binds with ATF4 preventing binding to the canonical binding site of ATF4 on the osteocalcin promoter [64].

1.7. Factor Inhibiting ATF4 Mediated Transcription – FIAT

FIAT is a 72-kDa protein transcribed from the *TXLNG* gene located on the X chromosome. It has three putative leucine zippers and a C-terminal coiled-coil region that is homologous amongst all taxilin family members, TXLNA and TXLNB [65]. The FIAT protein does not contain a DNA binding domain but is able to bind to ATF4 through its second leucine zipper. This binding effectively makes an inactive dimer as ATF4 is no longer capable of binding to the canonical OSE1 site within the osteocalcin promoter [66]. Overexpression of *Fiat* in both primary and immortalized osteoblasts was shown to inhibit Osteocalcin expression and reduce mineralization [67]. In contrast, siRNA knockdown of *Fiat* expression increased all ATF4 functions including increased binding to the OSE1 site, osteocalcin transcription, *Bsp* gene transcription and type I collagen synthesis. Mineralization and nodules numbers were also increased in FIAT-depleted osteoblasts [68].

Transgenic mice that express the human full length 1.8kb *FIAT* cDNA under the 2.3-kb *Col1a1* promoter were created to assess the physiological role of FIAT in bone. These mice, which had an increased expression of *FIAT* specifically in osteoblasts, were osteopenic. Bones from *FIAT* transgenic mice showed decreased bone mineral density, bone volume, and mineral apposition rates. The osteopenic phenotype also presented with a decrease in bone biomechanical properties resulting in a lower bone strength in transgenic mice when compared to wildtype littermates. No changes in osteoblast proliferation or apoptosis were observed in these mice but osteoblasts derived from these mice showed an impaired osteoblast activity [66]. The phenotype of the *FIAT* transgenic mice closely resembled that of the *Atf4* null mouse.

A global *Fiat* knockout mouse was created using a Cre-LoxP recombination driven by the cytomegalovirus promoter. *Fiat*$^{-/y}$ mice exhibited an increase in bone volume, affecting both the trabecular and cortical bone. An increase in the rate of mineral apposition was noted. The changes in bone mass and microarchitecture lead to an increase in bone strength and stiffness. Primary osteoblasts derived from this mouse model showed increase mineralization and osteoblast-specific markers like those found in siRNA mediated knockdown cells [69]. The two *Fiat* mouse models show that FIAT can impact both trabecular and cortical bone formation suggesting that inhibition of FIAT could result in meaningful gains in bone mass and strength. The findings validate the exploration of the ATF4-FIAT interaction as a drug target for bone regeneration.

1.8. Targeting a protein-protein interaction

Traditional druggable targets consist of a receptor and ligand or a hormone disrupter. These targets are in general easier to target by either creating a receptor antagonist/protagonist [70]. Increasingly protein-protein interactions are being targeted for drug development. It has been documented that the interaction between leucine zippers can be inhibited through small molecules. The advantages of targeting a transcriptional interaction, especially those achieved through leucine zippers, is the specificity and lowered risk of off target effects. Protein-protein interactions are more challenging as they require a small molecule to disrupt the interaction domain between the proteins and need increased specificity especially if the interaction domains share commonalities with those within the same family of proteins. [71]

Although protein-protein interactions can be identified and monitored through co-immunoprecipitation assays, they are costly, time consuming and the final readout cannot be easily scaled for high throughput screening. There are many systems that can be used to assess protein-protein interactions that have the positive attributes outlined above. These systems are bioluminescence resonance energy transfer (BRET), fluorescence resonance energy transfer (FRET) and luciferase reporter gene expression [72].

In brief, a luciferase assay works by inserting a response element (promoter region, canonical binding site, etc) upstream of a luciferase coding region. The binding of a protein to the response element drives downstream expression of the luciferase coding region resulting in luciferase production. The amount of luciferase is quantified after cell lysis by adding substrate specific to the luciferase used producing light which can be detected in a luminometer [73]. Although the traditional luciferase gene is derived from the firefly, a newer luciferase from Metridia has been gaining popularity due to its ease of use. Metridia luciferase is secreted and can be quantified from the tissue culture medium directly. The secretion of the luciferase eliminates the step of cell lysis of the traditional firefly luciferase. As well, secreted luciferase allows for the system to be “blanked” at the beginning of an experiment by replacing the cell medium, removing the previously produced luciferase, and reading the luciferase at a predetermined time afterwards [74]. In traditional firefly reporter, luciferase production begins shortly after transfection and continues until cell lysis. The ability to “blank” the luciferase in the secreted system lends itself to drug testing as the system can be reset and luciferase production be assessed in the presence of a drug.

The mammalian two hybrid system is an effective way to assess and quantify the amount of protein-protein interaction. This system is based on the properties of transcription factors, which can be divided into two independent parts: the DNA binding domain and the activation domain. The system is robust, using the GAL4 binding domain derived from yeast, and the VP16 activation domain, derived from the herpes simplex virus. When linked through a covalent peptide bond, the GAL4-VP16 recombinant protein is a strong transcriptional activator. The two protein moieties can also been recombined using protein-protein interaction motifs. For example, leucine zippers can be cloned in-frame with either the GAL4 or VP16 domain. Through interaction of the leucine zipper motifs, the GAL4 and VP16 domains are essentially tethered

together, and a robust transcription factor is reconstituted. The transcription factor binds to a response element, in this case a canonical GAL4 binding site repeated five times. This response element can be inserted upstream of a quantifiable readout [75]. For our purposes this response element was inserted upstream of a metridia luciferase coding region allowing the interaction to be quantified via light production. The system has a very low background and high dynamic range when used in mammalian cells that do not express the GAL4 protein or related family members.

1.9. Drug Development pipeline

The drug discovery pipeline can be broken down into multiple phases that build upon the work of the previous phase (Figure 3). The first phase is the pre-discovery phase. In this phase research is conducted to gather information about a disease using *in vitro* studies to identify the genetic or molecular target that leads to the phenotype of the disease. After identification, further *in vitro* studies identify pathway and other protein or ligand partners that interact with the target of interest. Once the target has been identified and explored extensively *in vitro*, the study moves onto the *in vivo* investigation of the target. The identified casual target is then either deleted or overexpressed in an *in vivo* animal model. The *in vivo* models allow for the understanding of the casual target globally, confirming it is the cause of the disease state.

After confirming the causal target of the disease state, the project is ready to move into the drug discovery phase. Generally, a high throughput screen is preformed to identify a promising lead compound that eventually could become a drug. Further detail about this stage will be expanded on later in this introduction.

Once a lead compound is identified, early safety tests are conducted. These tests can be done in silico, *in vitro* and eventually *in vivo*. The most common types of tests conducted are pharmacokinetics, pharmacodynamics, and computer modeling of the interaction of the lead compound and the target protein. Should the previous testing generate undesirable results such as instability of the lead compound, poor solubility, or short half life, the lead compound can be optimized through consultation with a medicinal chemist. By changing the structure of the lead molecule many of these pitfalls can be remedied. As well, different resuspension formulas can be used to increase solubility and delivery methods of the lead compound.

After lead optimization, the pipeline then moves onto pre-clinical testing. In this phase, *in vitro* and *in vivo* testing are done to determine the safety and efficacy of the lead compound. *In vitro* testing can confirm the targeting and specificity of the lead compound to the intended protein target. As well as confirm the function of the drug-protein interaction in the causal target pathway. Primary *in vivo* studies conducted are dose ranging to determine the safety and tolerability of the drug in animal models. After which, an appropriate dose is determine and used in subsequent pre-clinical testing [76].

The gold standard of pre-clinical testing is rescuing the disease state model. In terms of a drug targeting a protein, this would be a rescue of the deletion or transgenic phenotype based on the nature of the interaction targeted. Further pre-clinical testing would be conducted in animal models that mimic the human version of the disease state, which could be different than the previously mentioned rescue study. *In vivo* studies are then conducted in higher mammalian animal models to further confirm the safety of the lead compound. Both *in vitro* and *in vivo* preclinical testing help to determine if the lead compound, which is now referred to as a drug, is safe enough for human testing [77].

Once the drug is determined to be safe enough to move out of pre-clinical testing, applications for clinical trial exceptions are filed with the appropriate authorities before clinical trials can begin. In human clinical trials are split into three phases. Phase 1 is initial testing of the drug in a small group of healthy individuals. This is to determine the safety of the drug in human use. In phase 2, the drug is tested in a small group of patients of the targeted disease state. The third and last phase of a clinical trial is testing the drug in a large group of patients. It is in phase 3 that the safety, efficacy of the drug in the primary patient population and information about side effects is collected.

After clinical trials are conducted application for marketing authorization is submitted to the appropriate authorities for approval and manufacturing with full scale production can begin. Between the application process and approval by the appropriate agencies for the drug to be approved for clinical use, phase 4 and ongoing studies are still conducted to monitor and checking the efficacy of the drug in use [76].

This thesis covers a large portion of the drug discovery and development pipeline. Previous studies in the lab had identified the target protein and the role of this protein in a

disease state. The interaction and effects of this protein on bone physiology was extensively researched by students who had come before me. The thesis begins at the drug discovery phase and continues until the pre-clinical testing phase, including *in vivo* testing of the lead compound in both a rescue study and a disease model study.

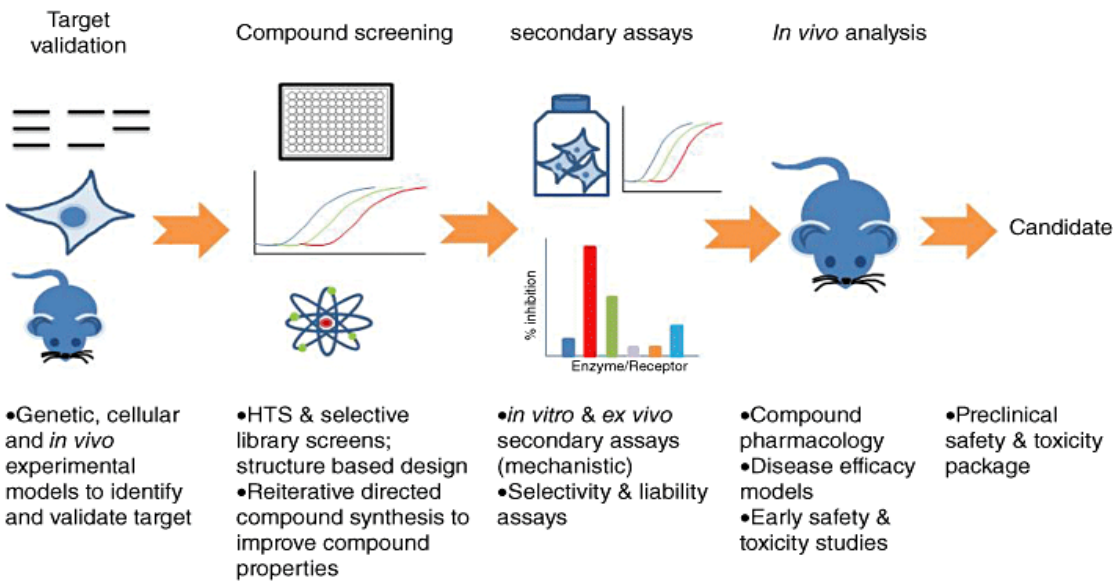

Figure 3. Schematic overview of the drug discovery pipeline.

In the pre-discovery phase research is conducted to gather information about a disease using *in vitro* studies to identify the genetic or molecular target that leads to the phenotype of the disease. In this phase a "Target" is identified that contributes to the phenotype further studies are conducted to understand the relationship between the target and the disease state phenotype. This target then becomes the basis for the drug discovery effort. An assay is developed to screen many compounds that can regulate the target identified. From there compounds identified in the screen are used in secondary assays to understand the mechanism between the compound, the target, and the disease phenotype. Secondary assays also explore the selectivity of the compound on the target. In this stage a lead compound is generally identified that had positive attributes *in vitro* and is selected for further studies *in vivo*. *In vivo* analysis is used to understand the safety and toxicity of the lead compound, the pharmacokinetics-pharmacodynamics of the lead compound, and the efficacy of the compound on the disease state models. Once the lead compound is determined to be safe enough to move out of pre-clinical testing, applications for clinical trial exceptions are filed with the appropriate authorities before clinical trials can begin. (Reproduced by permission from John Wiley and Sons: British Journal of Pharmacology, Principles of early drug discovery, Philpott et al. 2011).

1.10. Rationale, hypothesis, and objectives

Our long-standing research on the transcriptional repressor FIAT (Factor Inhibiting ATF4-mediated Transcription) has characterized it as a valid target for drug development. FIAT interacts with the osteoanabolic ATF4 transcription factor to prevent its binding to cognate response elements and thus, as its acronym implies, inhibit ATF4-mediated transcription. *FIAT* transgenic mice are osteopenic, while *Fiat*-deficient mice show a reciprocal high bone mass phenotype, supporting the selection of FIAT as a drug development target [66, 69]. **We hypothesized that compounds preventing the interaction of FIAT with ATF4 would be osteoanabolic, leading to beneficial gains in bone mass and strength.** We used cell biological approaches and preclinical models to test our hypothesis with three specific aims:

1. Perform a high-throughput screen to identify compounds that block the interaction of FIAT with ATF4;
2. Characterize the compound(s) identified through the screen;
3. Test the safety and efficacy of the compound(s) to increase bone mass *in vivo*.

In the body of the thesis, we show that a lead compound identified in the screen (code-named C73 for intellectual property protection issues, at behest of counsel) increases osteoblastogenesis *in vitro*, stimulating the expression of osteoblastic differentiation markers and mineralization. The compound is well tolerated *in vivo* and able to rescue the osteopenic phenotype of *FIAT* transgenic mice. We also demonstrated that treatment with C73 prevents as well as rescues the low bone mass phenotype of ovariectomized female mice, a standard preclinical model of metabolic bone disease used in bone regenerative medicine.

Chapter II: MATERIALS AND METHODS

2.1. Mammalian two hybrid vectors

Using the vectors provided in the CheckMate Mammalian Two-Hybrid System (Promega, Madison, WI) the interaction domain of ATF4 (Q136-A344, 208 amino acids, Mus musculus) was subcloned into the pACT Vector using BamHI and NotI restriction sites that were added during the PCR step, amplified from mouse cDNA. The interaction domain of FIAT (Q186-Y424, 238 amino acids, Homo sapiens) was subcloned into the pBIND vector using BamHI and NotI restriction sites cut from a pCDNA3.1_FIAT plasmid. A Gal4-VP16 expression vector (71728, Addgene, Watertown, MA), was used as a positive control vector for the mammalian two hybrid system. This vector expresses a fusion construct of Gal4 DNA binding domain (same as found in the pBIND vector) and a VP16 activating domain (same as found in the pACT vector). The five Gal4 binding sites and the minimal TATA box from the pG5Luc vector of the CheckMate Mammalian Two-Hybrid system was subcloned upstream of the Metridia luciferase gene in the pMetLuc2 vector from The Ready-To-Glow secreted reporter vector kit (Takara, Mountain View, CA) using KpnI, BglII, SacII and BamHI restriction sites. All generated vectors were verified by sequencing. Primer sequences and plasmids are available upon request.

2.2. Creation of stable cell lines HEK293

HEK293 cells (American Type Culture Collection, Manassas, VA) were cultured in Dulbecco's modified Eagle's medium (DMEM, Gibco, Grand Island, NY) supplemented with 10% fetal bovine serum (FBS, Gibco), 100 U/ml penicillin and 100 µg/ml streptomycin at 37°C in a humidified atmosphere at 5% CO_2. HEK293 cells were seeded at a density of 30,000 cells/cm^2 in 100mm tissue culture plates (Corning, Corning, NY) 24 hours before transfection. Two and a half micrograms (2.5µg) of pG5MetLuc2 reporter vector were transfected using the Lipofectamine Reagent kit following the manufacturer's instructions (Invitrogen, Carlsbad, CA). Two and a half micrograms (2.5µg) of pACT-ATF4 and pBD-FIAT or 2.5µg of Gal4-VP16 expression vector (71728, Addgene) were co-transfected. Twenty-Four (24) hours post transfection medium was changed. Six hours later 100 µl of medium was transferred to a 96 well plate in triplicate. The Ready-To-Glow secreted luciferase assay was performed according to manufacturer's protocol (Takara). Briefly, 5 µl of a 1X substrate/reaction buffer was added to 50 µl of cell culture medium from transfected cells in a 96 well plate in triplicates. Luciferase signal

was measured using a VICTOR Nivo multimode microplate reader (Perkin Elmer, Waltham, MA).

Transfected cells were treated with Geneticin (G418, Gibco) at a concentration of 1400 µg/ml for three days to select for the expression vectors. After selection was confirmed via the death of the killing control HEK293 plate, cells were seeded at a low density and allowed to expand over a week until individual colonies of cells could be identified. Monoclonal colonies of cells were selected with the application of a small circular Whatman Filter Paper (Sigma-Aldrich, St. Louis, MO) soaked in 0.25% trypsin (Gibco) placed over the cell cluster. The cell-carrying Whatman Filter Paper was transferred to a 96 well plate and DMEM medium supplemented with 10% FBS was added to the well. Cells were allowed to adhere over 48 hours at which point the Whatman filter paper was removed, and the cell viability was visually assessed via microscope. Cells that survived the lysis were expanded under G418 selection pressure and luciferase signal was assessed using the technique described above.

A stable cell line continuously expressing the pG5MetLuc2 vector reporter was selected for a signal that gave a relative luciferase signal closest to those of untransfected HEK293 cells. This line will henceforth be referred to as the negative control cell line. A stable cell line continuously expressing pG5MetLuc2, pACT-ATF4 and pBIND-FIAT vectors was selected for a signal that gave the highest amount of luciferase signal when compared to the negative control cell line. This line will henceforth be referred to as the experimental control cell line. A stable cell line continuously expressing the pG5MetLuc2 and Gal4-VP16 expression vector was selected for a signal that gave the highest difference in luciferase signal when compared to the experimental control cell line. This cell line will henceforth be referred to as the positive control cell line.

All stable cell lines were expanded under G418 selection pressure and frozen in a solution of FBS and 10% DMSO (ThermoFisher Scientific, Waltham, MA). Cells were stored long term in liquid nitrogen before being transferred to the high throughput screening platform.

2.3. High throughput screen methods & secreted luciferase

The high throughput screen was conducted using the services and facilities at the Institute for Research in Immunology and Cancer (IRIC) located within the University of Montreal Campus. The compound library at IRIC consists of 120,000 compounds that are either commercially available or proprietary. The flowthrough of the initial high throughput screen pipeline was as follows: 10 µM of compound was plated in singlicate in a 384 well plate. Seven thousand and five hundred (7,500) cells suspended in 25 µl of media were seeded per cell on top of the compound. Cells were allowed to attach overnight at conditions previously described. Plates were then allowed to equilibrate at room temperature for 30 minutes. After which 25ul of Ready-To-Glow luciferase substrate (Takara) was added per well and incubated for 20 minutes at room temperature. Luciferase signal was read 24 hours after cell seeding.

The initial screening was conducted with all 120,000 compounds in the screening library using the negative control cell line and the experimental cell line. A compound that reduced the luciferase signal of the experimental cell line close to that of the negative control cell line was considered positive hit.

A counter screen was conducted between the experimental cell line and the positive control cell line to identify and discard false positives. The experimental set up was the same as the initial screen except for the compound being plated in triplicate.

A final dose ranging screen was performed on the experimental cell line. Compounds were plated between 0.2 µM and 10 µM in quadruplicates following the same experimental set up of the previous screens.

Eight (8) candidate compounds were retained for further characterization.

2.4. Cell culture systems

MC3T3-E1 (subclone 4) osteoblastic cell line (a gift from Dr. Renny T. Franceschi, University of Michigan, Ann Arbor, MI) was cultured in minimum essential medium alpha (α-MEM, Gibco) supplemented with 10% FBS, 100 U/ml penicillin, and 100 µg/ml streptomycin at 37°C in a humidified atmosphere at 5% CO_2.

Primary osteoblasts were isolated from calvariae of 5-day old C57Bl6 mice. Calvariae were dissected and washed with phosphate-buffered saline (PBS). Calvariae were incubated in 5 ml of digestion solution (0.0625% Trypsin, 0.8 mg/ml collagenase type II [270 u/mg; Life Technologies], 0.025% EDTA in PBS) while rotating at 37°C for 20 minutes. Following incubation with the digestion solution, the supernatant which contained the isolated osteoblasts were transferred to a new tube. The remaining calvariae were washed with 3 ml of αMEM and 700 µl of FBS to inhibit trypsin activity. The supernatant of this wash was added to the supernatant of the previous digestion. Cells were spun and resuspended in complete αMEM and plated in 6-well plates (fraction 1). The digestion step was repeated three more times to obtain fractions 2 through 4. Cells were allowed to expand for 5 days before being passed for experiments. Fractions 3 and 4, representing the more mature osteoblast population, were used for experiments in this study.

Primary human osteoblasts were thawed (C-12720, Promocell, Heidelberg, Germany) and seeded in proprietary osteoblast growth medium (C27001, Promocell). Cells were passed once to allow for sufficient proliferation using DetachKit (C-41200, Promocell) before being seeded for experiments.

2.5. Cell proliferation assay

MC3T3-E1 cell proliferation and viability in the presence of the candidate compounds were measured using the MTT (3-[4,5-dimethylthiazol-2-yl]-2,5-diphenyl tetrazolium bromide, Si) assay (Sigma-Aldrich). Cells were plated at 7,500 cells/well in 96 well plates. After 24 hours, the medium was replaced with fresh medium containing various concentrations of the candidate compound starting at 100 µM, diluting 1:2 until 0.78 µM. After 48 hours of treatment cells were incubated with 0.5 µg/µl MTT in medium for three hours. Media was removed and cells were solubilized with DMSO and absorbance monitored at 570 nm.

2.6. Alkaline phosphatase assay

Alkaline phosphatase enzymatic activity was measured as a marker of osteoblast differentiation using the SIGMAFAST p-Nitrophenyl phosphate (pNPP) Tablets (Sigma-Aldrich). MC3T3-E1 cells were seeded at 7,500 cells/well. After 24 hours, the medium was replaced with fresh osteoblastic differentiation medium containing various concentrations of the

candidate compounds at either a high dose regime, starting at 12 µM, diluting 1:2 until 0.375 µM, or a low dose regime, starting at 2 µM, diluting 1:2 until 0.125 µM. To induce osteoblast differentiation of MC3T3-E1 cells, the αMEM medium was supplemented with 50 µg/ml of ascorbic acid (Sigma-Aldrich) and 10 mM of β-glycerophosphate (Sigma-Aldrich). Medium was changed every 2 days for the duration of the experiment containing the appropriate concentration of cadidate compounds. After 6 days the cells were washed 2 times with PBS. Thirty (30) µl of a lysis buffer (10 mM Tris pH 7.5, 0.2% Nonidet P-40, 1 mM phenylmethylsufonyl fluoride [PMSF]) was added per well. Cells were subjected to two rounds of freeze thaw between -80°C and 37°C respectively for 15 minutes each. Two hundred (200) µl of the pNPP substrate solution was added to each well and the alkaline phosphatase activity in the supernatant was determined spectrophotometrically at wavelength 405 nm.

2.7. Alizarin red staining

MC3T3-E1 cells and primary calvarial mouse osteoblasts were plated at 50,000 cells/cm^2. To induce osteoblast differentiation of MC3T3-E1 cells and primary calvarial osteoblasts, cells were incubated in αMEM supplemented with 50 µg/ml of ascorbic acid (Sigma-Aldrich) and 10 mM of β-glycerophosphate (Sigma-Aldrich). Medium was changed every 2 days for the duration of the experiment containing the appropriate concentration of candidate compounds. Primary human osteoblasts were seeded at 50,000 cells/cm^2 on collagen coated plates. To induce osteoblast differentiation, Osteoblast Mineralization Medium (C27020, Promocell) was used and changed every 2 days.

Alizarin red staining was performed on all cell types on day 14 of osteogenic differentiation. Cells were fixed in 70% ethanol for 1 hour at -20°C and subsequently washed twice with ddH_2O. Cells were incubated with alizarine red solution (40 mM, pH 4.2) (Sigma-Aldrich) for 15 minutes at room temperature. Cells were then washed five times with ddH_2O to remove excess staining and incubated in PBS for 15 minutes at room temperature. After which, cells were air dried and photographed.

2.8. RNA isolation and quantitative real-time PCR

Total RNA was extracted from cells or tissues using TRIzol reagent following the manufacturer's protocol (Invitrogen). Briefly, cells were collected, or tissue was homogenized in 1 mL of TRIzol and 200 µl of chloroform was added to the reaction. After centrifugation, the clear upper aqueous phase was extracted, and RNA was precipitated by adding 500 µl of isopropanol. The RNA pellet was washed twice with 75% ethanol before being resuspended in RNase-free water. For bone samples, after collection, bone marrow was flushed with PBS and then flash frozen in liquid nitrogen before storing at -80°C. Samples were thawed and homogenized in TRIzol using a tissue homogenizer (Polytron). One microgram (1 µg) of RNA was reversed-transcribed using the high-capacity cDNA reverse transcription kit following the manufacturer's instructions (ThermoFisher Scientific). Briefly, 10 µl of RNA at a total concentration of 1 µg was combined in 2X reverse-transcription master mix in a 96 well plate. The plate was sealed and loaded into a thermal cycler. The conditions for the thermal cycler were as follows: 25°C for 10 minutes, 37°C for 120 minutes, 85°C for 5 minutes and 4°C indefinitely.

Gene expression was assessed using the TaqMan Fast Advanced Master Mix (ThermoFisher Scientific) and the following TaqMan primers:

Gene	Taqman
Runx2	Mm00501578
Col1α1	Mm00801666_g1
Sp7	Mm00504574_m1
Alpl	Mm00475834_m1
Bglap2	AIWR1XJ
Tnfsf11	Mm00441906_m1
Tnfrsf11b	Mm00435454_m1
Gapdh	Mm99999912_g1
Atf4	Mm00515325_g1
Atf3	Mm00476033_m1
Ddit3	Mm01135937_g1
Txlng	Mm00769506_m1

RUNX2	Hs00231692_m1
SP7	Hs01866874_s1
BLGAP	Hs01587814_g1
APLP	Hs1029144_m1
GAPDH	Hs02786624_g1
COL1α1	Hs00164004_m1
TNFSF11	Hs00243522_m1
TNFRSF11B	Hs00900358_m1
ATF4	Hs00909569_g1
ATF3	Hs00231069_m1
DDIT3	Hs00358796_g1
TXLNG	Hs01085867_m1

Table 1. List of TaqMan probes

All reactions were carried out in a QuantStudio 7 Flex Real-Time PCR system (ThermoFisher Scientific).

2.9. GST pulldown

To generate pGST-*Atf4*, the mouse *Atf4* coding sequence was PCR amplified from pCMV6-*Atf4* (MR205957, Origene, Rockville, MA) and subcloned into the pGEX-4T-3 vector (Pharmacia Canada) using BamHI and NotI restriction sites. Recombinant GST-ATF4 fusion protein and GST control protein were expressed in T7 Express *E. coli* strain (New England Biolabs) and allowed to grow overnight at 30°C before being purified using anti-GST magnetic beads (Cell Signaling Technology, Danvers, MA) according to standard manufacturer's protocols. Briefly, the pellet obtained from the overnight growth of *E. coli* was lysed with RIPA buffer (50 mM Tris-HCl, pH 8.0, 150 mM NaCl, 1% Nonidet P-40, 0.5% deoxycholate, 0.1% SDS, 5 mM EDTA, 2.5 mM $Na_4P_2O_7$, 1 mM β-glycerophosphate, 1 mM Na_3VO_4, 1 mM PMSF, 1x protease inhibitor cocktail [Sigma-Aldrich]) and sonicated at 20% amplitude on ice, for a 30 seconds on/30 seconds off cycle for a total of 1.5 minutes of active sonication. Lysate was

clarified via centrifugation and incubated for 30 minutes at room temperature with anti-GST magnetic beads, with gentle rotation. Prey proteins such as: pCMV6-Txlng-Myc-Flag (MR226588, Origene), pCMV6-Cjun-Myc-Flag (MR227043, Origene), pCMV6-Ddit3-Myc-Flag (MR201400, Origene), pCMV6-Cebpb-Myc-Flag (MR227563, Origene) and pCMV6-Fosb-Myc-Flag (MR227058, Origene), were *in vitro* transcribed and expressed using TNT Quick Coupled Transcription/Translation system (Promega) according to manufacturer's instructions. Briefly, 1 µg of plasmid is incubated with 50 µl TnT quick master mix for 60 minutes at 30°C. GST-fusion protein-bound beads were incubated with the prey protein in a GST-pulldown buffer (20 mM Tris-HCl pH 7.5, 150 mM NaCl, 0.1% Nonidet P-40, 10% Glycerol with protease/phosphatase inhibitor mixture [Sigma]) for 30 minutes at room temperature. After 30 minutes 0.25 µM of Compound 73 or equivalent volume of DMSO were added to the GST-fusion protein-bound beads and prey protein and incubated for an additional 30 minutes at room temperature. After washing five times with the pulldown buffer, the beads were eluted in 2x Laemmli buffer and boiled for 5 minutes before being analyzed by SDS-PAGE and Western blotting.

2.10. SDS-PAGE & Western blotting

Prepared samples from the GST pulldowns were loaded onto a hand-poured 1.5 mm thick 12.5% SDS-polyacrylamide gel (PAGE) and migrated by electrophoresis in Tris-glycine SDS running buffer. Proteins were transferred to a PVDF membrane (Amersham, UK) for 1.5 hours at 100 volts. The membrane was blocked for 1 hour in 10% non-fat dry milk suspended in Tris buffered saline and 0.01% Tween-20 (TBST). After blocking, the membrane was incubated with a primary antibody diluted 1:1,000 in 5% bovine serum albumin (BSA) in TBST, overnight at 4°C with gentle agitation. The membrane was then incubated with horseradish-peroxidase, anti-rabbit, diluted 1:20,000 in 5% non-fat dry milk suspended in TBST. Western Lightening Chemiluminescence kit (Perkin Elmer) was used for development and the protein bands were visualized by exposure to film. The blots were probed with the following antibodies: rabbit-anti-TXLNG (HPA000841, Prestige Antibodies, Sigma-Aldrich) and rabbit-anti-Myc (71D10, Cell Signaling).

2.11. Chromatin immunoprecipitation

MC3T3-E1 cells were plated at 50,000 cells/cm^2 in 150 mm cell culture dishes. To induce osteoblast differentiation, cells were incubated in αMEM medium supplemented with 50 µg/ml of ascorbic acid (Sigma-Aldrich) and 10 mM of β-glycerophosphate (Sigma-Aldrich). Medium was also supplemented with 0.25 µM of Compound 73 or the equivalent concentration of DMSO for the duration of differentiation. Medium was changed every other day for the duration of the 7-day experiment. Cells were fixed for 10 minutes at room temperature with gentle agitation by adding the appropriate amount of 16% methanol free formaldehyde (28908, ThermoFisher Scientific) directly to the culture medium for a final concentration of 1% formaldehyde. The fixation reaction was stopped by adding an appropriate amount of 1M glycine for a final concentration of 0.125M in the culture medium and incubating for 5 minutes at room temperature with gentle agitation. Fixed cells were washed twice and scraped in cold PBS. Cells were spun down for 5 minutes at 500g. To isolate the nuclei, cells were successively resuspended and centrifuged three times in nucleus-chromatin preparation (NCP) buffer 1 (10 mM HEPES, pH 6.5, 10 mM EDTA, 0.5 mM EGTA, 200 mM NaCl).

The nuclear pellet was lysed by resuspension in 1 mL of cold RIPA buffer. Lysate was sonicated for 24 minutes using a 1 ml AFA fiber milliTUBE and a Focused-Ultra sonicator M220 (Covaris, Woburn, MA) set at 10% duty cycle, 75 watts intensity and 200 cycles per burst. Sonicated lysates were centrifuged at 13000g for 10 minutes. Chromatin immunoprecipitation (ChIP) was performed at 4°C overnight on a rotating platform by combining sonicated lysate with 1.5mg of Dynabeads protein G (ThermoFisher Scientific) conjugated to either normal rabbit IgG (2729, Cell Signaling) or rabbit anti-ATF4 (SD20-92, Invitrogen).

The protein-DNA-bead complexes were washed four times with RIPA buffer and four times with lithium chloride buffer (100 mM Tris-HCl, pH 8.0, 500 mM LiCl, 1% Nonidet P-40, 1% deoxycholate). Beads were then washed one time with 100 mM Tris-HCl pH 8.0. Complexes were eluted from the beads by adding 150 µl of 1% SDS and heating at 65°C for 10 minutes. Cross-links were reversed by heating the samples at 65°C for 5 hours.

DNA was purified by using UltraPure Phenol:Chloroform:Isoamyl alcohol (Invitrogen) extraction and precipitated using ethanol and 20 µg of glycogen (Invitrogen) as a carrier. The chromatin from input and ChIP Samples were resuspended in 50 µl of TE buffer (10 mM Tris-HCl, pH 8.0, 1 mM EDTA). *Bglap2* promoter fragments were amplified using 5′-AGGCAGCTGCAATCACCA-3′ forward and 5′-GCACCCTGCAGCATCCA-3′ reverse, *Ddit3* (7015) and *Atf3* (13059) promoter fragments were amplified using SimpleChip (Cell Signaling). Reactions were performed using 10 µl 2X PowerUP SYBR green master mix (ThermoFisher Scientific), 5 µl of a mixture of forward and reverse primers at 1.2 µM or SimpleChip reagent and 5 µl of ChIP sample in a 96 well plate. All reactions were carried out in a QuantStudio 7 Flex Real-Time PCR system (ThermoFisher Scientific).

2.12. Animal studies

All animal procedures were reviewed and approved by the McGill Institutional Animal Care and Use Committee and followed the guidelines of the Canadian Council on Animal Care, conforming to the relevant regulatory standards. Mice were kept in an environmentally controlled barrier animal facility with a 12-h light/12-h dark cycle and were fed standard mouse chow (D12450B, 10% fat; Charles River Laboratories International, Wilmington, MA) and water ad libitum unless otherwise noted.

Wild-type C57Bl6N (027) and CD1 (022) mice were purchased from Charles River. Mice were allowed to acclimate for 1 week in the animal facility before being used in experiments.

Creation of the *FIAT* transgenic mice were previously described and are a C57bl6N background [66]. Briefly, *FIAT* transgenic mice were generated using a 2.3 kb α1(I)collagen promoter fragment and the 1.8-kb full-length *FIAT* cDNA.

2.13. Mouse genotyping

Genotyping was performed using PCR amplification on genomic DNA prepared from ear clipping samples. Samples were digested overnight at 55°C in lysis buffer (0.1 mM Tris-HCl, pH 8.0, 0.2 M NaCl, 5 mM EDTA, 0.4% SDS, 250 µg proteinase K). DNA was precipitated with

isopropanol, washed with 75% ethanol, dried and resuspended in TE buffer. The following primers were used in genotyping the *FIAT* transgenic mice: 5′-ATCCATCAAAGCGCCATCAAAGCG-3′ and 5′-ACAAATAAAGCAATAGCATCACAA-3′. PCR products were resolved on an agarose gel.

2.14. Dose ranging study

Both male and female C57Bl6 were used in the dose ranging experiments. At 8 weeks of age, 5 mice of each sex were given an intraperitoneal (IP) injection of compound 73 or equivalent DMSO suspended in injection solution (40% Peg 400, 2% Tween 80, ddH_2O) five times a week for two weeks. Injections were performed in the morning. The following doses were used: 0.01 mg/kg, 0.1 mg/kg, 1 mg/kg and 10 mg/kg. Weight and behavior were monitored daily.

2.15. Serum & whole blood collection

At sacrifice, blood was collected from the mice by cardiac puncture. Serum was isolated using a serum separator tube (BD microtainer tubes, BD Franklin Lakes, NJ) by centrifugation at 3600 rpm for 8 minutes and stored at -80°C. Whole blood was collected for complete blood count in tubes containing 0.5 M K_3-EDTA at a ratio of 1:10 of whole blood. Frozen serum and whole blood were taken to the Comparative Medicine and Animal Resources Center (CMARC) at McGill University for hematological and blood biochemistry assays.

2.16. Pharmacokinetics-Pharmacodynamics

Eight (8)-week-old wild-type female CD1 mice (Charles River) were administered 10 mg/kg of compound 73 solution via IP injection in the morning. At designated time points, over 24 hours, blood, from groups of 3 mice each, was collected at sacrifice by cardiac puncture. Serum was isolated using a serum separator tube (BD microtainer tubes, BD Franklin Lakes, NJ) following the manufacturer's instructions and stored at -80°C. Frozen serum was taken to the Proteomics and Molecular Analysis Platform at the Research Institute of the McGill University

Health Centre (RI-MUHC). Here the serum was analyzed using liquid chromatography-mass spectrometry (LC-MS) to determine the concentration of the compound and the main metabolite.

Other tissues were collected at time of sacrifice including brain, pancreas, liver, lung and vertebrae. Tissues were cleaned and snap frozen in liquid nitrogen before being stored at -80°C long term. Tissues were crushed into a fine powder in liquid nitrogen with mortar and pestle before being transferred to the RI-MUHC platform for analysis.

2.17. Wild Type long term steady-state study

Wild-type male and female C57Bl6 mice (Charles River) were used in this experiment. Eight (8)-week-old mice were administered 10 mg/kg of compound 73 or DMSO solution via IP injection. Injections were given 5 times a week for 6 weeks. Injections were performed in the morning. Mice were sacrificed the day after the last injection was administered. At sacrifice blood and the following tissues were collected: calvaria, femurs, tibias, $L_2 – L_5$ vertebrae, subcutaneous fat pad, interscapular fat pad, and visceral fat pad.

2.18. Transgenic rescue

The transgenic *FIAT* mouse and wild type littermates were used in the transgenic rescue experiments. Both male and female mice were used in this experiment. Wild-type and transgenic cohorts were subdivided into control and treated mice. At 12 weeks of age mice were administered 10 mg/kg of compound 73 or DMSO solution via IP injection or oral gavage. Injections or oral gavage were given 5 times a week for 10 weeks. Injections or oral gavage was performed in the morning. Mice were sacrificed the day after the last dose was administered. At sacrifice blood and the following tissues were collected: calvaria, femurs, tibias, $L_2 – L_5$ vertebrae, subcutaneous fat pad, interscapular fat pad, and visceral fat pad.

2.19. High fat diet study

Wild-type female C57Bl6N mice (Charles River) were used in this study. Mice were divided between groups on a normal chow diet and a high fat chow diet (HFD; TD.06414, 60% fat; 31% lard 3% soybean oil, Envigo, Indianapolis, IN). Twelve (12)-week-old mice were

administered 10 mg/kg of compound 73 or DMSO solution via IP injection. Injections were given 5 times a week for 6 weeks. Injections were performed in the morning. Mice were sacrificed the day after the last injection was administered. At sacrifice blood and the following tissues were collected: calvaria, femurs, tibias, L_2 – L_5 vertebrae, subcutaneous fat pad, interscapular fat pad, and visceral fat pad.

2.20. Ovariectomized mouse prevention study

Wild-type C57Bl/6 or CD1 mice (Charles River) were used in this study. At 8 weeks of age, mice were subjected to either sham or ovariectomy surgery. Mice were placed under anesthesia via isoflurane and a dorsal skin incision was made to access the abdomen. The ovaries were surgically removed, and the incision site was sutured closed. In sham mice the procedure was the same, but the ovaries remained intact. The mice were allowed to recover for a week post-surgery to allow adequate healing of the surgical site. After recovery, mice were treated for 10 weeks through IP injections of either DMSO or compound 73, at a dose of 10 mg/kg, 5 times a week. Mice were sacrificed the day after the last injection was administered. At sacrifice blood and the following tissues were collected: calvaria, femurs, tibias, L_2 – L_5 vertebrae, subcutaneous fat pad, interscapular fat pad, and visceral fat pad.

2.21. Ovariectomized mouse rescue study

Wild-type C57Bl/6 or CD1 mice (Charles River) were used in this study. At 8 weeks of age, mice were subjected to either sham or ovariectomy surgery. Mice were placed under anesthesia via isoflurane and a dorsal skin incision was made to access the abdomen. The ovaries were then surgically removed, and the incision site was sutured closed. In sham mice the procedure was the same, but the ovaries remained intact. The mice were allowed to recover for a week post-surgery to allow adequate healing of the surgical site. Mice were allowed to age for an additional 8 weeks after recovery to achieve loss of bone mass. After 8 weeks had passed, mice were treated for 10 weeks through IP injections of either DMSO or compound 73, at a dose of 10 mg/kg, 5 times a week. Mice were sacrificed the day after the last injection was administered. At

sacrifice blood and the following tissues were collected: calvaria, femurs, tibias, L_2 – L_5 vertebrae, subcutaneous fat pad, interscapular fat pad, and visceral fat pad.

2.22. Micro-Computed tomography

Femurs and L_3-L_5 vertebrae from studied mice were dissected and immediately fixed in 4% paraformaldehyde for 24 hours at 4°C. Bones were washed 3 times in PBS and soaked overnight in 50% ethanol at 4°C. Bones were then transferred to 70% ethanol and kept at 4°C until analysis. Micro-computed tomography (μCT) was performed using a SkyScan 1272 high-resolution μCT scanner (Bruker SkyScan, Kontich, Belgium) connected to a Hamamatsu 10-megapixel camera. Femoral images were captured at 53 kV, 158 μA, using a detection pixel of 6 μm and a 0.25-mm aluminum filter. Integration time was set at 558 ms, and 2 images were captured every 0.40° through 180° rotation. Vertebral images were captured at 71 kV, 140 μA, using a detection pixel of 5 μm and a 0.25-mm aluminum filter. Integration time was set at 564 ms, and 2 images were captured every 0.40° through 180° rotation. Reconstruction was performed using SkyScan Recon software and analyzed using SkyScan CT Analysis software. Femoral trabecular parameters were measured on 369 slides (2.21 mm) of trabecular bone starting 74 slides (0.04mm) below the distal growth plate. Vertebral trabecular parameters of the L_4 vertebrae were measured on 450 slides (2.25 mm) of trabecular bone between the two growth plates. Cortical femur parameters were measured on 148 slides (0.88 mm) at midshaft. The following parameters were assessed: bone volume (BV, mm^3), tissue volume (TV, mm^3), the bone volume percent (BV/TV, %), cortical thickness (Ct.Th, mm), trabecular thickness (Tb.Th, mm), trabecular separation (Tb.Sp, mm), and trabecular number (Tb.N, mm^{-1}).

2.23. Three-point bending

Femoral mid-diaphyseal mechanical properties were measured via three-point bending. Femurs from studied mice were dissected, cleaned, and kept frozen at −20°C in PBS-soaked gauze until testing. Frozen femurs were equilibrated to room temperature and loaded to failure in a three-point bending assay using an Instron model 5943 single column table frame machine (Instron Corporation, Norwood, MA). Samples were positioned on the anterior surface down and

loaded centrally at a crosshead speed of 0.05 mm/s and a support distance of 7 mm. Whole-bone mechanical properties were assessed by the generated force vs. displacement data generated by Bluehill Universal software. The following parameters were assessed: stiffness (Young's Modulus, N/mm), load at yield (N), maximum load (N), and work to break (J).

2.24. Vertebral compression testing

L_2 vertebral mechanical properties were measured via compression testing. L_2 vertebrae from studied mice were dissected, cleaned, and kept frozen at −20°C in PBS-soaked gauze until testing. Frozen vertebrae were equilibrated to room temperature and loaded to failure via compression using a Bose Electroforce 3200 Series III test instrument (Bose Corporation – ElectroForce Systems Group, Eden Prairie, MN). The dorsal part of the vertebrae was loaded onto the sample holder within the compression area. Using a 225N load cells, samples were compressed at a rate of 0.1mm/s until failure. Data was collected in Wintest 7 software and analyzed using Matlab. The following parameters were assessed: stiffness (Young's Modulus, N/mm), load at yield (N), maximum load (N), and work to break (J).

2.25. Statistical analysis

Data are presented as means ± one standard deviation (SD). Comparisons were made by analysis of variance (ANOVA) with *post hoc* tests (Bonferroni's test), or unpaired t-tests. A probability (P) value lower than 0.05 was accepted as significant. Statistical analyses were performed utilizing GraphPad Prism 9 (GraphPad Software).

Chapter III: A high throughput screen, targeting the interaction domains of ATF4 and FIAT, identifies a lead compound.

3.1. Establishing stable cell lines expressing the interaction domains of ATF4 and FIAT in the mammalian two hybrid assay for high throughput screening

To successfully screen a large library of compounds a robust assay with a quantifiable readout is needed. We chose to use the mammalian two hybrid assay for our screening method as it is an effective system to assess and quantify the amount of protein-protein interaction. Previous work in our laboratory determined it was FIAT's second leucine zipper that is responsible for the interaction with ATF4. As the interaction between the two proteins are dependent on this specific structural motif, a former colleague of the lab subcloned these portion of each respective protein into expression plasmids to use within the mammalian two hybrid.

The second leucine zipper of FIAT spans amino acids positions 194 to 222, but a larger domain was subcloned in-frame with the Gal4 DNA binding domain from the pBIND vector due to the location of convenient restriction enzyme sites (Q186-Y424, 238 amino acids, Homo sapiens). The leucine zipper of ATF4 encompasses amino acids positions 306 to 334 but for the same reasons, a larger domain was subcloned in-frame with the VP16 activation domain of the pACT vector (Q136-A344, 208 amino acids, Mus musculus). A secreted luciferase reporter was created by subcloning the DNA binding site and promoter region from the mammalian two hybrid system upstream of reporter plasmid containing the secreted metridia luciferase reporter gene from the Takara ready to glow system (pG5MetLuc2) (Figure 4). The advantage of using a secreted luciferase is there is no cell lysis step, instead cell media is used. This allows for the luciferase count to be set to 0 when the media is changed, allowing for an accurate read-out of luciferase production after a compound has been added.

When all three plasmids, pG5MetLuc2, pACT-ATF4 and pBIND-FIAT, were co-transfected in HEK293 cells using lipofectamine, luciferase could be detected using the Takara ready to glow detection system. Three stable cells lines were created to carry out the high throughput screen. A negative control cell line (Met7) that stably expresses the pMET plasmid and produced no relative luciferase units (RLUs). An experimental cell line (F15) that stably expresses pG5MetLuc2, pACT-ATF4 and pBIND-FIAT and produces high RLUs. Lastly, a

positive control cell line (V29) that stably expresses pMET and GAL4-VP16 plasmid, a positive control plasmid for the Mammalian two hybrid assay that expresses a fusion GAL4-VP16 protein and produces high RLUs (Figure 5). Once these three stable cell lines were established and expanded, we used the services at the University of Montreal, Institute for Research in Immunology and Cancer, to preform a high throughput screen to identify compounds that disrupt the ATF4-FIAT interaction.

3.2. A high throughput screen identifies 8 compounds that potentially affect the ATF4-FIAT interaction

The initial screening of the 120,000-compound library used the Met7 negative control and F15 experimental cell lines. A compound was considered a "positive hit" if it reduced the RLUs of the experimental cell line by at least 50%. In this screen, 2,000 compounds were identified as positive hits. A counter screen was preformed on the 500 compounds that decreased RLUs by the highest margin in the initial screen. This counter screen was conducted using the experimental cell line versus the positive control cell line (V29) and the aim was to exclude false positives. A false positive could occur if a compound interfered with luciferase production, the luciferase assaying or caused cell death. The counter screen identified 262 compounds that affected luciferase expression in the experimental cell line and had no effect on the positive control cell line. Finally, a dose response screen of the top 19 compounds identified in the counter screen was completed using the experimental cell line. The top eight compounds that responded well in a dose response manner were further investigated *in vitro* to identify a lead compound (Table 1).

3.3. Assessing the biological significance of the 8 selected compounds identifies a lead compound, C73

Seven out of the eight compounds identified in the screen were "novel" while one was the FDA approved drug spironolactone. Each compound identified in the screen was given a code designation for intellectual property considerations, except for spironolactone as it has a proper drug name. Since most of the compounds had no published information for use in cell culture, determining the correct dose for downstream studies was prudent.

A MTT viability assay was used to find an adequate dose for each identified compound. MC3T3-E1 cells were plated and treated at various concentrations of each compound in a serial dilution of 1:2 starting at a maximum concentration of 100 μM. After 48 hours, the MTT viability assay was conducted according to manufacturer's protocol. At 25 μM most compounds were toxic. A second MTT study was preformed at a lower concentration. For a majority of the compounds, viability was maintained until 6 μM, at which point cell death began (Figure 6).

To determine the effect of the compounds on differentiation a pNPP assay was preformed to investigate the alkaline phosphatase activity of MC3T3-E1 cells differentiated in the presence of each compound. MC3T3-E1 cells were plated and differentiated for six days in the presence of each compound at a maximum concentration of 12 μM. Subsequent concentrations were evaluated in a serial dilution of 1:2. An increase in alkaline phosphatase was observed in cells treated with C56 and C73. In cells treated with C56, an increase in alkaline phosphatase levels were observed at 6 μM. In cells treated with C73, an increase in alkaline phosphatase levels were observed at concentrations of 1.5 μM and lower (Figure 7A). A second pNPP assay was preformed at a lower concentration of C73, where the maximum concentration was 2 μM. In this assay, a concentration of 0.25 μM of C73 had the largest effect on alkaline phosphatase (Figure 7B).

From the MTT and pNPP assays we were able to determine the appropriate concentration for each compound for a longer, more robust investigation on the effects of the compound on osteoblast differentiation. For compounds C21, C73, and C84 a concentration of 0.25 μM would be used for all subsequent studies. For compounds C56, C95, Spironolactone (Sp), M51, and A75 a concentration of 6 μM would be used for all subsequent studies.

To investigate the effect of the candidate compounds on mineralization, MC3T3-E1 cells were plated at confluency and differentiated for 14 days in the presence of each compound at the predetermined concentration. Treatment with compounds C73 and C56 showed an increase in calcium deposits, as assessed by alizarin red staining (Figure 8A). In addition to increased mineralization, C73 increased the expression of classical osteoblastic markers such as alkaline phosphatase (*Alpl*), *Runx2*, *Col1a1*, osteocalcin (*Bglap*), and Osterix (*Sp7*) (Figure 8B). No

changes in osteoblast markers were observed in cells treated with C56 (data not shown). These results identified C73 as the lead compound to be investigated further.

To ensure that the observed effects were not restricted to an established cell line, we performed *in vitro* differentiation assays with primary osteoblasts derived from both murine and human sources. Murine primary osteoblasts that were differentiated in the presence of 0.25 μM C73 showed an increase in calcium deposits when assessed by alizarin red staining (Figure 9A). An increase in mineralization was also accompanied by an increase in expression of osteocalcin (*Bglap*), alkaline phosphatase (*Alpl*), *Col1a1*, Osterix (*Sp7*), and *Runx2* (Figure 9B). When human primary osteoblasts were differentiated in the presence of 0.25 μM C73, an increase in calcium deposits was observed by alizarin red staining (Figure 9C). RT-qPCR analysis showed an increase in expression of alkaline phosphatase (*Alpl*) and Osterix (*Sp7*) (Figure 9D).

These results establish C73 as the lead compound identified in the high throughput screen targeting the ATF4-FIAT interaction. Osteoblasts, both immortalized and primary, treated with C73 throughout differentiation exhibited an increase in mineralization and expression of osteoblastic markers.

3.4. FIGURES AND TABLES

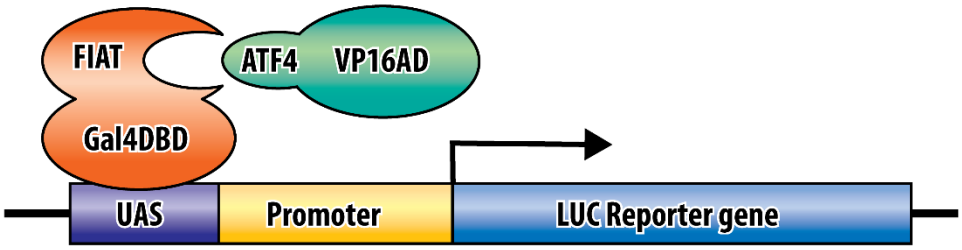

Figure 4. Schematic representation of the mammalian two hybrid assay.

A schematic representation of the mammalian two hybrid system showing FIAT and ATF4 subcloned into their respective domains. The LUC reporter gene in the system is the secreted Metridia luciferase.

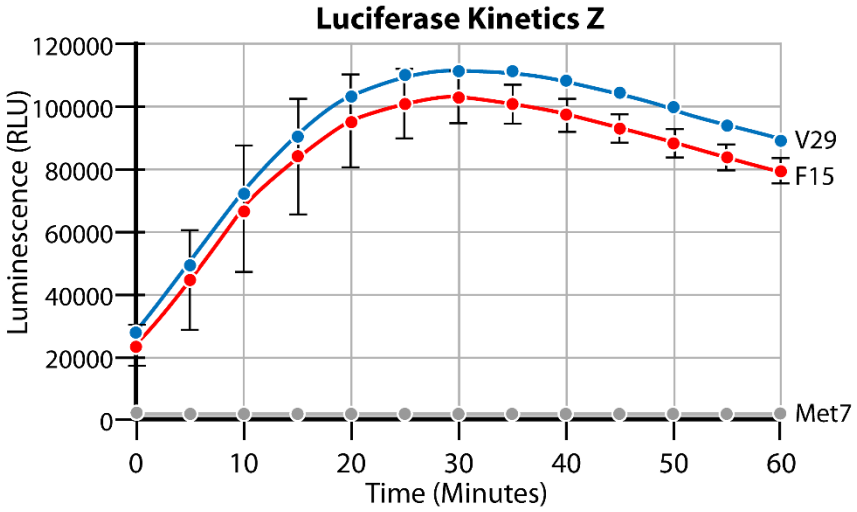

Figure 5. Luciferase Kinetics of the three cell lines.

High RLUs are observed in the positive (V29, blue) and experimental (F15, red) cell lines throughout the 60-minute kinetics test after luciferase substrate had been added to the system. A low RLU baseline is observed in the negative (Met7, grey) cell line.

Compound ID	Max % Inh (F15)	Max % Inh (V29)	ΔMax % Inh (F15-V29)
UM0006004	80.461	31.288	49.17
UM0073132	57.982	19.268	38.71
UM0118410	50.435	14.118	36.32
UM0015538	52.957	19.105	33.85
UM0092942	34.642	4.669	29.97
UM0055162	45.426	16.338	29.09
UM0070891	55.056	28.017	27.04
UM0008317	45.354	21.398	23.96
UM0046961	91.944	69.664	22.28
UM0121391	25.866	3.710	22.16
UM0044935	106.268	86.376	19.89
UM0000364	53.377	33.899	19.48
UM0076022	105.843	86.992	18.85
UM0050179	48.734	33.180	15.55
UM0070855	84.221	69.280	14.94
UM0119468	36.933	23.314	13.62
UM0013011	49.513	36.537	12.98
UM0019765	77.677	81.659	-3.98
UM0016497	79.859	91.422	-11.56

Table 2. Dose Response testing of top 19 compounds identified in the high throughput screen.

Results from a dose response test of the top 19 compounds identified in the high throughput screen. The first column identifies the compound name in the library, as assigned by the core facility at IRIC. The second column represents the maximum percent inhibition of RLUs of each compound as tested in the experimental cell line, F15. The third column represents the maximum percent inhibition of RLUs of each compound as tested in the positive control cell line, V29. The last column represents the change in maximum percent inhibition taken as the maximum percent inhibition of the F15 cell line minus the maximum percent inhibition of V29 cell line. The top eight compounds which showed the greatest change in maximum percent inhibition were further investigated *in vitro*.

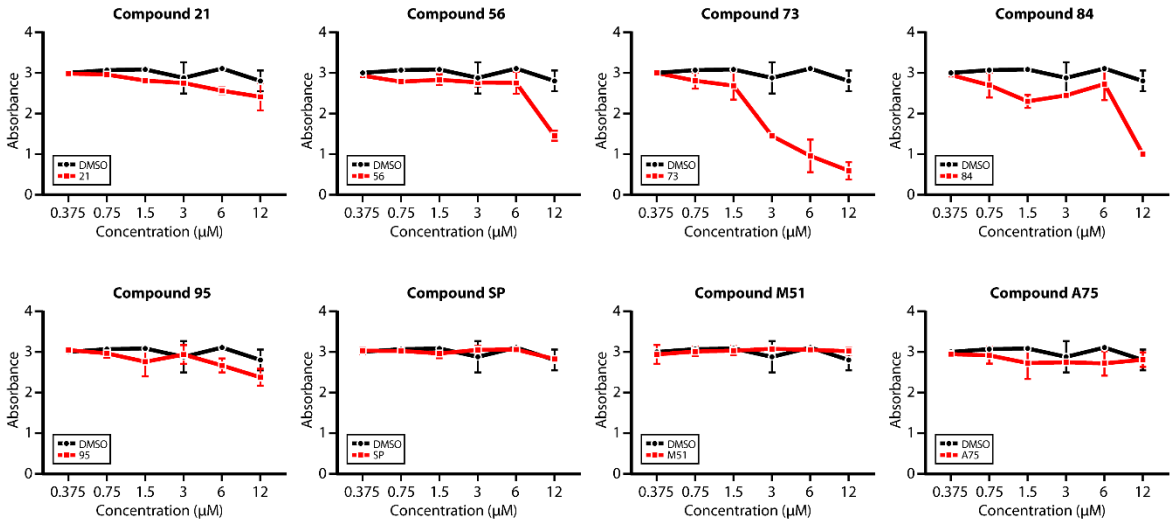

Figure 6: MTT viability assay of compounds identified in the high throughput screen in MC3T3-E1

MC3T3-E1 cells were treated with increasing concentrations of the compounds identified in the high throughput screen or DMSO. After 48 hours the viability of the cells was determined using the MTT viability assay according to the manufacturer's protocol. Each point represents the mean value and the error bars represent the SD between replicate cultures in that group.

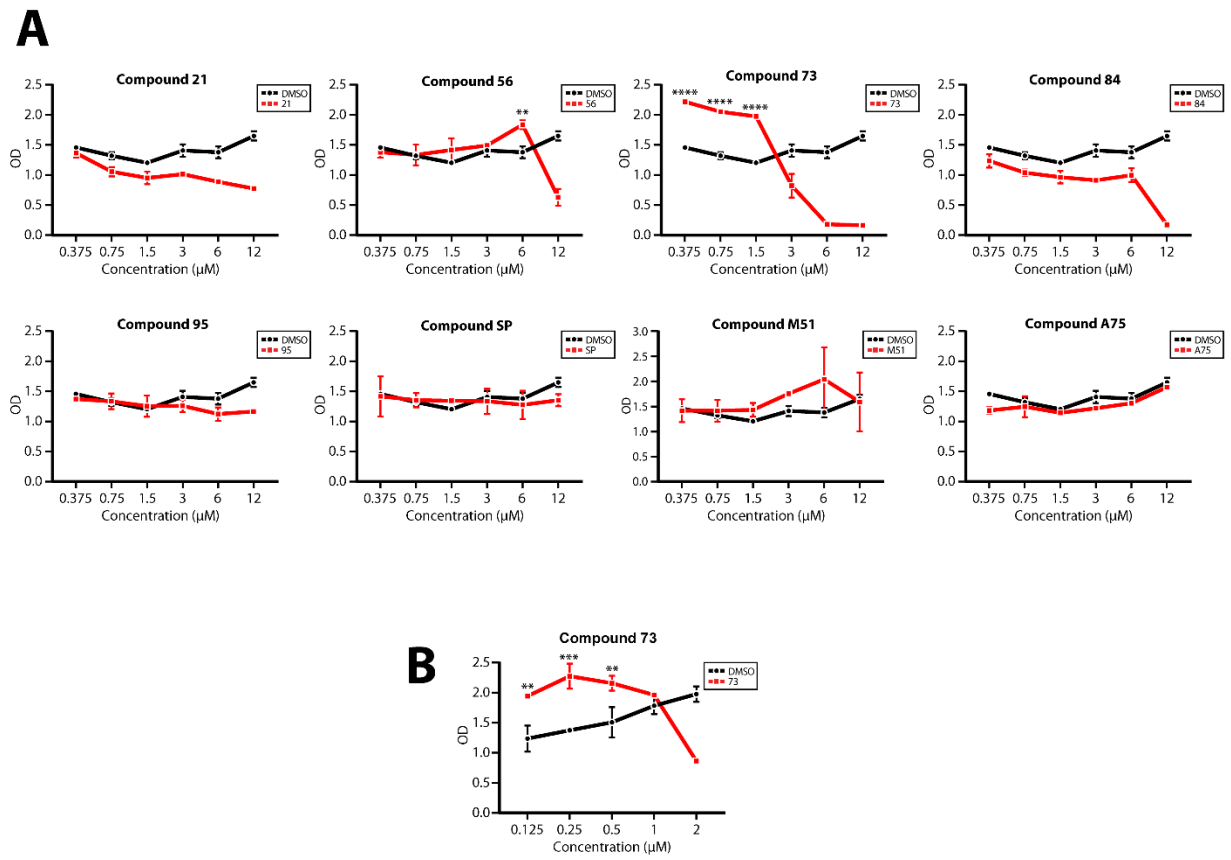

Figure 7: Alkaline phosphatase activity of MC3T3-E1 cells after treatment with compounds identified in the high throughput screen.

MC3T3-E1 cells were differentiated in the presence of the compounds identified in the high throughput screen for six days. **A**. Using a maximum concentration of each compound at 12 μM and subsequent lower concentrations of a 1:2 serial dilution. Alkaline phosphatase activity was assessed using a pNPP assay according to manufacturer's protocol. **B**. Using a maximum concentration of 2 μM of C73 and subsequent lower concentrations of a 1:2 serial dilution. Alkaline phosphatase activity was assessed using a pNPP assay according to manufacturer's protocol. Each point represents the mean value and the error bars represent the SD between replicate cultures in that group. **, $P < 0.01$; ***, $P < 0.001$; ****, $P < 0.0001$.

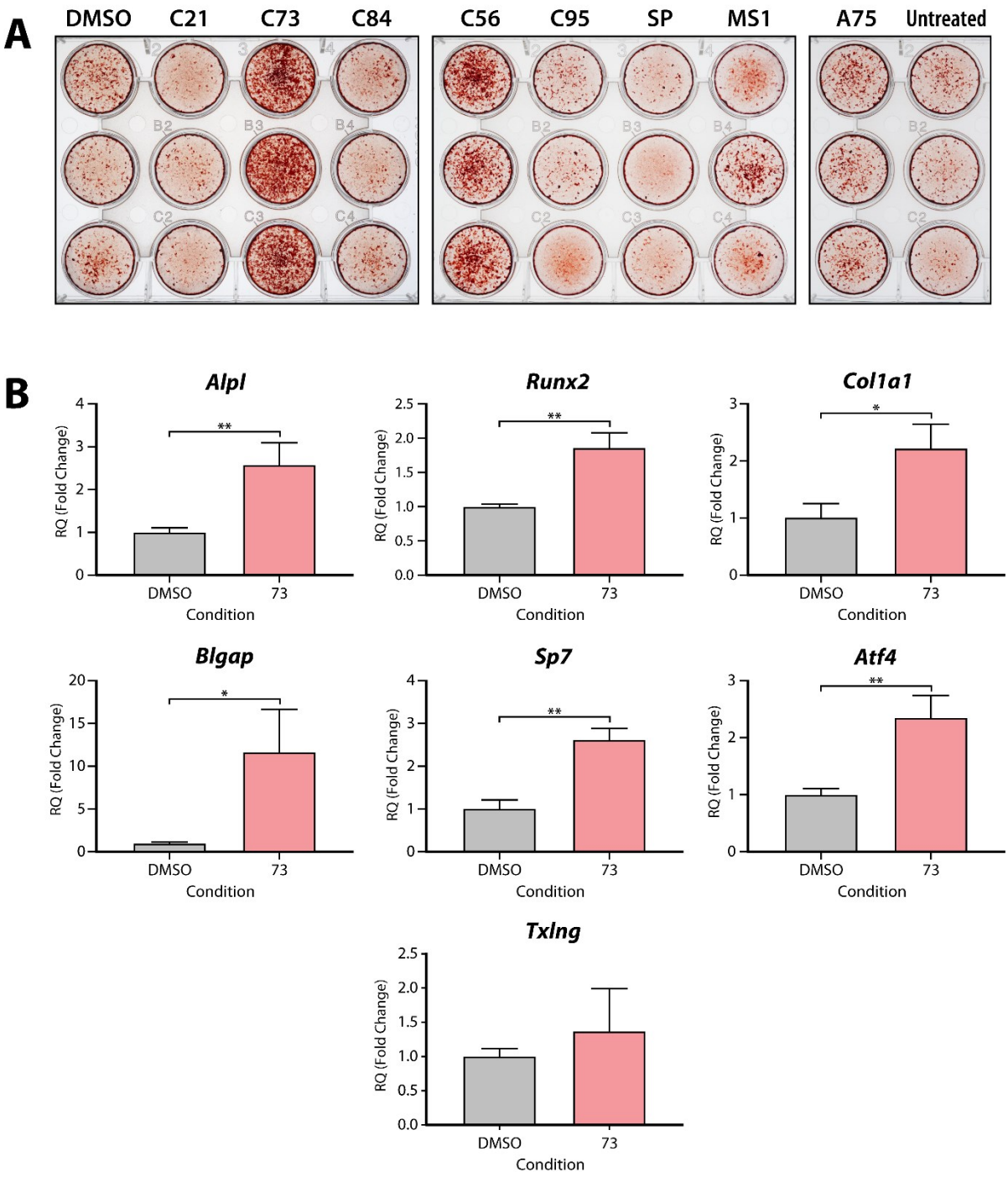
A
DMSO
C21
C73
C84
C56
C95
SP
MS1
A75
Untreated
B
Alpl
Runx2
Col1a1
Bglap
Sp7
Atf4
Txlng
RQ (Fold Change)
Condition
DMSO
73

Figure 8: MC3T3-E1 differentiated in the presence of compounds identified in the high throughput screen.

MC3T3-E1 cells were plated at confluency and differentiated for 14 days in the presence of the identified compounds. C21, C73 and C84 were at a concentration of 0.25 μM, while the rest of the compounds were at a concentration of 6 μM. **A**. Alizarin red staining on day 14 of differentiation **B.** Gene expression analysis of osteogenic markers in C73-treated cells. Quantitative RT-qPCR using TaqMan probes against osteoblast differentiation markers, normalized to *Gapdh*, was performed on RNA isolated from MC3T3-E1 cells grown for 14 days in osteogenic medium supplemented with 0.25 μM C73. Data are expressed relative to levels measured of MC3T3-E1 cells which received a vehicle treatment and are presented as the means ± SEM of triplicate determinations. *, $P < 0.05$; **, $P < 0.01$; ***

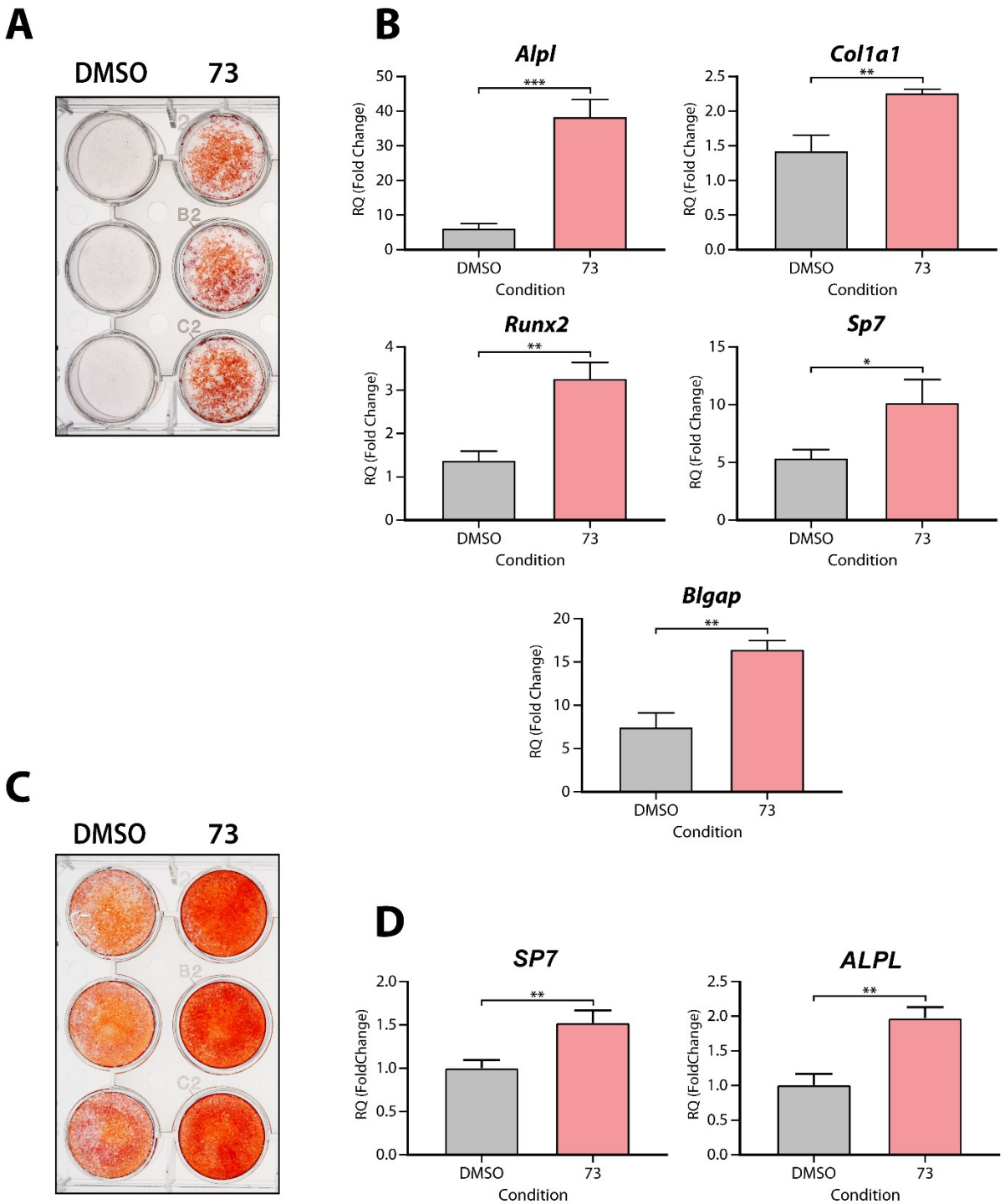
A
DMSO
73
B2
C2
B
Alpl
***
RQ (Fold Change)
50
40
30
20
10
0
DMSO
73
Condition
Col1a1
**
2.5
2.0
1.5
1.0
0.5
0.0
Runx2
4
3
2
1
Sp7
*
15
10
5
Blgap
20
C
D
SP7
RQ (FoldChange)
ALPL

Figure 9. Effects of C73 are not limited to immortalized cell lines.

Primary mouse and human osteoblasts were differentiated in the presence of 0.25 μM of C73. **A**. Alizarin red staining of differentiated primary mouse osteoblasts on day 14. **B.** Gene expression analysis of osteogenic markers. **C**. Alizarin red staining of differentiated primary human osteoblasts on day 14. **D.** Gene expression analysis of osteogenic markers. Quantitative RT-qPCR using TaqMan probes against osteoblast differentiation markers, normalized to *Gapdh*, was performed on RNA isolated from either mouse or human primary osteoblasts differentiated for 14 days in osteogenic medium supplemented with 0.25 μM C73. Data are expressed relative to levels measured of MC3T3-E1 cells which received a vehicle treatment and are presented as the means ± SEM of triplicate determinations. *, $P < 0.05$; **, $P < 0.01$; ***

Chapter IV: C73 disrupts the ATF4-FIAT interaction, but not other ATF4 interactions, allowing ATF4 to bind to its canonical binding site, OSE1, in the promoter region of *Bglap*

4.1. Treatment with C73 leads to decreased interaction between ATF4 and FIAT

Previous studies have shown that a change in the ATF4-FIAT interaction, via knockdown of FIAT, has a positive impact on mineralization. As the high throughput screen targeted the interaction domains of these two proteins, we hypothesize that C73 decreases or disrupts the ATF4-FIAT interaction. Using GST pulldowns, we assessed the effect of C73 on the ATF4-FIAT interaction. Halfway through the incubation period between the full-length GSH–*S*-transferase ATF4 fusion protein (GST-ATF4) purified from *Escherichia coli* bacteria and the *in vitro* translated MYC-tagged FIAT protein, 0.25 μM of C73 or equivalent volume of DMSO was added to the reaction. A strong signal can be observed at 72 kDa in the DMSO control treated lane denoting the interaction between ATF4 and FIAT. A decrease in signal is observed after 0.25 μM C73 is added to the system (Figure 10). We interpret these results to support our hypothesis that C73 is disrupting the ATF4-FIAT interaction.

4.2. Treatment with C73 does not affect interaction of ATF4 with other bZIP members, cJUN, FOSB, C/EBPβ, CHOP

FIAT is not the sole binding partner of ATF4. ATF4 has been shown to have various binding partners that have differing roles in the modulation of downstream ATF4 targets. Although the high throughput screen targeted the specific interaction domains of FIAT and ATF4, we needed to examine if C73 could disrupt other ATF4 binding partners that also interact through a leucine zipper. We examined four known ATF4 binding partners: cJUN, FOSB, C/EBPβ, and CHOP [60, 78]. We *in vitro* translated the four MYC-tagged proteins (cJUN, FOSB, C/EBPβ, and CHOP) and added 0.25 μM C73 to the reaction halfway through the incubation with GST-ATF4 protein. There is no change in interaction between ATF4 and the respective reciprocal protein when C73 is added to the system (Figure 11). We conclude that C73 specifically inhibits the ATF4/FIAT interaction, suggesting that C73 acts through binding FIAT, and not the ATF4 moiety of the heterodimer.

4.3. Treatment with C73 increases the binding of ATF4 to the OSE1 site in the promoter region of *Bglap*

The primary mode in which FIAT impacts mineralization is through modulating the binding of ATF4 to the OSE1 site in the promoter region of Osteocalcin (*Bglap*). A previous

study from our laboratory demonstrated FIAT inhibits the binding of ATF4 to an OSE1 oligonucleotide probe in an electrophoretic mobility shift assay (EMSA) [66]. Our previous GST pulldown results show that C73 can decrease the binding between ATF4 and FIAT. We hypothesized that the decrease in binding between FIAT with ATF4 can lead to a meaningful gain in ATF4 binding to the OSE1 site. Chromatin immunoprecipitation (ChIP) was performed on MC3T3-E1 cells differentiated for 7 days in the presence of 0.25 μM C73 or volume equivalent of DMSO. Using an anti-ATF4-specific antibody, results show a significant enrichment of ATF4 binding to the OSE1 site in DMSO-treated cells when compared to naïve IgG. This enrichment was further enhanced when cells were treated with C73 (Figure 12). This data supports our preferred hypothesis that C73 disrupts the ATF4-FIAT interaction, allowing ATF4 to bind to the OSE1 site in the osteocalcin promoter and leading to increased osteoblast differentiation and mineralization.

4.4. FIGURES AND TABLES

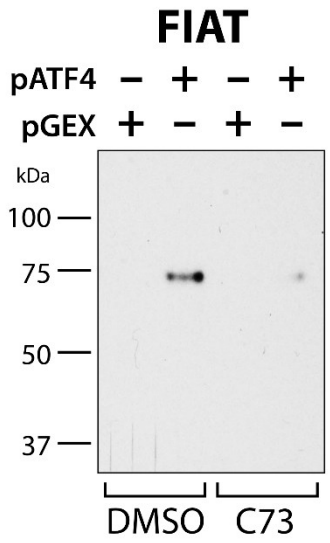

Figure 10. Treatment with C73 leads to a decrease in the ATF4-FIAT interaction.

GST-ATF4 fusion protein or GST alone was expressed in bacteria and incubated with *in vitro* translated FIAT. Halfway through incubation DMSO or 0.25 μM C73 was added to the system and the interaction was evaluated by SDS-PAGE and Western blot analysis.

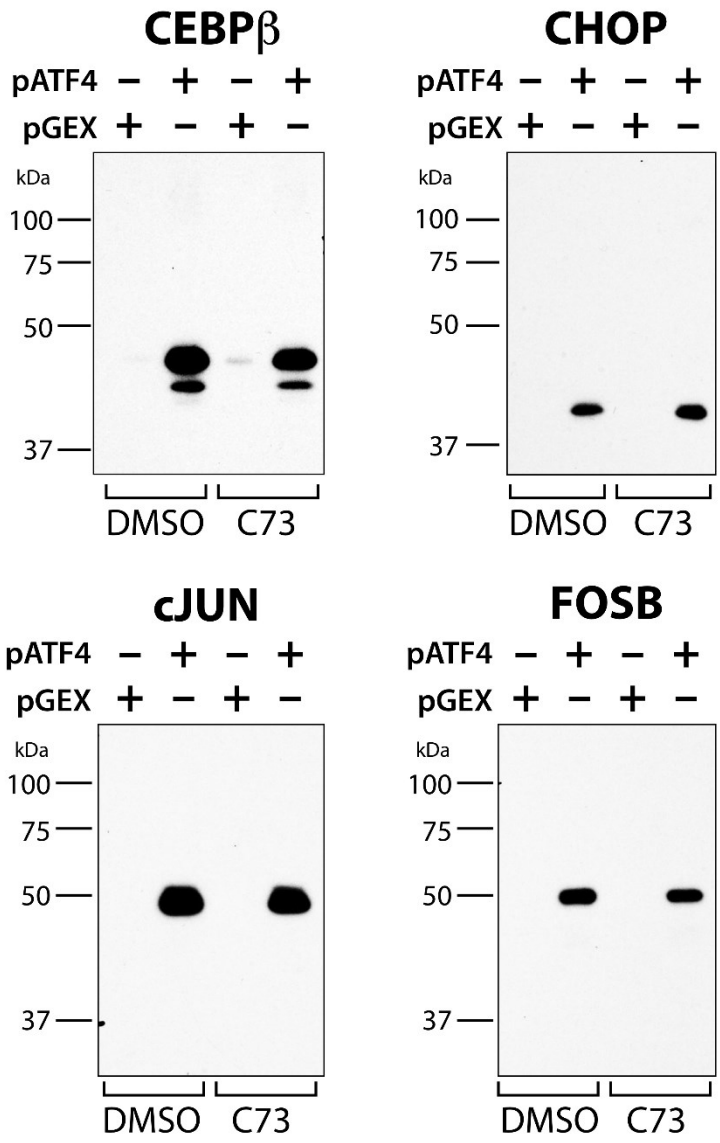

Figure 11. Treatment with C73 does not affect the binding of ATF4 to other bZIP members

GST-ATF4 fusion protein or GST alone was expressed in bacteria and incubated with *in vitro* translate C/EBPβ, FOSB, CHOP, CJUN. Halfway through incubation DMSO or 0.25 μM C73 was added to the system and the interaction was evaluated by SDS-PAGE and Western blot analysis.

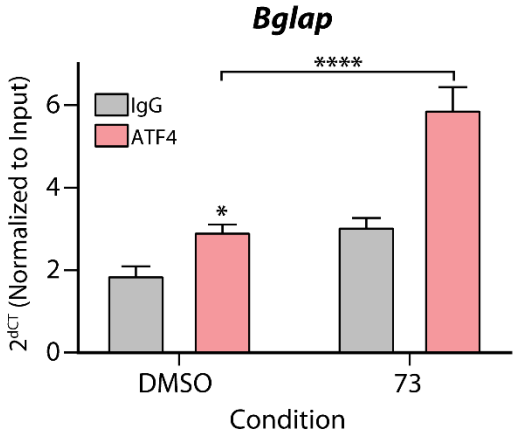

Figure 12. Treatment with C73 enhances ATF4 binding to the OSE1 site in the *Bglap* promoter.

Quantitative chromatin immunoprecipitation (ChIP) assays performed on MC3T3-E1 cells differentiated for 7 days under treatment with DMSO or 0.25 μM of C73 and using a pan-specific anti-ATF4 antibody or naive IgG as negative control. Input and ChIP products were amplified by SYBR green PCR using specific primers flanking the OSE1 site in the *Bglap* promoter. ChIP values were normalized to corresponding input values. Results are presented as 2^−ΔCT and are mean ± SEM of triplicate determinations. *, $P < 0.05$; ****, $P < 0.0001$.

Chapter V: C73 is well tolerated *in vivo*, has positive pharmaco-dynamics/kinetics parameters and long-term treatment has a positive impact on bone mass accrual.

5.1. *In vivo* dose ranging testing shows no negative impacts on mouse health through IP injection.

Given the results from the *in vitro* testing, a dose ranging experiment was conducted to explore the tolerability and safety of C73 *in vivo*. Using both sexes, C57bl6 mice at 8 weeks of age were injected intraperitoneally (IP) with either C73 or DMSO control. The doses tested were: 0.01mg/kg, 0.1 mg/kg, 1 mg/kg and 10 mg/kg. For the doses of 1 mg/kg and less, C73 was dissolved in 0.22 µM filtered ddH_2O. For a concentration of 10 mg/kg C73 was insoluble in water. To increase solubility at this concentration a solution comprised of PEG 400, Tween 80, and C73 was used to create a microemulsion. In the control group DMSO was substituted in place of C73 in the microemulsion solution.

Injections were administered 5x a week for two weeks. Mice were weighed before each injection, and regardless of treatment group, gained weight appropriately (Figure 13A). C73 had no effect on weight gain over the treatment regime. No abnormal behavior was observed over the course of the experiment in C73 treated mice.

After the two weeks, mice were sacrificed and whole blood and plasma were collected for processing. When comparing the blood biochemistry between the DMSO control and C73 treated mice, there was no significant difference between the groups in the doses investigated. Of note, no changes occurred in markers relating to liver function (total bilirubin), kidney function (BUN urea) nor heart function (AST), with all values falling within the expected range for proper organ function within a mouse (Figure 13B). These results suggest that, on a systemic level, C73 is tolerated as well as DMSO control and does not negatively affect major organ functions.

The collected whole blood was sent for complete blood count (CBC). No significant differences were observed between the DMSO control and C73 treated mice for any dose. Red blood cells count and white blood cell count, and platelet count were comparable between the groups (Figure 13C). This suggests that there is no change in bone marrow function of blood cell production, or inflammation occurring with the treatment of C73.

Given the data collected in the dose ranging experiment *in vivo*, we concluded that C73 is well tolerated *in vivo* and that we could proceed to investigate the efficacy of the compound for

bone mass accrual. Given the tolerability of the highest dose of 10 mg/kg, we chose this dose for all subsequent *in vivo* experiments.

5.2. Preliminary PK/PD data for C73

Using the expertise of the Proteomics and Molecular Analysis Platform at the Research Institute of the McGill University Health Center, we sought to determine a concentration-time curve and the half-life of C73 in a murine model. Using 12-week-old CD-1 mice, a timed study was conducted in which mice were given 10 mg/kg C73 via IP injection. Serum samples were then collected at predetermined time intervals over three hours. Using LC-MS, a pharmacokinetics curve for C73 after IP injection was generated. Five (5) minutes after injection, C73 was quantifiable in serum. A peak concentration of C73 was observed at 15 minutes post injection, and the half-life was measured as approximately 45 minutes after injection. C73 was still detectable at 60 minutes post injection but after 3 hours the compound was undetectable in serum (Figure 14A).

As the target tissue for C73 is bone tissue, the vertebra (L_2-L_5) from the pharmacokinetics study was collected in tandem with the serum. Vertebra were cleaned of tissue, intervertebral discs, and spinal cord before being snap frozen in liquid nitrogen. Vertebra were homogenized under cryogenic conditions using mortar and pestle. Using LC-MS, C73 was detectable in vertebral tissue 15 minutes after IP injection (Figure 14B). This data confirms C73 rapidly reaches its target tissue.

5.3. Long term steady state treatment with C73 in a low bone mass mouse strain increases osteoblast differentiation markers, bone mass and bone biomechanical properties of long bone and vertebrae.

Although the effect of drugs on a cellular level can occur rapidly, the effect at the tissue level takes longer. The two-week administration of C73 was too short to observe meaningful changes in bone mass when assessed by 3 point-bending and μCT analysis (data not shown). A long-term steady state experiment was conducted to investigate if: 1. C73 is tolerated well with prolonged use and 2. C73 could increase bone mass in a mouse strain exhibiting a comparably low bone mass under steady-state homeostatic conditions.

Eight-week-old female C57bl6 mice were administered 10 mg/kg of C73 or DMSO control via IP injection 5x a week for 6 weeks. Throughout the study, no abnormal behavior or aberrant weight change occurred in the treated cohort. RT-qPCR analysis RNA extracted from the tibial bone showed an increase in osteoblastic markers: *Alpl*, *Col1a1*, *Runx2*, *Sp7, and Atf4.* No changes were observed in the RNA expression of *Fiat* (*Txlng*). A slight increase in *Rankl* expression was observed, which is a downstream target of ATF4. No changes were observed in *Opg* expression. Of note, an increase in *Bglap* was observed, which is the downstream target of the ATF4-FIAT interaction (Figure 15)

Static histomorphometry of distal femurs obtained by μCT showed an increase in both the trabecular and cortical bone compartments of C73 treated mice. Treatment with C73 showed an increase in trabecular compartment. Although the percent bone volume (BV/TV) was not significant the C73 treated mice showed significant increase in trabecular thickness when compared to the control treated mice. (Figure 16A). Cortical tissue showed an increase in tissue area (T.Ar), tissue perimeter (T.Pm), bone area (B.Ar) and cortical thickness (Cs.Th) (Figure 16B). To investigate if increase in bone mass of the C73 treated mice was associated with increased bone strength, we assessed the biomechanical and structural properties of C73 treated bones. Using three-point bending, we tested the whole-bone mechanical properties of femurs at mid-diaphysis. Femurs of C73 treated mice exhibited an increase in maximum load and load at break suggesting an increase in overall bone strength (Figure 16C). There were no changes in the other parameters measured (data not shown). Furthermore, we assessed the changes in the mechanical properties of the vertebral body using compression testing. The compression data of the L_2 vertebra of C73 mice showed an increase in load at yield and work to yield (Figure 16D). The increase in the load at yield suggests that C73-treated vertebra can sustain more load and energy before it suffers permanent damage.

The long-term steady state experiment demonstrated that prolonged use of C73 at a dose of 10 mg/kg is well tolerated. Using a mouse that has a naturally occurring low bone mass phenotype, we were able to increase osteoblastic differentiation markers in marrow flushed tibias assessed by RT-qPCR. In addition, an increase in bone mass was observed both in the cortical and trabecular compartment of the bone tissue. This increase in bone mass in the femur correlates with an increase in bone biomechanical properties when assessed by 3-pt-bending,

namely an increase in the amount of load the femur can sustain before fracture occurs. Furthermore, an increase in the load at yield and energy to yield of the vertebral body also confirms bone biomechanical properties are being affected in other areas of the skeleton, not exclusively in the long bone. These promising data obtained under steady-state homeostatic conditions and supporting an osteoanabolic activity prompted the testing of C73 in preclinical models of low bone mass.

5.4. FIGURES AND TABLES

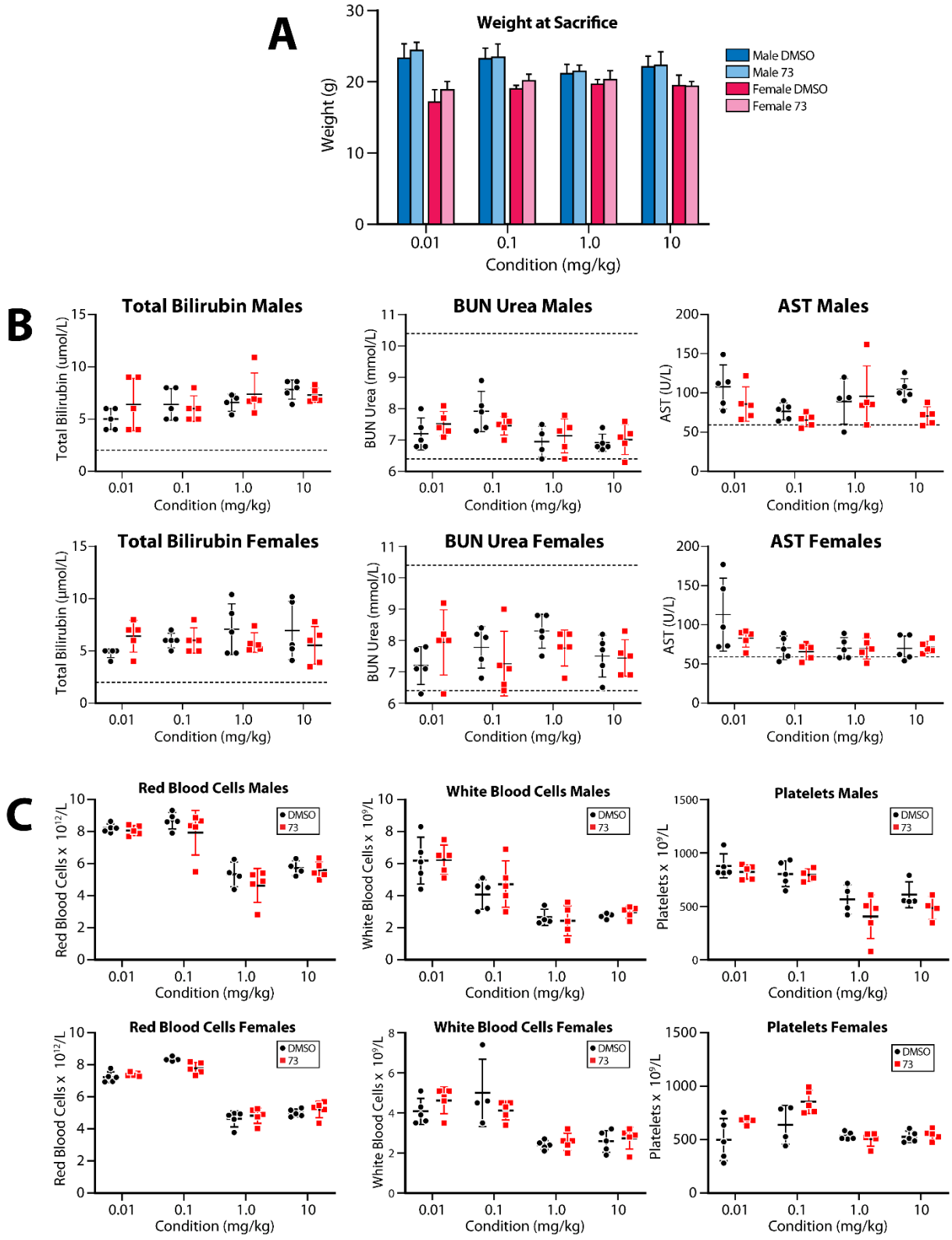

Figure 13. Safety testing of C73 *in vivo*; weight, blood biochemistry and complete blood count

Using both sexes, C57bl6 mice at 8 weeks of age were injected intraperitoneally (IP) with either C73 or DMSO control. Injections were given five days a week for two weeks. **A**. Weight at sacrifice **B**. Blood biochemistry assessing Total bilirubin, Bun Urea and AST. Dashed lines indicate the suggested ranges for mice as reported by CMARC. **C**. CBC investigating red blood cell, white blood cell and platelet counts. N=5

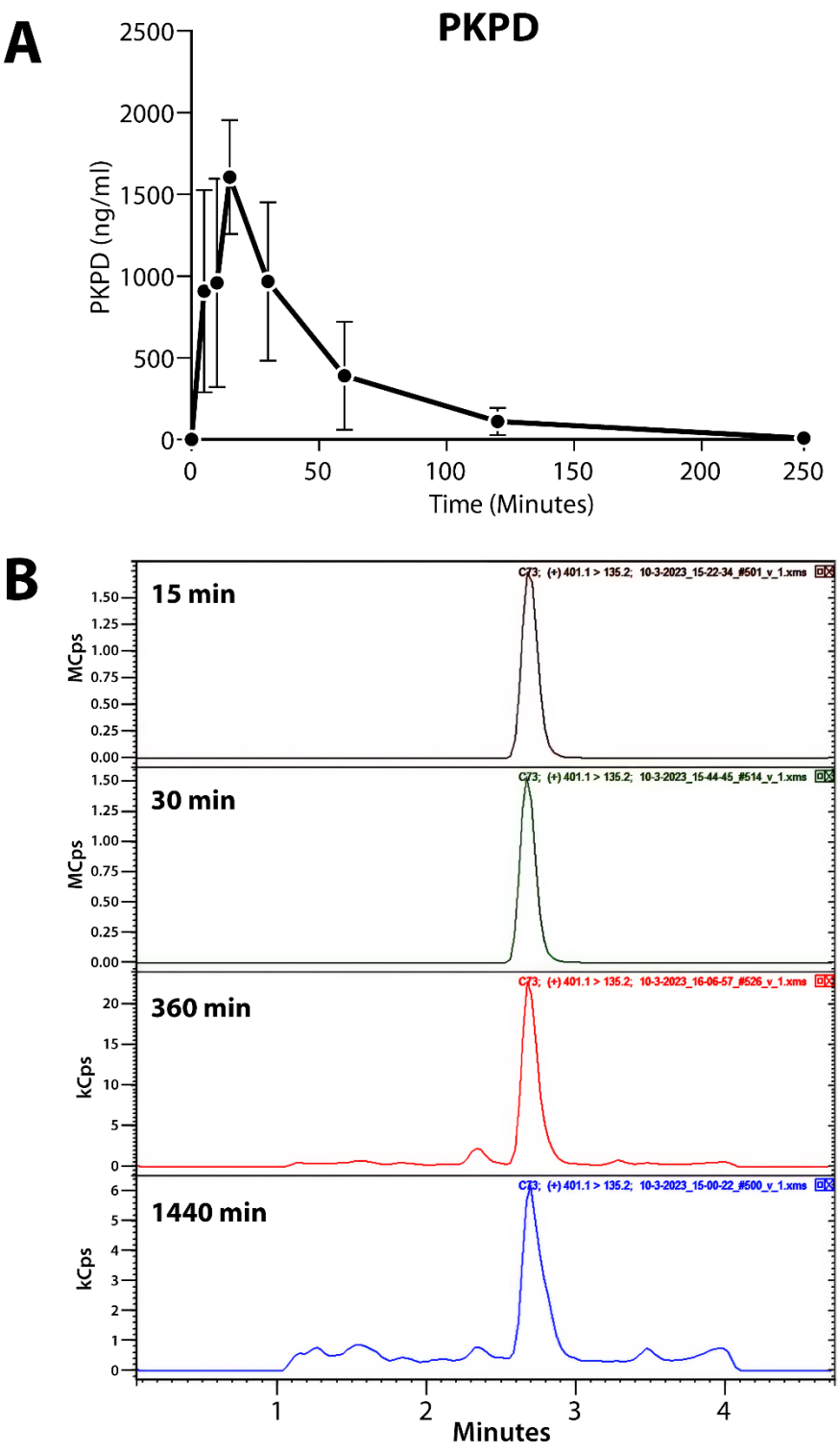
A
PKPD
PKPD (ng/ml)
2500
2000
1500
1000
500
0
0
50
100
150
200
250
Time (Minutes)
B
15 min
30 min
360 min
1440 min
MCps
kCps
Minutes
1
2
3
4

Figure 14. Pharmacokinetics/Pharmacodynamics of C73 at 10 mg/kg in CD1 mice via intraperitoneal injection.

A. A pharmacokinetics curve plotting the concentration of C73 in the serum over time post injections. Each point represents the mean value, and the error bars represent the SD. N = 3. **B**. Chromatogram of LC-MS/MS derived from vertebral tissue at different time points post injection. The spike denotes the presence of C73 in the sample.

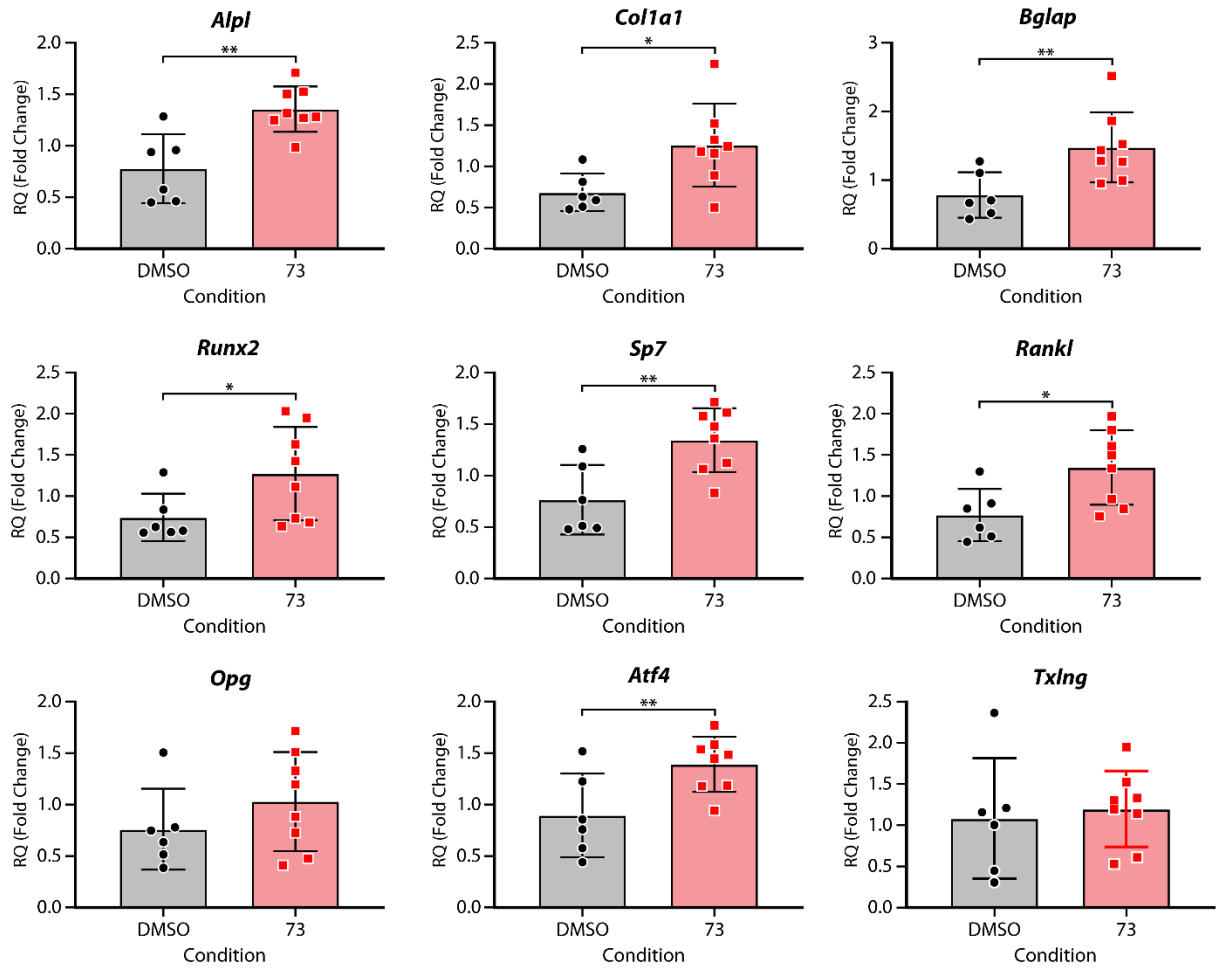

Figure 15. Long term in vivo treatment with C73 enhances mRNA osteogenic markers.

C57bl6 Female mice at 8 weeks of age were injected intraperitoneally with either C73 (10 mg/kg) or DMSO control, 5x a week for 6 weeks (N=8 or 6). Quantitative RT-qPCR using TaqMan probes against osteoblast differentiation markers was performed on RNA isolated from marrow flush tibias. Results are normalized to *Gapdh* expression and are given as means ± SD. *, $P < 0.05$; **, $P < 0.01$

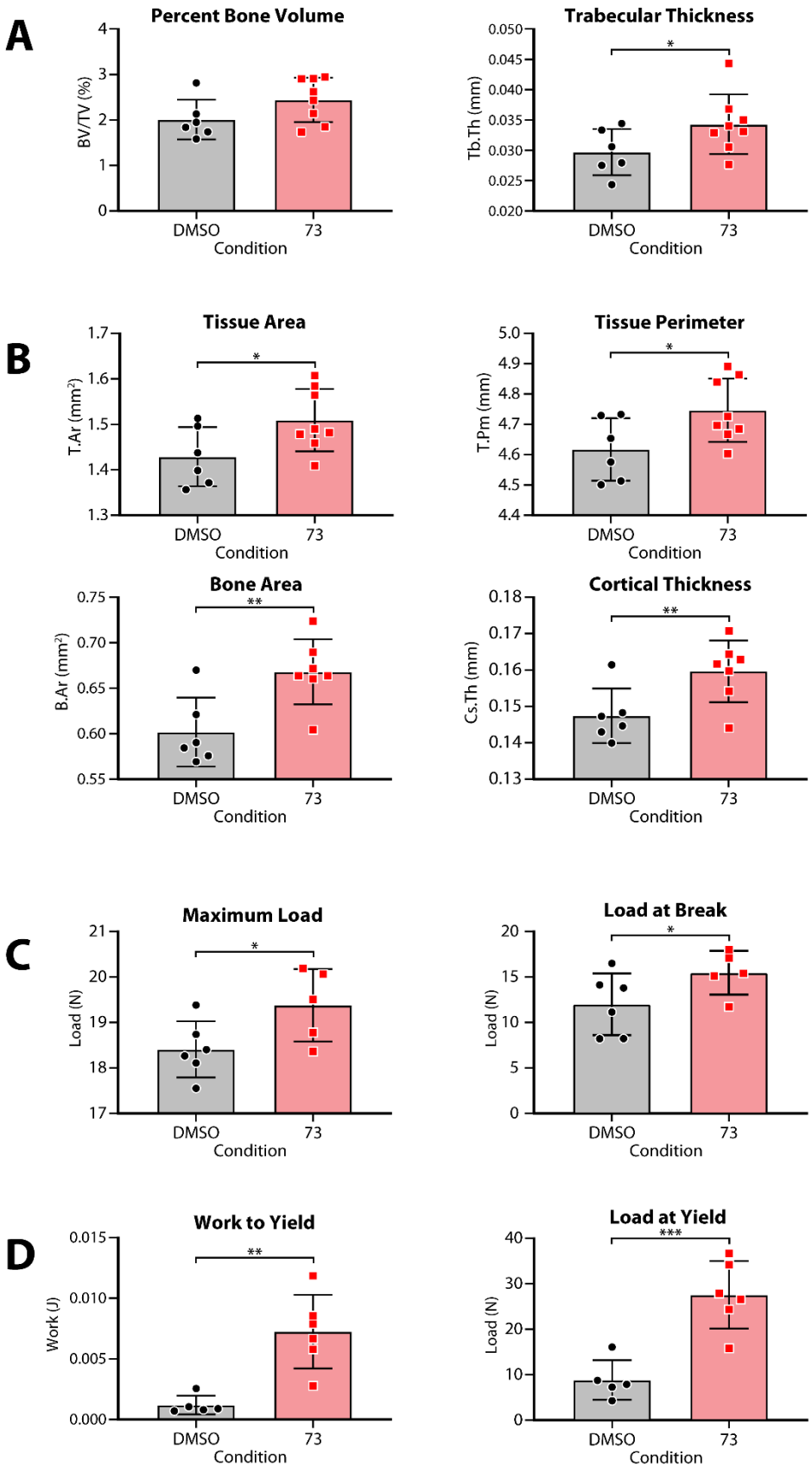
A
Percent Bone Volume
BV/TV (%)
0
1
2
3
4
DMSO
73
Condition
Trabecular Thickness
Tb.Th (mm)
0.020
0.025
0.030
0.035
0.040
0.045
0.050
*
DMSO
73
Condition
B
Tissue Area
T.Ar (mm²)
1.3
1.4
1.5
1.6
1.7
*
DMSO
73
Condition
Tissue Perimeter
T.Pm (mm)
4.4
4.5
4.6
4.7
4.8
4.9
5.0
*
DMSO
73
Condition
Bone Area
B.Ar (mm²)
0.55
0.60
0.65
0.70
0.75
**
DMSO
73
Condition
Cortical Thickness
Cs.Th (mm)
0.13
0.14
0.15
0.16
0.17
0.18
**
DMSO
73
Condition
C
Maximum Load
Load (N)
17
18
19
20
21
*
DMSO
73
Condition
Load at Break
Load (N)
0
5
10
15
20
*
DMSO
73
Condition
D
Work to Yield
Work (J)
0.000
0.005
0.010
0.015
**
DMSO
73
Condition
Load at Yield
Load (N)
0
10
20
30
40
***
DMSO
73
Condition

Figure 16. Long term *in vivo* treatment with C73 enhances bone mass and biomechanical properties.

C57bl6 Female mice at 8 weeks of age were injected intraperitoneally with either C73 (10 mg/kg) or DMSO control, 5x a week for 6 weeks (N=8 or 6). Histograms representing trabecular (**A**) and cortical (**B**) structural parameters obtained by μCT analyses. C73 treated mice show a significant increase in trabecular (**A**) and cortical (**B**) indices. Trabecular parameters are percent bone volume (BV/TV), and trabecular thickness (Tb.Th). Cortical parameters are tissue area (T.Ar), tissue perimeter (T.Pm), bone area (B.Ar) and cortical thickness (Cs.Th). Results are given as means ± SD. Three-point bending testing (**C**) of femurs. C73 treated mouse femurs show an increase in maximum load and load at break. Results are given as means ± SD. Vertebral compression (**D**) of L_2 vertebra. C73 treated mouse L_2 vertebra show an increase work to yield and load at yield. Results are given as means ± SD.

Chapter VI: Treatment with C73 rescues the low bone mass phenotype of *FIAT* transgenic mice.

6.1. Treatment with C73 rescues the low bone mass phenotype and the reduced bone strength of *FIAT* transgenic mice

To assess the drug-target efficacy of C73, we sought to rescue the low bone mass phenotype of the *FIAT* transgenic mouse, previously described by our laboratory [66]. Twelve (12)-week-old *FIAT* transgenic mice of both sexes were administered C73 at a dose of 10 mg/kg, 5x a week for 10 weeks via IP injection. No aberrant changes in body weight trends nor abnormal behavior were observed during the experiment.

In the male cohort, static histomorphometry of distal femurs obtained by μCT showed the expected decrease in trabecular bone associated with the *FIAT* transgenic mouse when comparing the DMSO control treated wild-type and transgenic mice. This measurement between the DMSO control groups confirms the low bone mass phenotype is still present in the murine model even after maintaining the strain in breeding for close to 20 years and allows to assess bone mass gain through intervention. To assess if the low bone mass phenotype was "rescued" we compared the bone parameters between the C73 treated *FIAT* transgenic mouse and the wild-type DMSO control treated mouse. An absence of significant differences between these two groups would allow us to conclude that the low bone mass phenotype was rescued.

Treatment with C73 had a significant effect on percent trabecular bone volume (BV/TV) and trabecular number in the transgenic littermates (Figure 17A). These parameters were comparable to the wild-type DMSO control treated mice; thus, we concluded that treatment with C73 was able to rescue the low bone mass phenotype in the trabecular bone compartment. There were no significant changes observed within the cortical bone compartment of the DMSO control treated mice between the wild-type and transgenic mouse (data not shown). Since there was no change in the cortical bone compartment, we could not accurately assess the effect of C73 treatment in this area.

Using three-point bending we tested the whole-bone strength of the femurs at mid-diaphysis collected from this study. No changes in bone strength were observed in the DMSO control treated mice between the wild-type and transgenic mouse (data not shown). Since there was no change in bone strength in the control mice, we could not accurately assess the effect of C73 treatment on this parameter.

Static histomorphometry of the vertebral body of the L_4 vertebrae obtained by μCT showed the expected decrease in trabecular bone in the DMSO control treated cohort between the wild-type and transgenic mice. This measurement between the DMSO control groups confirms the low bone mass phenotype is present in the vertebral body as this area was not investigated during the initial phenotyping study conducted in our laboratory [66]. A gain in the trabecular compartment of the vertebral body, as shown by the increase in percent bone volume (BV/TV) and trabecular number, can be observed after treatment with C73 (Figure 17B). Furthermore, we assessed the changes in the mechanical properties of the vertebral body using compression testing. The compression data from the L_2 vertebra showed a decrease in load at yield and work to yield between the wild-type and FIAT transgenic DMSO control treated mice. A rescue of these parameters was seen in the FIAT transgenic mice treated with C73 (Figure 17C). The increase in the load at yield suggests that C73 treated FIAT transgenic vertebra can sustain more load and energy before suffering permanent damage.

In the female cohort, static histomorphometry of distal femurs obtained by μCT showed no changes in the trabecular or cortical bone in the DMSO control treated cohort between the wild-type and transgenic mice (data not shown). Furthermore, when using three-point bending to assess the whole-bone mechanical properties of femurs at mid-diaphysis, no changes in bone strength were observed regardless of phenotype or treatment (data not shown).

Static histomorphometry of the vertebral body of the L_4 vertebrae obtained by μCT showed the expected decrease in trabecular bone in the DMSO control treated cohort between the wild-type and transgenic female mice. A subsequent rescue of percent bone volume and trabecular number can be observed with the treatment of C73 (Figure 18A). Furthermore, we assessed the changes in the mechanical properties of the vertebral body using compression testing. The compression data from the L_2 vertebra showed a decrease in load at yield and work to yield between the wild-type and FIAT transgenic DMSO control treated mice. A rescue of these parameters was seen in the FIAT transgenic mice treated with C73 (Figure 18B). The increase in the load at yield suggests that C73 treated FIAT transgenic vertebra can sustain more load and energy before it suffers permanent damage.

This data supports the drug efficacy of C73 by rescuing the low bone mass phenotype of the *FIAT* transgenic mouse. Although only the male cohort showed a difference in long bone

parameters at the trabecular level, both sexes showed meaningful bone mass accrual upon treatment in the vertebral body.

6.2. Oral administration of C73 rescues the low bone mass phenotype of the *FIAT* transgenic mouse.

Although C73 was efficient at rescuing the low bone mass when given through IP injection, it was unknown if the same effect could be achieved when administered orally. Using the *FIAT* transgenic mice, we conducted an identical study to the one described above but C73 was given through oral gavage. No aberrant changes in body weight trends nor abnormal behavior were observed during the experiment. Although both sexes were investigated in this study, as of writing only the female cohort had been analyzed.

In the female cohort, μCT analysis of L_4 vertebral body showed a significant decrease in the following trabecular bone parameters in the DMSO control treated cohort between the wild-type and transgenic mouse: percent bone volume (BV/TV) and trabecular thickness. These parameters were non-significant between the wild-type DMSO control treated group and the *FIAT*-transgenic C73 group (Figure 19A). We concluded that administration of C73 through oral gavage was able to rescue the low bone mass phenotype observed in the L_4 vertebral body of the FIAT-transgenic mouse.

To assess if these structural changes influenced the mechanical properties of the vertebral body, compression of the L_2 vertebra was assessed. The compression testing of the vertebra showed a decrease in the following parameters assessing bone strength between the wild-type and *FIAT* transgenic DMSO control treated mice: load at yield, work to yield, work to max load and work to break. A rescue of these parameters was seen in the *FIAT* transgenic mice treated with C73, as noted by the non-significant changes between this group and the wild-type DMSO control treated group. (Figure 19B). The increase in the load at yield suggests that C73 treated *FIAT* transgenic vertebra can sustain more load and energy before it suffers permanent damage.

As of writing, the structural changes of the femur in the female cohort have yet to be assessed via μCT analysis. Preliminary bone strength data, using three-point bending testing on the mid-diaphysis of the femur, showed a decrease in maximum load and work to maximum load parameters between the wild-type and *FIAT* transgenic mice in the DMSO control group. These

strength parameters were rescued with the treatment of C73 given through oral gavage (data not shown).

The effect of C73 on bone mass accrual and strength has been shown to be effective when given through IP injection. In the patient population, medicine that requires multiple injections have lower rates of compliance than those that can be taken orally. Using the *FIAT* transgenic mouse model, we were able to rescue a low bone mass phenotype by administering C73 orally. The rescue of the low bone mass phenotype was comparable to when C73 was given through IP injections. Mice given an oral gavage of C73 exhibited no discernable off target effects and tolerated the drug well throughout treatment.

6.3. FIGURES AND TABLES

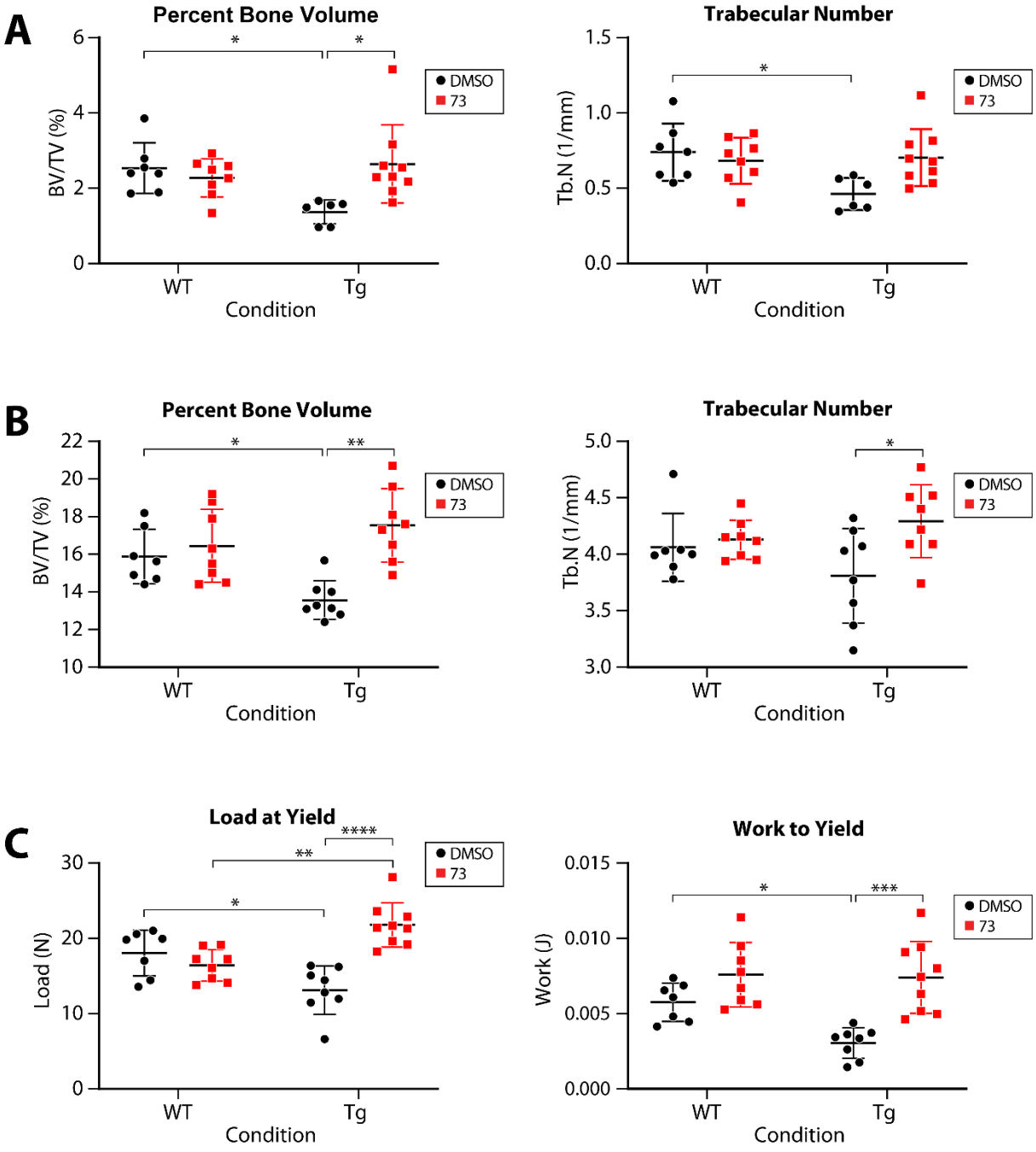

Figure 17. Treatment with C73 rescues the low bone mass phenotype and reduced bone strength of the *FIAT*-transgenic in male mice.

Wild type or *FIAT*-transgenic male mice at 12 weeks of age were injected intraperitoneally with either C73 (10 mg/kg) or DMSO control, 5x a week for 10 weeks (N=8 or 7). Histograms representing femoral trabecular (**A**) structural parameters obtained by μCT analyses. C73 treated mice show a significant increase in trabecular indices (**A**). Trabecular parameters are percent bone volume (BV/TV), and trabecular number (Tb.N). Results are given as means ± SD. Histograms representing vertebral trabecular (**B**) structural parameters obtained by μCT analyses. C73 treated mice show a significant increase in trabecular indices. Trabecular parameters are percent bone volume (BV/TV), and trabecular number (Tb.N). Results are given as means ± SD. Vertebral compression (**C**) of L_2 vertebra. C73 treated mouse L_2 vertebra show an increase work to yield and load at yield. Results are given as means ± SD. *, $P < 0.05$; **, $P < 0.01$; ***, $P < 0.001$; ****, $P < 0.0001$.

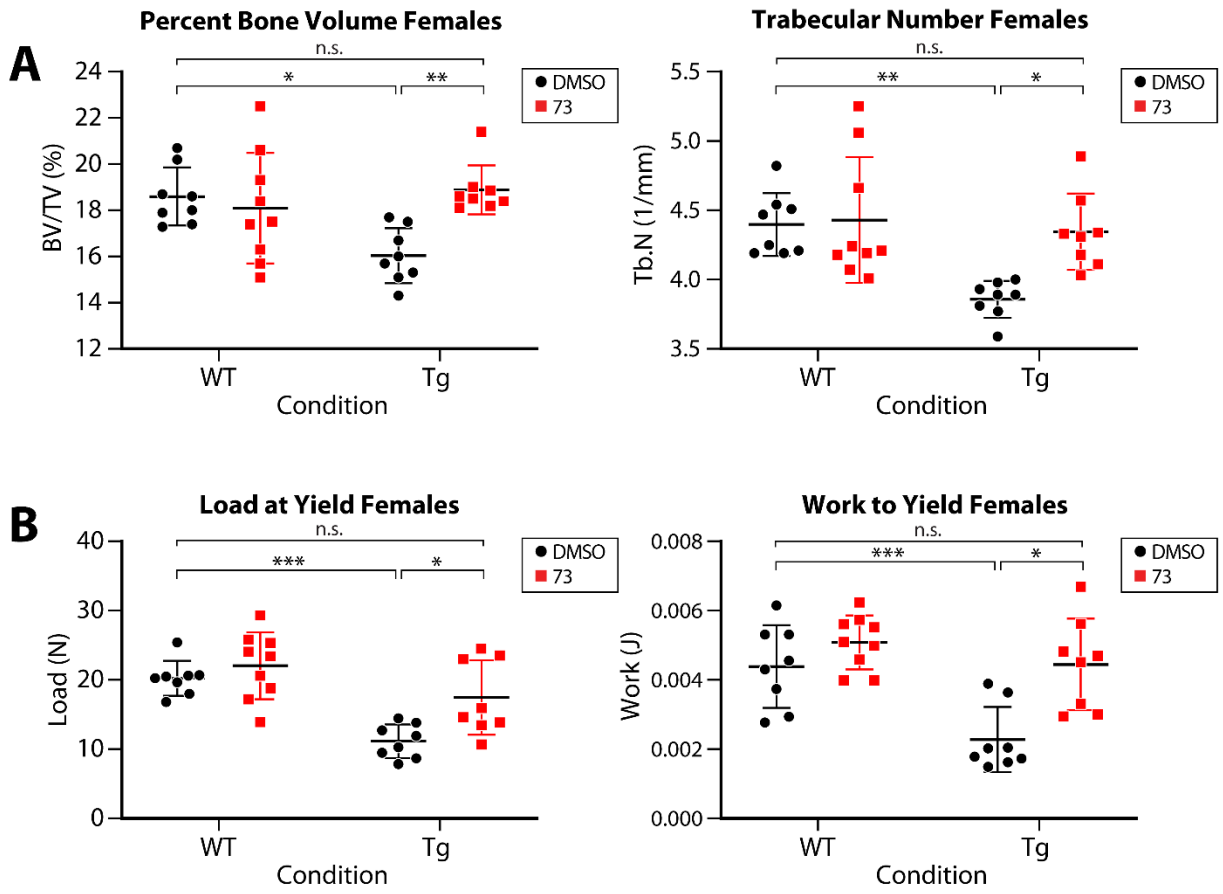

Figure 18. Treatment with C73 rescues the low bone mass phenotype and reduced bone strength of the FIAT-transgenic in female mice.

Wild type or FIAT-transgenic female mice at 12 weeks of age were injected intraperitoneally with either C73 (10 mg/kg) or DMSO control, 5x a week for 10 weeks (N=8 or 9). Histograms representing vertebral trabecular (**A**) structural parameters obtained by µCT analyses. C73 treated mice show a rescue of the trabecular indices. Trabecular parameters are percent bone volume (BV/TV), and trabecular number (Tb.N). Results are given as means ± SD. Vertebral compression (**B**) of L_2 vertebra. C73 treated mouse L_2 vertebra show a rescue of the following biomechanical properties: load at yield and work to yield. Results are given as means ± SD. *, $P < 0.05$; **, $P < 0.01$; ***, $P < 0.001$

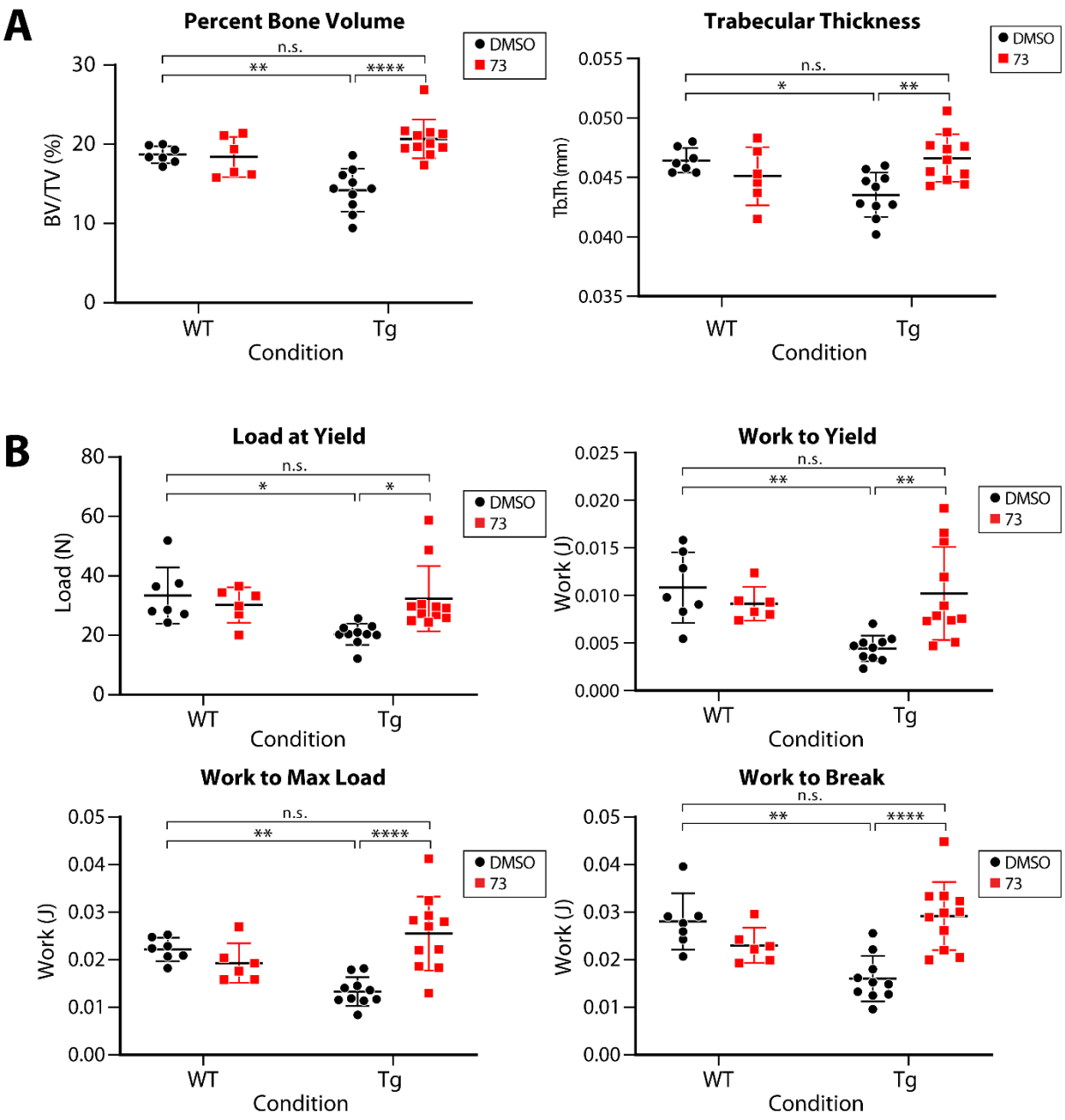
A
Percent Bone Volume
BV/TV (%)
30
20
10
0
n.s.
**
****
DMSO
73
WT
Tg
Condition
Trabecular Thickness
TbTh (mm)
0.055
0.050
0.045
0.040
0.035
n.s.
*
**
DMSO
73
WT
Tg
Condition
B
Load at Yield
Load (N)
80
60
40
20
0
n.s.
*
*
DMSO
73
WT
Tg
Condition
Work to Yield
Work (J)
0.025
0.020
0.015
0.010
0.005
0.000
n.s.
**
**
DMSO
73
WT
Tg
Condition
Work to Max Load
Work (J)
0.05
0.04
0.03
0.02
0.01
0.00
n.s.
**
****
DMSO
73
WT
Tg
Condition
Work to Break
Work (J)
0.05
0.04
0.03
0.02
0.01
0.00
n.s.
**
****
DMSO
73
WT
Tg
Condition

Figure 19. Oral administration of C73 rescues the low bone mass phenotype and reduced bone strength of the *FIAT*-transgenic in female mice.

Wild type or *FIAT*-transgenic female mice at 12 weeks of age received either C73 (10 mg/kg) or DMSO control through oral gavage, 5x a week for 10 weeks (N=6, 7 or 10). Histograms representing vertebral trabecular (**A**) structural parameters obtained by μCT analyses. C73 treated mice show a rescue of trabecular indices. Trabecular parameters are; percent bone volume (BV/TV), and trabecular thickness (Tb.Th). Results are given as means ± SD. Vertebral compression (**B**) of L_2 vertebra. C73 treated mouse L_2 vertebra show a rescue of the following biomechanical properties: load at yield, work to yield, work to max load and work to break. Results are given as means ± SD. *, $P < 0.05$; **, $P < 0.01$; ***, $P < 0.001$; ****, $P < 0.0001$.

Chapter VII: C73 prevents and rescues ovariectomy-induced bone loss.

7.1. C73 treatment maintains bone mass and bone biomechanical properties as a preventative treatment in ovariectomized mice.

Ovariectomized mice (OVX) are used in bone research to recapitulate the bone loss phenotype experienced by post-menopausal women. Although C73 could rescue the low bone mass phenotype of the *FIAT* transgenic mouse, it was unknown if it could rescue a similar phenotype in a well-studied preclinical bone loss model. In this model the ovaries of female mice are surgically removed promoting rapid bone loss. Generally, mice are then left to age for a predetermined amount of time, in which bone loss occurs. This resulting bone loss mimics the effects seen in post-menopausal women, which is generally when intervention occurs. We questioned if administering C73 a week after OVX surgery could be used as a preventative measure against the OVX-induced bone loss. In this experiment, 12-week-old CD1 female mice had either an ovariectomy or a sham surgery and were allowed to recover for a week. After recovery mice were given C73 at a dose of 10mg/kg for 8 weeks via IP injection. To confirm the success of the ovariectomy, uterine weight was recorded at sacrifice (Figure 20A). The measured reduction in uterine weight confirmed that the removal of the ovaries was achieved.

To assess if the low bone mass phenotype of the OVX treatment was "prevented" we compared the bone parameters between the C73 treated OVX mice and the DMSO control treated SHAM mice. If there was no significant difference between these two groups, we concluded that intervention with C73 was sufficient to prevent the OVX induced bone loss.

μCT analysis of L_4 vertebral body showed the expected bone loss phenotype between the SHAM and OVX DMSO control treated mice. A decrease was observed in the following parameters between the DMSO control treated SHAM and OVX mice: percent bone volume (BV/TV), trabecular thickness, trabecular separation, and trabecular number. After treatment with C73, these parameters were non-significant between the DMSO SHAM and C73 treated OVX, suggesting a prevention of the low bone mass phenotype associated with the OVX mouse model (Figure 20B).

The observed decrease in trabecular bone structure of the vertebral body in the OVX-DMSO group was also associated with a decrease in bone strength. Compression testing of the L_2 vertebra from the OVX DMSO treated group showed a decrease in load at yield and maximum load when compared to the DMSO SHAM mice. These parameters did not differ

between the DMSO treated SHAM mice and the C73 treated OVX mice (Figure 20C). The compression testing results suggest that C73 can prevent the associated poor biomechanical properties that lead to an increased fracture risk following loss of ovarian function.

Although we observed the rescue of osteopenic phenotype in the *FIAT*-transgenic mouse model, we were curious if the associated bone loss from ovariectomy could be prevented with early intervention of C73. In CD1 mice, treatment of ovariectomized mice with C73 was able to prevent trabecular bone loss and in turn, prevent the decrease in biomechanical properties.

7.2. C73 treatment rescues the low bone mass phenotype and decreased bone biomechanical properties observed in an ovariectomy study.

In the previous experiment, we demonstrated that treatment with C73 could act as a preventative intervention in post-menopausal induced bone loss. Although prevention would be a prudent approach to treating post-menopausal bone loss, most interventions do not occur until a patient complains of pain and has noticeable changes in bone mass, usually assessed through a DEXA scan. To test if treatment with C73 could rescue the low bone mass associated with OVX, ample time was allotted in the experimental design to ensure that sufficient bone loss had occurred after surgery before intervention occurred. Twelve (12)-week-old female C57bl6 mice either had their ovaries removed or underwent sham surgery. The mice were allowed to age without intervention for 8 weeks to allow for discernable bone loss. After this time, mice were given C73 at a dose of 10 mg/kg for 8 weeks via IP injection. To confirm the success of the ovariectomy, uterine weight was recorded at sacrifice (Figure 21A).

To assess if the low bone mass phenotype of the OVX treatment was “rescued” we compared the bone parameters between the C73 treated OVX mice and the DMSO control treated SHAM mice. If there was no significant difference between these two groups, we concluded that intervention with C73 was able to rescue the OVX induced bone loss.

μCT analysis of L_4 vertebral body showed the expected bone loss phenotype between the SHAM and OVX DMSO control treated mice. A decrease was observed in the following parameters between the DMSO control treated SHAM and OVX mice: percent bone volume (BV/TV) and trabecular thickness. After treatment with C73, these parameters were non-

significant between the DMSO SHAM and C73 treated OVX, suggesting a rescue of the low bone mass phenotype associated with the OVX mouse model (Figure 21B).

The observed decrease in trabecular bone structure of the vertebral body in the OVX-DMSO group was also associated with a decrease in bone strength. Compression testing of the L_2 vertebra from the OVX DMSO treated group showed a decrease in load at yield and maximum load when compared to the DMSO SHAM mice. These parameters did not differ between the DMSO treated SHAM mice and the C73 treated OVX mice (Figure 21C). The compression testing results suggest that C73 can rescue the associated poor biomechanical properties that lead to an increased fracture risk associated with reduced ovarian function.

Ovariectomy is a common method to study the osteopenic phenotype experienced in post-menopausal women. The aim of the experiment was to determine if C73 is effective in a post-menopausal mouse model after bone loss had already occurred. In C57bl6 mice, intervention with C73 was able to rescue the low trabecular bone mass in the vertebrae of ovariectomized mice. Also, the bone strength of the OVX-C73 mice were comparable to the control treated SHAM mice, suggesting a rescue of whole bone strength as well.

7.3. FIGURES AND TABLES

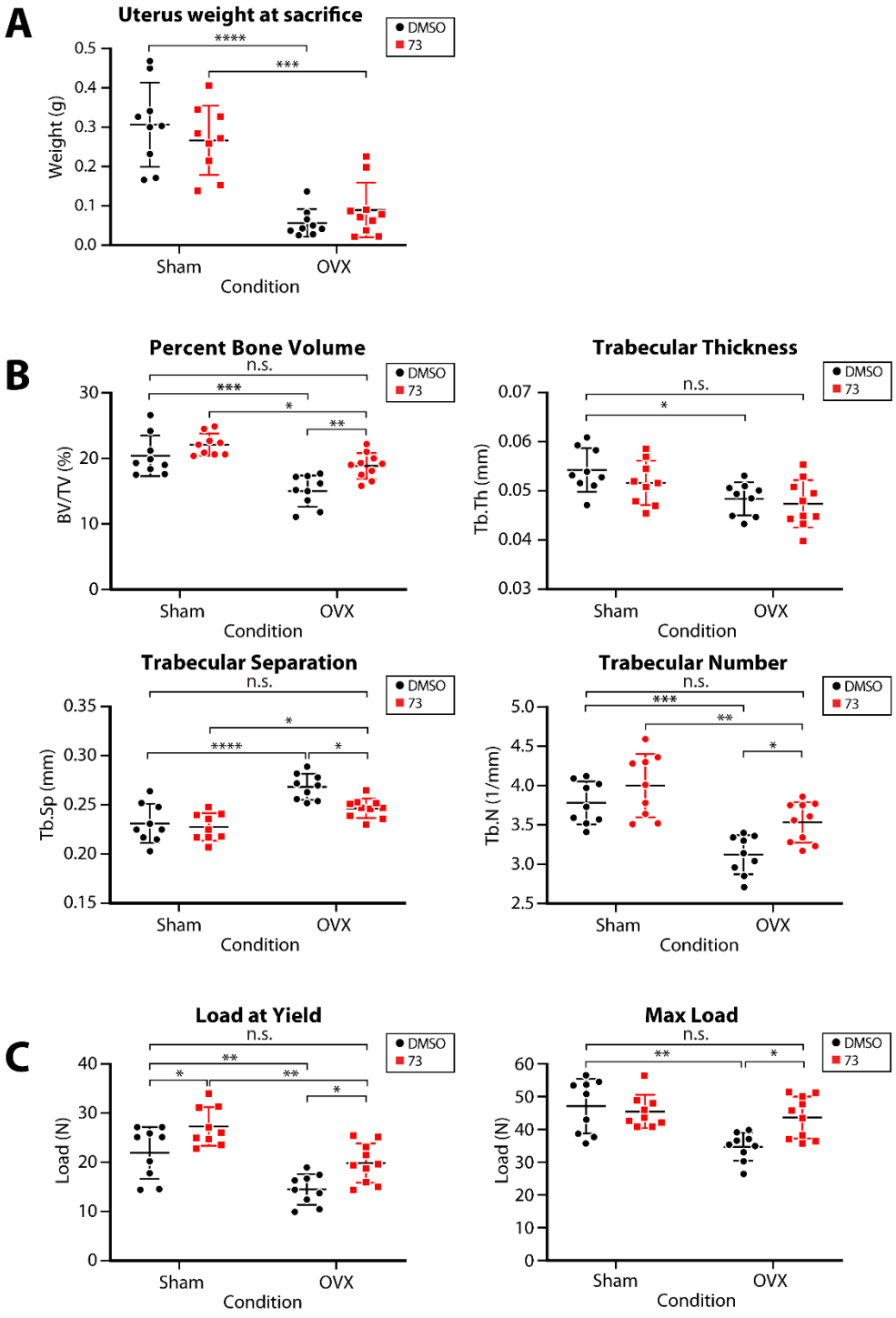

Figure 20. C73 treatment maintains bone mass and bone biomechanical properties as a preventative treatment in ovariectomized mice

CD1 female mice at 12 weeks of age underwent either SHAM or ovariectomy surgery. The following week mice were injected intraperitoneally with either C73 (10 mg/kg) or DMSO control, 5x a week for 8 weeks (N= 9). **A**. The uterine weight was taken at sacrifice, showing a significant decrease in mass in the ovariectomized mice. Histograms representing vertebral trabecular (**B**) structural parameters obtained by μCT analyses. C73 treated mice show a rescue of the trabecular indices. Trabecular parameters are percent bone volume (BV/TV), trabecular thickness (Tb.Th), trabecular separation (Tb.S) and trabecular number (Tb.N). Results are given as means ± SD. Vertebral compression (**C**) of L_2 vertebra. C73 treated mouse L_2 vertebra show a rescue of the following biomechanical properties: load at yield and max load. Results are given as means ± SD. *, $P < 0.05$; **, $P < 0.01$; ***, $P < 0.001$; ****, $P < 0.0001$.

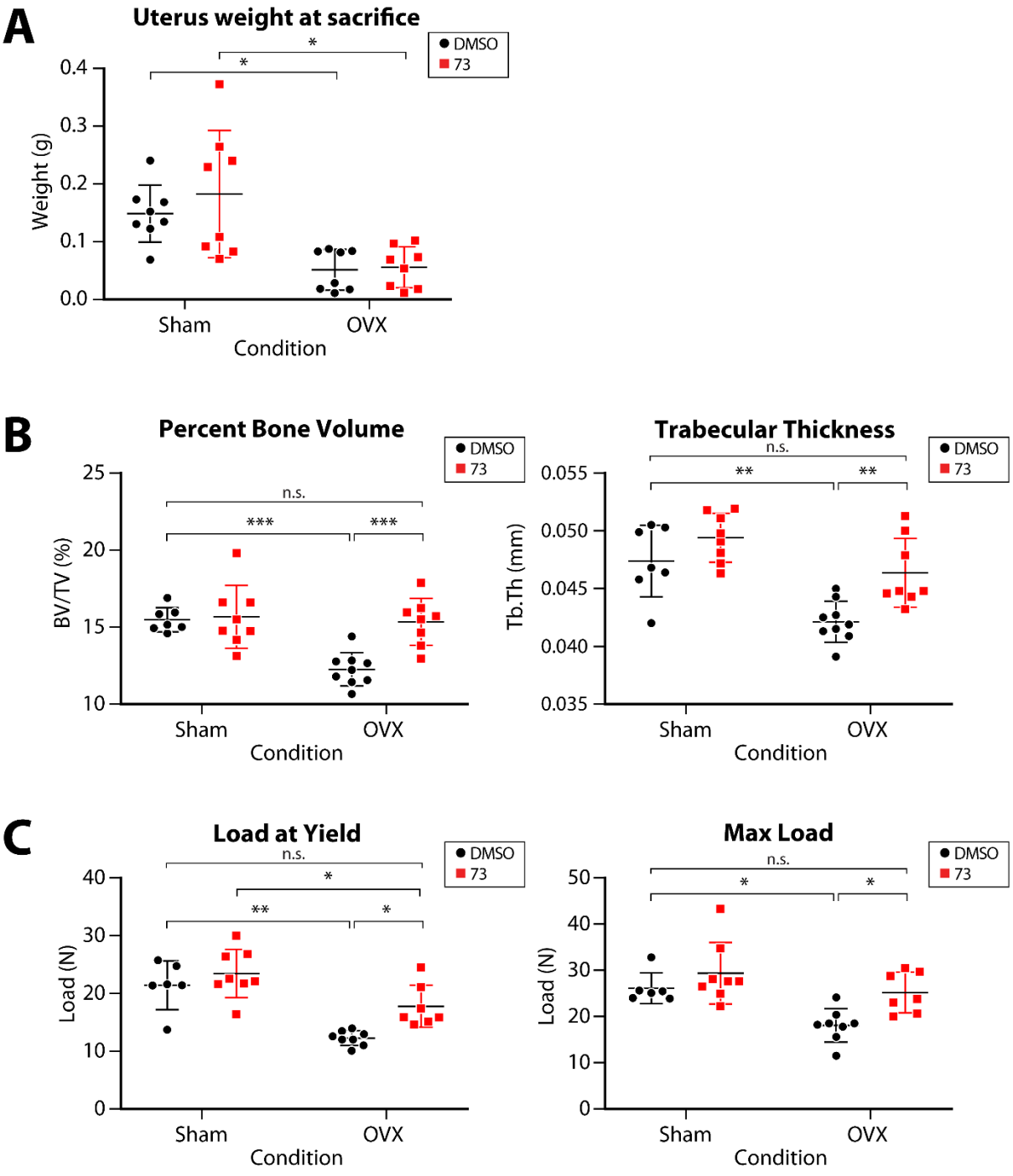
A
Uterus weight at sacrifice
DMSO
73
*
*
Weight (g)
0.4
0.3
0.2
0.1
0.0
Sham
OVX
Condition
B
Percent Bone Volume
DMSO
73
n.s.
***
***
BV/TV (%)
25
20
15
10
Sham
OVX
Condition
Trabecular Thickness
DMSO
73
n.s.
**
**
Tb.Th (mm)
0.055
0.050
0.045
0.040
0.035
Sham
OVX
Condition
C
Load at Yield
DMSO
73
n.s.
*
**
*
Load (N)
40
30
20
10
0
Sham
OVX
Condition
Max Load
DMSO
73
n.s.
*
*
Load (N)
50
40
30
20
10
0
Sham
OVX
Condition

Figure 21. C73 treatment rescues the low bone mass phenotype and decreased bone biomechanical properties observed in an ovariectomy study.

C57bl6 female mice at 12 weeks of age underwent either SHAM or ovariectomy surgery. The mice were allowed to age without intervention for 8 weeks, after which they were injected intraperitoneally with either C73 (10 mg/kg) or DMSO control, 5x a week for 8 weeks (N= 7 or 8). **A**. The uterine weight was taken at sacrifice, showing a significant decrease in mass in the ovariectomized mice. Histograms representing vertebral trabecular (**B**) structural parameters obtained by μCT analyses. C73 treated mice show a rescue of the trabecular indices. Trabecular parameters are percent bone volume (BV/TV), trabecular thickness (Tb.Th), trabecular separation (Tb.S) and trabecular number (Tb.N). Results are given as means ± SD. Vertebral compression (**C**) of L_2 vertebra. C73 treated mouse L_2 vertebra show a rescue of the following biomechanical properties: load at yield and max load. Results are given as means ± SD. *, $P < 0.05$; **, $P < 0.01$; ***, $P < 0.001$;

Chapter VIII: DISCUSSION and FUTURE EXPERIMENTS

In this thesis I have identified C73, a small molecule compound targeting FIAT, that has potential as a novel first-in-class osteoanabolic drug. The compound increases osteoblastogenesis in vitro and was able to rescue the low bone mass phenotype of several preclinical models of metabolic bone diseases.

The *Fiat* cDNA was initially cloned using a yeast two-hybrid screen with a bait consisting of the NACA transcriptional coregulator cDNA [66]. The interaction between NACA and FIAT was independently confirmed [65, 79] and its potential relevance to the work described herein will be discussed below.

In silico analysis of the *Fiat* sequence highlighted the fact that FIAT contains putative leucine zippers, a known protein-protein interaction motif [59, 67, 80]. Previous work from our laboratory explored whether FIAT could form homodimeric or heterodimeric interactions. Through two-hybrid assays using FIAT as bait, it was found that FIAT could not homodimerize but was able to heterodimerize with the osteoanabolic transcription factor, ATF4 [56, 66]. The initial in silico analysis determined that FIAT does not contain a DNA binding domain [66]. Combined with results showing that its interaction with ATF4 prevents the binding of ATF4 to its target genes promoters [66], these observations allowed us to speculate that FIAT could act as a dominant-negative repressor of ATF4 activity [66]. Indeed, in bone cells, an excess of FIAT inhibits mineralization and diminishes expression of ATF4-dependent osteoblast differentiation markers [66]. Reciprocally, knockdown of *Fiat* expression stimulates osteoblast activity by increasing ATF4-dependent functions [68].

The relevance of the FIAT/ATF4 interaction in bone tissue became apparent when our group studied the physiological effects of altering this interaction *in vivo*. The first *in vivo* characterization was conducted using a transgenic mouse model which expressed the human full length 1.8kb *FIAT* cDNA under the 2.3kb *Col1a1* promoter, limiting the overexpression of the *FIAT* transgene to osteoblast cells. The transgenic mice were osteopenic and osteoblasts derived from these mice exhibited impaired activity. The expression level of the *FIAT* transgene resulted in a rather slight increase in total *FIAT/Fiat* mRNAs when quantified by real-time RT-PCR [66]. Even though the overexpression of *FIAT* was modest it was enough to modulate bone mass in this mouse model. That minor changes in FIAT activity could elicit a tissue response hinted at the potential for FIAT as a drug target.

Since increasing FIAT expression in bone specific cells could result in decreased bone mass, the next question was what happens if FIAT expression is depleted? To explore this question a global *Fiat* knockout mouse was created using a Cre-LoxP recombination driven by the cytomegalovirus promoter. As *Fiat* is a X-linked gene that escapes X-inactivation, male mice were used in this study to ensure a true knockout. *Fiat* $^{-}$/y mice exhibited an increase in bone volume, affecting both the trabecular and cortical bone. An increase in the rate of mineral apposition was noted. The global knockout attempt was efficient as *Fiat* mRNA was not detectable in the calvaria, spleen, brain, or heart tissue. FIAT protein expression was undetectable in primary osteoblasts isolated from mutant mice. No obvious off target effects were noted in mutant mice. The mutant mice were fertile without morphological abnormalities and had similar body weights to their wild-type littermates throughout the study [69]. These results support the role of FIAT in bone physiology and the validity of FIAT as a drug target. We reasoned that blocking FIAT activity would lead to beneficial gains in bone mass and strength.

We used a mammalian two-hybrid system to identify small molecules that prevent the FIAT/ATF4 interaction. This high throughput strategy used the second leucine zipper of FIAT fused in-frame with the GAL4-DNA Binding Domain to generate a DBD-FIAT ‘bait’. The leucine zipper of ATF4 was fused in-frame with the VP16 Activation Domain to produce the AD-ATF4 ‘target’. Interaction of the bait with the target through the leucine zipper interface reconstitutes a strong transcriptional activator and induces high levels of expression from a luciferase reporter vector. This system is an artificial expression system that we exploited to assess the efficacy of compounds to disrupt the interaction; the readout was inhibition of luciferase expression compared to vehicle-treated cells. One of the limitations of this system is that it does not represent the endogenous expression levels of either protein. It also disregards the innate location of each protein within the subcellular compartments. While FIAT can be detected in both the cytoplasm and the nucleus, the interaction between FIAT and ATF4 occurs in the nucleus [66].

Traditionally, drug discovery efforts have focused on protein targets that naturally bind ligands or substrates, such as enzymes, G-protein coupled receptors (GPCRs), ion channels, transporters, and nuclear hormone receptors [70]. Small molecules targeting these proteins can be engineered to bind to the region, usually a deep pocket, on the protein that the naturally

occurring substrate or ligand would occupy, effectively modulating the function. The other class of therapeutic agents traditionally exploited in drug discovery is protein-based therapeutics, also known as biologics [81].

While disruption of transcription factors' protein-protein interaction (PPI) or protein-DNA interaction is challenging, it presents the advantage of exhibiting minimal off-target effects as opposed to upstream targets like signaling kinases. The main hurdle of targeting a PPI is the structural conformation of the protein and interaction domain. Many of these proteins are 'flat', lacking a deep hydrophobic pocket and have extended contact surfaces with their interacting partner [82]. Due to these attributes, traditional drug discovery techniques of exploiting a hydrophobic pocket with a small molecule or targeting with a larger biologic cannot be employed. Additionally, transcription factors are intracellularly localized, often exclusively within the nucleus. Having a molecule pass into the nucleus presents its own challenges and limitations. For a molecule to pass through the nuclear envelope, via passive diffusion, it must be smaller than 45 kDa. Any molecule larger than this requires a specific targeting signal, or it will be excluded from the nucleus [83]. Fortunately, small molecules with the proper physicochemical characteristics can diffuse to the nucleus.

One of the first PPI to be targeted and successfully "drugged" was the MYC/MAX interaction. The MYC oncogene family is involved in many cellular processes but became of interest for drug discovery due to its role in cancer [84]. Deregulation of MYC is observed in approximately 70% of human malignancies in various cancer types and is overexpressed in approximately 50% of triple-negative breast cancers [85]. MYC is a transcription factor that is composed of a helix-loop-helix interaction and DNA binding domain. It forms heterodimers with another transcription factor, MAX. Over thirty small molecules targeting this interaction have been characterized. The mechanisms of action disrupting the MYC/MAX interaction fall into three categories: direct disruptors of MYC/MAX heterodimerization, disruptors of MYC/MAX heterodimer binding to DNA or stabilizers of Max/Max homodimerization [86].

The binding of the cFOS/cJUN heterodimer to DNA is another interaction that has been successfully targeted and for which a lead compound has reached phase II in clinical trials. The T-5224 compound was shown to inhibit the binding of the cFOS/cJUN AP-1 heterodimer to its canonical response element and protect joints from destruction in a mouse model of rheumatoid

arthritis. T-5224 showed specificity for inhibiting the binding activity of AP-1 family members (cFOS/cJUN and cJUN/cJUN) without affecting other transcription factors such as NFkb, MyoD, C/EBPα, ATF-2, and Sp-1 [87, 88]. Although T-5224 did not continue past phase II for its effectiveness in arthritis, it has been shown to possess anticancer activity and studies are ongoing studying the synergistic effect between T-5224 and other FDA approved cancer therapies [89].

These drug efforts serve as a proof of concept for the viability of targeting a PPI such as the ATF4/FIAT heterodimerization. The interaction between ATF4 and FIAT occurs through a leucine zipper interaction domain, an interface that does not exhibit a strict amino acid sequence but rather relies on the alignment of leucine residues on the same face of an alpha helix [59]. The chance of aberrant inhibition of related interactions has been a drawback to targeting protein-protein interactions, since leucine zipper factors usually interact with many different binding partners [60]. In our study, we assessed the effect of C73 on other ATF4 heterodimers and saw no interference in the binding of ATF4 to C/EBPß, CHOP, cJUN and FOSB [60, 78]. We conclude that C73 specifically inhibits the ATF4/FIAT interaction which suggests that C73 acts through binding FIAT, and not the ATF4 moiety of the heterodimer. This model could be tested using saturation transfer difference (STD) NMR to look for direct binding of C73 to FIAT [90]. The STD assay has the advantage that irradiation of the protein leads to enhancement of signals in the part of the ligand that contacts the protein. This provides invaluable information on ligand-protein interactions for structure refinement. Alternatively, fluorescence polarization (FP) assays could be developed to assess direct binding [91].

Additional results presented in this thesis support the model through which C73 interacts with FIAT to disrupt the ATF4/FIAT heterodimer, thus freeing ATF4 from the FIAT inhibitor and allowing increased amounts of ATF4 binding to target promoters. For example, Chromatin-immunoprecipitation (ChIP) studies showed an increase in ATF4 binding to its cognate site within the Osteocalcin (*Bglap*) promoter following C73 treatment. The rescue of the osteopenic phenotype of *FIAT* transgenic mice also confirms the efficacy of the C73 compound to block the activity of an overexpressed *FIAT* sequence and support the preferred model for the mechanism of action of compound C73.

We determined a preliminary safety profile for C73 administration *in vivo*. Animals tolerated the compound up to the 10 mg/kg bw dose (maximum solubility) and there was no

deleterious impact on complete blood counts or detrimental effects on heart, liver or kidney function as assessed by blood markers. Throughout the 10-week treatment duration used in rescue protocols, mice receiving C73 gained weight at the same pace as vehicle-treated mice. As any final drug would be used for even longer-term therapy, it will be important to assess the potential for off-target effects. To this end, we could screen C73 in a standard SafetyScreen44 panel [92] which encompasses a range of targets identified by pharmaceutical companies as potential liabilities.

We also reason that the mechanism of action of C73 limits its potential for side-effects. ATF4 is a widely studied protein and the regulation, expression and signalling pathways it is involved in have been extensively studied. ATF4 is ubiquitously expressed but the protein is only enriched in osteoblasts. Through post translational modifications, ATF4 is ubiquitinated and marked for proteasomal degradation in most other cell types [52]. Only in situations of endoplasmic reticulum stress or unfolded protein responses is ATF4 proteasomal degradation halted, and the protein allowed to accumulate [58]. Thus, a drug acting to increase ATF4 activity should preferentially act on bone in the absence of comorbidities.

FIAT is ubiquitously expressed [65] but few studies beyond ours have defined a precise biological function for the protein. Association studies have linked differential expression of *FIAT* to various pathologies without mechanistic data [93-101]. A 2009 study from Hotokezaka et al. suggested that NACA is an initiator of ER stress and mentioned that FIAT might also be implicated in the pathway [102, 103]. Our own results have shown that NACA can enhance the inhibitory activity of FIAT on ATF4-mediated transcription [79]. Thus, in osteoblasts, the biological relevance of the FIAT/NACA interaction would also be negated by compounds blocking FIAT activity, such as C73.

Pharmacokinetic-pharmacodynamics (PKPD) studies demonstrated that C73 exhibits a decent half-life of approximately 45 minutes when administered intraperitoneally. C73 was detected in bone 15 minutes post-injection, confirming that the compound is reaching the target tissue of interest. An additional PKPD investigation is in progress to determine the half-life and bioavailability of C73 when administered orally, which is the preferred mode of administration for a drug.

We have not measured changes in *Fiat* mRNA expression in cultured osteoblasts or in bone tissue treated with C73. However, increased *Atf4* transcription levels were observed in cultured osteoblasts treated with C73. A possible mechanism involves C/EBPβ binding to the *Atf4* promoter [104]. It is not clear if C/EBPβ canonically binds as a homodimer or a heterodimer on this promoter region but it has been proposed that ATF4 might be a heterodimerization partner in this interaction [105]. In C73-treated osteoblasts, ATF4 is freed to bind with other bZIP family members such as C/EBPβ. This could create a feed forward loop increasing the binding of this heterodimer to the ATF4 promoter and increasing transcription. This model could be tested using ChIP assays with ATF4 antibodies and *Atf4* promoter-specific primers.

C73 has a promising efficacy and safety profile. However, it would be interesting to improve the potency and pharmacokinetics of C73 through medicinal chemistry. While safety has been demonstrated in mice, it was for a relatively short-term treatment only, whereas osteoanabolic treatment in patients is likely to be long-term. Moreover, it is not uncommon for toxicity to arise when moving to other animals and eventually humans. The normal approach in a pharmaceutical company is to de-risk compounds for toxicity as they develop and have at least one reliable backup to a lead compound should unforeseen toxicity arise. As it will likely be necessary to engage with a pharmaceutical company to commercialize the osteoanabolics that we develop, having a portfolio of de-risked compounds instead of a single lead compound will improve the chances for successful clinical trials and commercialization. Fortunately, C73 is a low molecular weight molecule that follows Lipinski's Rule of Five. Lipinksi's rules are a scoring template for different attributes a molecule possesses which correlates to the likelihood of it being successfully orally administered. The ideology behind Lipinski's rules is that an orally active drug will have less than 5 H-bond donors, 10 H-bond acceptors, the molecular weight is less than 500, and the calculated Log P (CLog P) is less than 5 [106]. These criteria can be used as predictors of absorption or permeation of small molecules. Starting the drug discovery pipeline with a small molecule that abides by these rules leaves a wider dynamic range for lead optimization. C73 meets the requirements of Lipinski's rules and allows for a range of modifications to be made that will still respect the rule.

On standard mouse chow, Fiat-deficient animals are glucose-tolerant. That metabolic advantage is neutralized when the mice are fed a high-fat diet [69]. We tested the impact of

treatment with C73 in mice receiving a high-fat diet. A modest increase in glucose tolerance could be measured in mice fed standard mouse chow and receiving C73 (data not shown). But the improved metabolic phenotype returned to baseline when mice were challenged with a high fat diet (data not shown). These results show that C73 treatment is not detrimental even under high-fat feeding conditions, but long-term osteoanabolic treatment with C73 could necessitate dietary adjustments in treated patients.

There are currently several therapies on the market to treat low bone mass disease that either stimulate osteoblastic bone formation (anabolic) or inhibit osteoclast resorption (anti-resorptive). In our study we showed that C73 can rescue the low bone mass phenotype of the *FIAT* transgenic mouse, and in a classical mouse model of post menopausal osteoporosis. A next step would be to compare the efficacy of C73 on bone mass accrual against drugs that are FDA approved for treatment of low bone mass. A study using ovariectomized mice or another low bone mass mouse model, comparing the effects of C73 vs. an intervention such as intermittent PTH treatment [107] would be sufficient. These experiments have yet to be conducted, but the information gained from them would be valuable.

One limitation of this study is that it does not actually formally demonstrate whether treatment with C73 acts as an osteoanabolic or anti-resorptive therapy. In the long-term steady state study, a blood biochemistry assay monitoring anti-resorptive marker, TRAcP5b, showed no changes in this marker between DMSO and C73 treated mice (Supplemental Figure 1). This result alone cannot determine classification of C73 as either osteoanabolic or anti-resorptive. Further investigation into this matter will be conducted using dynamic histomorphometry to compare mineral apposition rates and bone formation rates between vehicle and C73-treated animals. Our preferred interpretation remains that C73 is an osteoanabolic compound.

As outlined in the introduction there are various drawbacks to the current FDA approved drugs for treating low bone mass. An experiment that could be fruitful is exploring if a synergistic effect could be obtained using C73 in tandem with an approved bone loss drug. This approach of coupling a small molecule and an FDA approved drug has been successful in other pathologies. When the AP-1 small molecule T-5224 stalled in clinical trials, a group explored if the compound could synergize with another known drug. In this case they used T-5224 and bortezomib in tandem to treat a clinically challenging subset of multiple myeloma. It was shown

that giving the therapies together enhanced the effectiveness of bortezomib in patients who were previously deemed resistant to bortezomib therapy [89]. It should be noted that T-2554 and bortezomib target two different pathways which could account for the enhanced therapeutic effectiveness in treating drug resistant multiple myeloma. C73 is novel because it exploits the ATF4/FIAT interaction. Current drug therapies exploit different pathways to enhance bone mass. Perhaps targeting two different pathways that can modulate bone mass could create a synergistic effect leading to enhanced outcomes.

FIAT is an X-linked gene that escapes X inactivation [108], and it has a Y homolog (*TXLNGY*) [109]. Of note, although TXLNGY transcripts can be detected in gene expression analysis, it is unclear if *TXLNGY* is a gene [110] or a pseudogene [111]. Interestingly, *FIAT* is overexpressed in Klinefelter Syndrome patients [112] , a frequent male chromosomal aneuploidy (47,XXY) with low bone mass [113]. The increased expression of *FIAT* in Klinefelter Syndrome patients has been proposed as a mechanism for the low bone mass observed in these individuals [114, 115]. This suggests that therapy with small molecules that target the FIAT protein, such as C73, could represent an interesting avenue for precision medicine in the treatment of the bone phenotype of Klinefelter Syndrome patients.

8.1. FIGURES AND TABLES

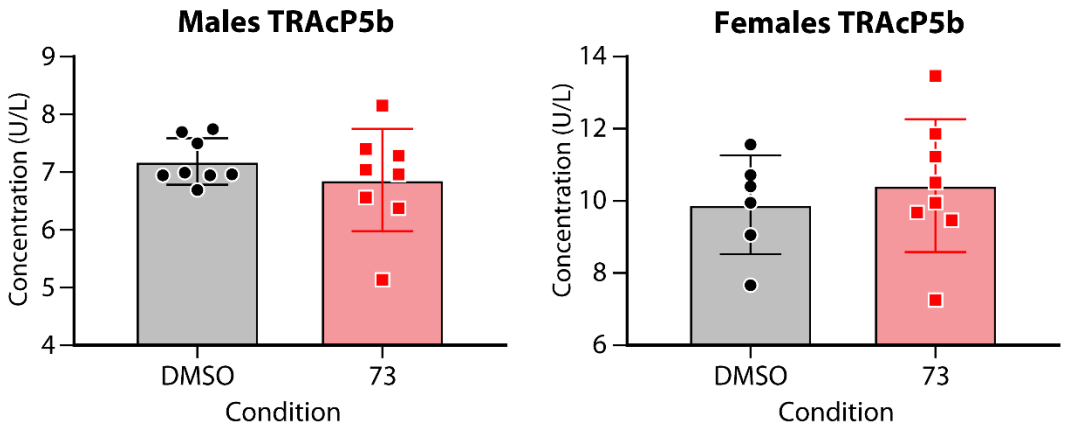

Figure 22. Blood biochemistry shows no changes in anti-resorptive marker in mice treated with C73.

C57bl6 female mice at 8 weeks of age were injected intraperitoneally with either C73 (10 mg/kg) or DMSO control, 5x a week for 6 weeks (N=8 or 6). Serum collected from these mice was used in an ELISA to quantify the concentration of TRAcP5b, an anti-resorptive marker, present at sacrifice. No changes were observed in this marker between the DMSO vehicle treated mice and the C73 treated mice in either sex.

Chapter IX: CONCLUSION

We have identified C73, an orally active osteoanabolic lead compound that blocks the activity of its target, FIAT, to increase bone mass. Because of this unique mechanism of action, C73 could become a first-in-class drug for the treatment of low bone mass metabolic bone diseases. An efficacious, orally administered osteoanabolic treatment remains a poorly met medical need and so our discovery represents a significant breakthrough.

Chapter X: REFERENCES

1. An, Y.H. and K.L. Martin, *Handbook of histology methods for bone and cartilage*. 2003: Springer.
2. Boskey, A.L. and P.G. Robey, *The Composition of Bone*, in *Primer on the Metabolic Bone Diseases and Disorders of Mineral Metabolism*. 2018. p. 84-92.
3. Han, Y., et al., *Paracrine and endocrine actions of bone—the functions of secretory proteins from osteoblasts, osteocytes, and osteoclasts.* Bone research, 2018. **6**(1): p. 16.
4. Asada, N., M. Sato, and Y. Katayama, *Communication of bone cells with hematopoiesis, immunity and energy metabolism.* BoneKEy reports, 2015. **4**.
5. Mera, P., M. Ferron, and I. Mosialou, *Regulation of energy metabolism by bone-derived hormones.* Cold Spring Harbor perspectives in medicine, 2018. **8**(6): p. a031666.
6. Nakashima, K. and B. de Crombrugghe, *Transcriptional mechanisms in osteoblast differentiation and bone formation.* TRENDS in Genetics, 2003. **19**(8): p. 458-466.
7. Teti, A., *Bone development: overview of bone cells and signaling.* Current osteoporosis reports, 2011. **9**: p. 264-273.
8. Pourquié, O., *Vertebrate segmentation: from cyclic gene networks to scoliosis.* Cell, 2011. **145**(5): p. 650-663.
9. Rutkovskiy, A., K.-O. Stensløkken, and I.J. Vaage, *Osteoblast differentiation at a glance.* Medical science monitor basic research, 2016. **22**: p. 95.
10. Ducy, P., et al., *Osf2/Cbfa1: a transcriptional activator of osteoblast differentiation.* cell, 1997. **89**(5): p. 747-754.
11. Nakashima, K., et al., *The novel zinc finger-containing transcription factor osterix is required for osteoblast differentiation and bone formation.* Cell, 2002. **108**(1): p. 17-29.
12. Capulli, M., R. Paone, and N. Rucci, *Osteoblast and osteocyte: games without frontiers.* Archives of biochemistry and biophysics, 2014. **561**: p. 3-12.
13. Bonewald, L.F., *The amazing osteocyte.* Journal of bone and mineral research, 2011. **26**(2): p. 229-238.
14. Franz-Odendaal, T.A., B.K. Hall, and P.E. Witten, *Buried alive: how osteoblasts become osteocytes.* Developmental dynamics: an official publication of the American Association of Anatomists, 2006. **235**(1): p. 176-190.
15. Poole, K.E., et al., *Sclerostin is a delayed secreted product of osteocytes that inhibits bone formation.* The FASEB journal, 2005. **19**(13): p. 1842-1844.
16. Delgado-Calle, J. and T. Bellido, *The osteocyte as a signaling cell.* Physiological reviews, 2022. **102**(1): p. 379-410.
17. Ross, F.P. and S.L. Teitelbaum, *αvβ3 and macrophage colony-stimulating factor: partners in osteoclast biology.* Immunological reviews, 2005. **208**(1): p. 88-105.
18. Suda, T., et al., *Modulation of osteoclast differentiation and function by the new members of the tumor necrosis factor receptor and ligand families.* Endocrine reviews, 1999. **20**(3): p. 345-357.
19. Takito, J., S. Inoue, and M. Nakamura, *The sealing zone in osteoclasts: a self-organized structure on the bone.* International journal of molecular sciences, 2018. **19**(4): p. 984.
20. Asagiri, M. and H. Takayanagi, *The molecular understanding of osteoclast differentiation.* Bone, 2007. **40**(2): p. 251-264.

21. Parfitt, A.M., *Targeted and nontargeted bone remodeling: relationship to basic multicellular unit origination and progression.* Bone, 2002. **30**(1): p. 5-7.
22. Bonewald, L.F., *The role of the osteocyte in bone and nonbone disease.* Endocrinology and Metabolism Clinics, 2017. **46**(1): p. 1-18.
23. Tang, Y., et al., *TGF-β1–induced migration of bone mesenchymal stem cells couples bone resorption with formation.* Nature medicine, 2009. **15**(7): p. 757-765.
24. Sims, N.A. and T.J. Martin, *Osteoclasts provide coupling signals to osteoblast lineage cells through multiple mechanisms.* Annual review of physiology, 2020. **82**: p. 507-529.
25. Feng, X. and J.M. McDonald, *Disorders of bone remodeling.* Annual Review of Pathology: Mechanisms of Disease, 2011. **6**: p. 121-145.
26. Fitzpatrick, L.A. *Secondary causes of osteoporosis*. in *Mayo Clinic Proceedings*. 2002. Elsevier.
27. Johnell, O., et al., *Predictive value of BMD for hip and other fractures.* Journal of bone and mineral research, 2005. **20**(7): p. 1185-1194.
28. Kannegaard, P.N., et al., *Excess mortality in men compared with women following a hip fracture. National analysis of comedications, comorbidity and survival.* Age and ageing, 2010. **39**(2): p. 203-209.
29. McClung, M.R., P.D. Miller, and S.E. Papapoulos, *Osteoporosis*, in *Primer on the Metabolic Bone Diseases and Disorders of Mineral Metabolism*. 2018. p. 393-397.
30. Compston, J.E., M.R. McClung, and W.D. Leslie, *Osteoporosis.* The Lancet, 2019. **393**(10169): p. 364-376.
31. Langdahl, B.L. and T. Harsløf, *Medical treatment of osteoporotic vertebral fractures.* Therapeutic Advances in Musculoskeletal Disease, 2011. **3**(1): p. 17-29.
32. Russell, R., et al., *Mechanisms of action of bisphosphonates: similarities and differences and their potential influence on clinical efficacy.* Osteoporosis international, 2008. **19**: p. 733-759.
33. Ott, S.M., et al., *Bone histomorphometric and biochemical marker results of a 2-year placebo-controlled trial of raloxifene in postmenopausal women.* Journal of bone and mineral research, 2002. **17**(2): p. 341-348.
34. Reid, I.R., et al., *Effects of denosumab on bone histomorphometry: the FREEDOM and STAND studies.* Journal of Bone and Mineral Research, 2010. **25**(10): p. 2256-2265.
35. Stone, J.A., et al., *Clinical and translational pharmacology of the cathepsin K inhibitor odanacatib studied for osteoporosis.* British journal of clinical pharmacology, 2019. **85**(6): p. 1072-1083.
36. Deal, C. and J. Gideon, *Recombinant human PTH 1-34 (Forteo): an anabolic drug for osteoporosis.* Cleveland Clinic journal of medicine, 2003. **70**(7): p. 585-6, 589.
37. Sleeman, A. and J.N. Clements, *Abaloparatide: A new pharmacological option for osteoporosis.* American journal of health-system pharmacy, 2019. **76**(3): p. 130-135.
38. Cosman, F., et al., *Romosozumab treatment in postmenopausal women with osteoporosis.* New England Journal of Medicine, 2016. **375**(16): p. 1532-1543.
39. Abrahamsen, B. and D. Prieto-Alhambra, *Adverse Effects of Drugs for Osteoporosis.* Primer on the Metabolic Bone Diseases and Disorders of Mineral Metabolism, 2018: p. 579-587.
40. Cramer, J.A., et al., *Compliance and persistence with bisphosphonate dosing regimens among women with postmenopausal osteoporosis.* Current medical research and opinion, 2005. **21**(9): p. 1453-1460.
41. Hayes, K.N., et al., *Duration of bisphosphonate drug holidays in osteoporosis patients: a narrative review of the evidence and considerations for decision-making.* Journal of Clinical Medicine, 2021. **10**(5): p. 1140.

42. Bandeira, L., E.M. Lewiecki, and J.P. Bilezikian, *Romosozumab for the treatment of osteoporosis*. Expert opinion on biological therapy, 2017. **17**(2): p. 255-263.
43. De Crombrugghe, B., et al., *Transcriptional mechanisms of chondrocyte differentiation*. Matrix Biology, 2000. **19**(5): p. 389-394.
44. Elefteriou, F., et al., *ATF4 mediation of NF1 functions in osteoblast reveals a nutritional basis for congenital skeletal dysplasiae*. Cell metabolism, 2006. **4**(6): p. 441-451.
45. Komori, T., *Roles of Runx2 in skeletal development*. RUNX Proteins in development and cancer, 2017: p. 83-93.
46. Komori, T., et al., *Targeted disruption of Cbfa1 results in a complete lack of bone formation owing to maturational arrest of osteoblasts*. cell, 1997. **89**(5): p. 755-764.
47. Otto, F., et al., *Cbfa1, a candidate gene for cleidocranial dysplasia syndrome, is essential for osteoblast differentiation and bone development*. Cell, 1997. **89**(5): p. 765-771.
48. Zhang, C., *Transcriptional regulation of bone formation by the osteoblast-specific transcription factor Osx*. Journal of orthopaedic surgery and research, 2010. **5**: p. 1-8.
49. Yoshida, C.A., et al., *SP7 inhibits osteoblast differentiation at a late stage in mice*. PloS one, 2012. **7**(3): p. e32364.
50. Zhou, X., et al., *Multiple functions of Osterix are required for bone growth and homeostasis in postnatal mice*. Proceedings of the National Academy of Sciences, 2010. **107**(29): p. 12919-12924.
51. Kawane, T., et al., *Dlx5 and mef2 regulate a novel runx2 enhancer for osteoblast-specific expression*. Journal of Bone and Mineral Research, 2014. **29**(9): p. 1960-1969.
52. Yang, X. and G. Karsenty, *ATF4, the osteoblast accumulation of which is determined post-translationally, can induce osteoblast-specific gene expression in non-osteoblastic cells*. Journal of Biological Chemistry, 2004. **279**(45): p. 47109-47114.
53. Xiao, G., et al., *Cooperative interactions between activating transcription factor 4 and Runx2/Cbfa1 stimulate osteoblast-specific osteocalcin gene expression*. Journal of Biological Chemistry, 2005. **280**(35): p. 30689-30696.
54. Yu, S., et al., *Critical role of activating transcription factor 4 in the anabolic actions of parathyroid hormone in bone*. PloS one, 2009. **4**(10): p. e7583.
55. Cao, H., et al., *Activating transcription factor 4 regulates osteoclast differentiation in mice*. The Journal of clinical investigation, 2010. **120**(8): p. 2755-2766.
56. Yang, X., et al., *ATF4 is a substrate of RSK2 and an essential regulator of osteoblast biology: implication for Coffin-Lowry syndrome*. Cell, 2004. **117**(3): p. 387-398.
57. Liu, Z., et al., *The Mechanotransduction Signaling Pathways in the Regulation of Osteogenesis*. International Journal of Molecular Sciences, 2023. **24**(18): p. 14326.
58. Harding, H.P., et al., *Regulated translation initiation controls stress-induced gene expression in mammalian cells*. Molecular cell, 2000. **6**(5): p. 1099-1108.
59. Landschulz, W.H., P.F. Johnson, and S.L. McKnight, *The leucine zipper: a hypothetical structure common to a new class of DNA binding proteins*. Science, 1988. **240**(4860): p. 1759-1764.
60. Hai, T. and T. Curran, *Cross-family dimerization of transcription factors Fos/Jun and ATF/CREB alters DNA binding specificity*. Proceedings of the national academy of sciences, 1991. **88**(9): p. 3720-3724.
61. Tominaga, H., et al., *CCAAT/enhancer-binding protein β promotes osteoblast differentiation by enhancing Runx2 activity with ATF4*. Molecular biology of the cell, 2008. **19**(12): p. 5373-5386.
62. Dobreva, G., et al., *SATB2 is a multifunctional determinant of craniofacial patterning and osteoblast differentiation*. Cell, 2006. **125**(5): p. 971-986.

63. Lian, N., et al., *Vimentin inhibits ATF4-mediated osteocalcin transcription and osteoblast differentiation*. Journal of biological chemistry, 2009. **284**(44): p. 30518-30525.
64. Chandhoke, T.K., et al., *Osteopenia in transgenic mice with osteoblast-targeted expression of the inducible cAMP early repressor.* Bone, 2008. **43**(1): p. 101-109.
65. Nogami, S., et al., *Identification and characterization of taxilin isoforms.* Biochemical and biophysical research communications, 2004. **319**(3): p. 936-943.
66. Yu, V.W., et al., *FIAT represses ATF4-mediated transcription to regulate bone mass in transgenic mice.* The Journal of cell biology, 2005. **169**(4): p. 591-601.
67. Yu, V.W., C. Gauthier, and R. St-Arnaud, *FIAT represses bone matrix mineralization by interacting with ATF4 through its second leucine zipper.* Journal of cellular biochemistry, 2008. **105**(3): p. 859-865.
68. Yu, V.W., J. El-Hoss, and R. St-Arnaud, *FIAT inhibition increases osteoblast activity by modulating Atf4-dependent functions.* Journal of cellular biochemistry, 2009. **106**(1): p. 186-192.
69. Hekmatnejad, B., et al., *FIAT Deletion Increases Bone Mass But Does Not Prevent High-Fat-Diet–Induced Metabolic Complications.* Endocrinology, 2017. **158**(2): p. 264-276.
70. Overington, J.P., B. Al-Lazikani, and A.L. Hopkins, *How many drug targets are there?* Nature reviews Drug discovery, 2006. **5**(12): p. 993-996.
71. Higueruelo, A.P., H. Jubb, and T.L. Blundell, *Protein–protein interactions as druggable targets: recent technological advances.* Current opinion in pharmacology, 2013. **13**(5): p. 791-796.
72. Blay, V., et al., *High-throughput screening: today's biochemical and cell-based approaches.* Drug Discovery Today, 2020. **25**(10): p. 1807-1821.
73. Smale, S.T., *Luciferase assay.* Cold Spring Harbor Protocols, 2010. **2010**(5): p. pdb. prot5421.
74. Stepanyuk, G.A., et al., *Expression, purification and characterization of the secreted luciferase of the copepod Metridia longa from Sf9 insect cells.* Protein expression and purification, 2008. **61**(2): p. 142-148.
75. Luo, Y., et al., *Mammalian two-hybrid system: a complementary approach to the yeast two-hybrid system.* Biotechniques, 1997. **22**(2): p. 350-352.
76. Sinha, S. and D. Vohora, *Drug discovery and development: An overview.* Pharmaceutical medicine and translational clinical research, 2018: p. 19-32.
77. Swinney, D.C. and J. Anthony, *How were new medicines discovered?* Nature reviews Drug discovery, 2011. **10**(7): p. 507-519.
78. Vinson, C.R., T. Hai, and S.M. Boyd, *Dimerization specificity of the leucine zipper-containing bZIP motif on DNA binding: prediction and rational design.* Genes & development, 1993. **7**(6): p. 1047-1058.
79. Hekmatnejad, B., et al., *SUMOylated αNAC potentiates transcriptional repression by FIAT.* Journal of Cellular Biochemistry, 2014. **115**(5): p. 866-873.
80. Kouzarides, T. and E. Ziff, *The role of the leucine zipper in the fos–jun interaction.* Nature, 1988. **336**(6200): p. 646-651.
81. Fauman, E.B., B.K. Rai, and E.S. Huang, *Structure-based druggability assessment—identifying suitable targets for small molecule therapeutics.* Current opinion in chemical biology, 2011. **15**(4): p. 463-468.
82. Gowthaman, R., E.J. Deeds, and J. Karanicolas, *Structural properties of non-traditional drug targets present new challenges for virtual screening.* Journal of chemical information and modeling, 2013. **53**(8): p. 2073-2081.

83. Talcott, B. and M.S. Moore, *Getting across the nuclear pore complex*. Trends in cell biology, 1999. **9**(8): p. 312-318.
84. Dang, C.V., *MYC on the path to cancer.* Cell, 2012. **149**(1): p. 22-35.
85. D'Avola, A., et al., *Spotlight on New Therapeutic Opportunities for MYC-Driven Cancers*. OncoTargets and Therapy, 2023: p. 371-383.
86. Ross, J., et al., *Targeting MYC: From understanding its biology to drug discovery.* European Journal of Medicinal Chemistry, 2021. **213**: p. 113137.
87. Aikawa, Y., et al., *Treatment of arthritis with a selective inhibitor of c-Fos/activator protein-1*. Nature biotechnology, 2008. **26**(7): p. 817-823.
88. Motomura, H., et al., *A selective c-Fos/AP-1 inhibitor prevents cartilage destruction and subsequent osteophyte formation*. Biochemical and biophysical research communications, 2018. **497**(2): p. 756-761.
89. Tang, S., et al., *The selective activator protein-1 inhibitor T-5224 regulates the IRF4/MYC axis and exerts cooperative antimyeloma activity with bortezomib.* Chemico-Biological Interactions, 2023. **384**: p. 110687.
90. Viegas, A., et al., *Saturation-transfer difference (STD) NMR: a simple and fast method for ligand screening and characterization of protein binding*. Journal of chemical Education, 2011. **88**(7): p. 990-994.
91. Fischer, J., et al., *Synthetically accessible non-secosteroidal hybrid molecules combining vitamin D receptor agonism and histone deacetylase inhibition*. Chemistry & Biology, 2012. **19**(8): p. 963-971.
92. Bendels, S., et al., *Safety screening in early drug discovery: an optimized assay panel*. Journal of pharmacological and toxicological methods, 2019. **99**: p. 106609.
93. Pottmeier, P., et al., *Sex-biased Gene Expression During Neural Differentiation of Human Embryonic Stem Cells*. 2023.
94. Sun, J., et al., *Development and validation of a hypoxia-related gene signature to predict overall survival in early-stage lung adenocarcinoma patients*. Therapeutic advances in medical oncology, 2020. **12**: p. 1758835920937904.
95. Li, H., et al., *Differences in the prognosis of gastric cancer patients of different sexes and races and the molecular mechanisms involved*. International journal of oncology, 2019. **55**(5): p. 1049-1068.
96. Sousa, A., et al., *Gender differential transcriptome in gastric and thyroid cancers.* Frontiers in Genetics, 2020. **11**: p. 537330.
97. Han, W., et al., *Prognostic Roles of LncRNA XIST and Its Potential Mechanisms in Human Cancers: A Pan-Cancer Analysis*. bioRxiv, 2021: p. 2021.06. 16.448675.
98. Wang, Y., et al., *Phenotype-Genotype analysis of caucasian patients with high risk of osteoarthritis*. Frontiers in Genetics, 2022. **13**: p. 922658.
99. Wang, Y., et al., *Upregulation of XIAP promotes lung adenocarcinoma brain metastasis by modulating ceRNA network*. Frontiers in Oncology, 2022. **12**: p. 946253.
100. Gonzalez, T.L., et al., *Sex differences in the late first trimester human placenta transcriptome*. Biology of Sex Differences, 2018. **9**: p. 1-23.
101. Wang, W., et al., *Detecting biomarkers of alzheimer's disease based on multi-constrained uncertainty-aware adaptive sparse multi-view canonical correlation analysis*. Journal of Molecular Neuroscience, 2022. **72**(4): p. 841-865.
102. Hotokezaka, Y., et al., *GSK-3β-dependent downregulation of γ-taxilin and αNAC merge to regulate ER stress responses*. Cell Death & Disease, 2015. **6**(4): p. e1719-e1719.
103. Hotokezaka, Y., et al., *αNAC depletion as an initiator of ER stress-induced apoptosis in hypoxia*. Cell Death & Differentiation, 2009. **16**(11): p. 1505-1514.

104. Dey, S., et al., *Transcriptional repression of ATF4 gene by CCAAT/enhancer-binding protein β (C/EBPβ) differentially regulates integrated stress response.* Journal of Biological Chemistry, 2012. **287**(26): p. 21936-21949.
105. Kaspar, S., et al., *Adaptation to mitochondrial stress requires CHOP-directed tuning of ISR.* Science advances, 2021. **7**(22): p. eabf0971.
106. Lipinski, C.A., et al., *Experimental and computational approaches to estimate solubility and permeability in drug discovery and development settings.* Advanced drug delivery reviews, 1997. **23**(1-3): p. 3-25.
107. St-Arnaud, R., et al., *NACA and LRP6 Are Part of a Common Genetic Pathway Necessary for Full Anabolic Response to Intermittent PTH.* International Journal of Molecular Sciences, 2022. **23**(2): p. 940.
108. Zhang, Y., et al., *Genes that escape X-inactivation in humans have high intraspecific variability in expression, are associated with mental impairment but are not slow evolving.* Molecular biology and evolution, 2013. **30**(12): p. 2588-2601.
109. Godfrey, A.K., et al., *Quantitative analysis of Y-Chromosome gene expression across 36 human tissues.* Genome research, 2020. **30**(6): p. 860-873.
110. Gegenschatz-Schmid, K., et al., *Genes located in Y-chromosomal regions important for male fertility show altered transcript levels in cryptorchidism and respond to curative hormone treatment.* Basic and clinical andrology, 2019. **29**: p. 1-8.
111. Rotondo Dottore, G., et al., *Genetic profiling of orbital fibroblasts from patients with Graves' orbitopathy.* The Journal of Clinical Endocrinology & Metabolism, 2021. **106**(5): p. e2176-e2190.
112. Zitzmann, M., et al., *Gene expression patterns in relation to the clinical phenotype in Klinefelter syndrome.* The Journal of Clinical Endocrinology & Metabolism, 2015. **100**(3): p. E518-E523.
113. Ferlin, A., et al., *Osteoporosis in Klinefelter's syndrome.* MHR: Basic science of reproductive medicine, 2010. **16**(6): p. 402-410.
114. Skakkebæk, A., et al., *DNA hypermethylation and differential gene expression associated with Klinefelter syndrome.* Scientific Reports, 2018. **8**(1): p. 13740.
115. Skakkebæk, A., et al. *Epigenetics and genomics in Klinefelter syndrome*. in *American Journal of Medical Genetics Part C: Seminars in Medical Genetics*. 2020. Wiley Online Library.

APPENDICES

COPYRIGHTS AND PERMISSIONS

Figure 1.

Figure 3.

REB APPROVAL FOR MICE STUDIES

RightsLink

View Orders

Displayed below are the orders associated with: The FIAT transcriptional repressor as a drug target for bone regeneration

Date	Order No	Type of Use	Fee	Publication	Title
May 10, 2024	5785560044328	Thesis/Dissertation	0.00 USD	Nature Reviews Molecular Cell Biology	Mechanisms of bone development and repair
Feb 21, 2024	5733760465516	Dissertation/Thesis	0.00 CAD	British Journal of Pharmacology	Principles of early drug discovery

Back

SPRINGER NATURE LICENSE
TERMS AND CONDITIONS

May 13, 2024

This Agreement between McGill University -- Caitlin Anderson ("You") and Springer Nature ("Springer Nature") consists of your license details and the terms and conditions provided by Springer Nature and Copyright Clearance Center.

License Number	5785560044328
License date	May 10, 2024
Licensed Content Publisher	Springer Nature
Licensed Content Publication	Nature Reviews Molecular Cell Biology
Licensed Content Title	Mechanisms of bone development and repair
Licensed Content Author	Ankit Salhotra et al
Licensed Content Date	Sep 8, 2020
Type of Use	Thesis/Dissertation
Requestor type	academic/university or research institute
Format	print and electronic
Portion	figures/tables/illustrations
Number of figures/tables/illustrations	1
Would you like a high resolution image with your order?	no
Will you be translating?	no
Circulation/distribution	1 - 29
Author of this Springer Nature content	no
Title of new work	The FIAT transcriptional repressor as a drug target for bone regeneration
Institution name	McGill University
Expected presentation date	Jun 2024

Portions	Fig. 1: Bone homeostasis.
Requestor Location	McGill University 1003 Bd Décarie Montreal, QC H4A 0A9 Canada Attn: McGill University
Total	**0.00 USD**

Terms and Conditions

Springer Nature Customer Service Centre GmbH Terms and Conditions

The following terms and conditions ("Terms and Conditions") together with the terms specified in your [RightsLink] constitute the License ("License") between you as Licensee and Springer Nature Customer Service Centre GmbH as Licensor. By clicking 'accept' and completing the transaction for your use of the material ("Licensed Material"), you confirm your acceptance of and obligation to be bound by these Terms and Conditions.

Grant and Scope of License

1. 1. The Licensor grants you a personal, non-exclusive, non-transferable, non-sublicensable, revocable, world-wide License to reproduce, distribute, communicate to the public, make available, broadcast, electronically transmit or create derivative works using the Licensed Material for the purpose(s) specified in your RightsLink Licence Details only. Licenses are granted for the specific use requested in the order and for no other use, subject to these Terms and Conditions. You acknowledge and agree that the rights granted to you under this License do not include the right to modify, edit, translate, include in collective works, or create derivative works of the Licensed Material in whole or in part unless expressly stated in your RightsLink Licence Details. You may use the Licensed Material only as permitted under this Agreement and will not reproduce, distribute, display, perform, or otherwise use or exploit any Licensed Material in any way, in whole or in part, except as expressly permitted by this License.

1. 2. You may only use the Licensed Content in the manner and to the extent permitted by these Terms and Conditions, by your RightsLink Licence Details and by any applicable laws.

1. 3. A separate license may be required for any additional use of the Licensed Material, e.g. where a license has been purchased for print use only, separate permission must be obtained for electronic re-use. Similarly, a License is only valid in the language selected and does not apply for editions in other languages unless additional translation rights have been granted separately in the License.

1. 4. Any content within the Licensed Material that is owned by third parties is expressly excluded from the License.

1. 5. Rights for additional reuses such as custom editions, computer/mobile applications, film or TV reuses and/or any other derivative rights requests require additional permission and may be subject to an additional fee. Please apply to journalpermissions@springernature.com or bookpermissions@springernature.com for these rights.

Reservation of Rights

Licensor reserves all rights not expressly granted to you under this License. You acknowledge and agree that nothing in this License limits or restricts Licensor's rights in or use of the Licensed Material in any way. Neither this License, nor any act, omission, or statement by Licensor or you, conveys any ownership right to you in any Licensed Material, or to any element or portion thereof. As between Licensor and you, Licensor owns and retains all right, title, and interest in and to the Licensed Material subject to the license granted in Section 1.1. Your permission to use the Licensed Material is expressly conditioned on you not impairing Licensor's or the applicable copyright owner's rights in the Licensed Material in any way.

Restrictions on use

3. 1. Minor editing privileges are allowed for adaptations for stylistic purposes or formatting purposes provided such alterations do not alter the original meaning or intention of the Licensed Material and the new figure(s) are still accurate and representative of the Licensed Material. Any other changes including but not limited to, cropping, adapting, and/or omitting material that affect the meaning, intention or moral rights of the author(s) are strictly prohibited.

3. 2. You must not use any Licensed Material as part of any design or trademark.

3. 3. Licensed Material may be used in Open Access Publications (OAP), but any such reuse must include a clear acknowledgment of this permission visible at the same time as the figures/tables/illustration or abstract and which must indicate that the Licensed Material is not part of the governing OA license but has been reproduced with permission. This may be indicated according to any standard referencing system but must include at a minimum 'Book/Journal title, Author, Journal Name (if applicable), Volume (if applicable), Publisher, Year, reproduced with permission from SNCSC'.

STM Permission Guidelines

4. 1. An alternative scope of license may apply to signatories of the STM Permissions Guidelines ("STM PG") as amended from time to time and made available at https://www.stm-assoc.org/intellectual-property/permissions/ permissions-guidelines/.

4. 2. For content reuse requests that qualify for permission under the STM PG, and which may be updated from time to time, the STM PG supersede the terms and conditions contained in this License.

4. 3. If a License has been granted under the STM PG, but the STM PG no longer apply at the time of publication, further permission must be sought from the Rightsholder. Contact journalpermissions@springernature.com or bookpermissions@springernature.com for these rights.

Duration of License

5. 1. Unless otherwise indicated on your License, a License is valid from the date of purchase ("License Date") until the end of the relevant period in the below table:

Reuse in a medical communications project	Reuse up to distribution or time period indicated in License
Reuse in a dissertation/ thesis	Lifetime of thesis
Reuse in a journal/magazine	Lifetime of journal/magazine
Reuse in a book/textbook	Lifetime of edition
Reuse on a website	1 year unless otherwise specified in the License
Reuse in a presentation/slide kit/poster	Lifetime of presentation/slide kit/poster. Note: publication whether electronic or in print of presentation/slide kit/poster may require further permission.
Reuse in conference proceedings	Lifetime of conference proceedings
Reuse in an annual report	Lifetime of annual report
Reuse in training/CME materials	Reuse up to distribution or time period indicated in License
Reuse in newsmedia	Lifetime of newsmedia
Reuse in coursepack/ classroom materials	Reuse up to distribution and/or time period indicated in license

Acknowledgement

6. 1. The Licensor's permission must be acknowledged next to the Licensed Material in print. In electronic form, this acknowledgement must be visible at the same time as the figures/tables/illustrations or abstract and must be hyperlinked to the journal/book's homepage.

6. 2. Acknowledgement may be provided according to any standard referencing system and at a minimum should include "Author, Article/Book Title, Journal name/Book imprint, volume, page number, year, Springer Nature".

Reuse in a dissertation or thesis

7. 1. Where 'reuse in a dissertation/thesis' has been selected, the following terms apply: Print rights of the Version of Record are provided for; electronic rights for use only on institutional repository as defined by the Sherpa guideline (www.sherpa.ac.uk/romeo/) and only up to what is required by the awarding institution.

7. 2. For theses published under an ISBN or ISSN, separate permission is required. Please contact journalpermissions@springernature.com or bookpermissions@springernature.com for these rights.

7. 3. Authors must properly cite the published manuscript in their thesis according to current citation standards and include the following acknowledgement: '*Reproduced with permission from Springer Nature*'.

License Fee

You must pay the fee set forth in the License Agreement (the "License Fees"). All amounts payable by you under this License are exclusive of any sales, use, withholding, value added or similar taxes, government fees or levies or other assessments. Collection and/or remittance of such taxes to the relevant tax authority shall be the responsibility of the party who has the legal obligation to do so.

Warranty

9. 1. The Licensor warrants that it has, to the best of its knowledge, the rights to license reuse of the Licensed

Material. **You are solely responsible for ensuring that the material you wish to license is original to the Licensor and does not carry the copyright of another entity or third party (as credited in the published version).** If the credit line on any part of the Licensed Material indicates that it was reprinted or adapted with permission from another source, then you should seek additional permission from that source to reuse the material.

9. 2. EXCEPT FOR THE EXPRESS WARRANTY STATED HEREIN AND TO THE EXTENT PERMITTED BY

APPLICABLE LAW, LICENSOR PROVIDES THE LICENSED MATERIAL "AS IS" AND MAKES NO OTHER

REPRESENTATION OR WARRANTY. LICENSOR EXPRESSLY DISCLAIMS ANY LIABILITY FOR ANY CLAIM

ARISING FROM OR OUT OF THE CONTENT, INCLUDING BUT NOT LIMITED TO ANY ERRORS,

INACCURACIES, OMISSIONS, OR DEFECTS CONTAINED THEREIN, AND ANY IMPLIED OR EXPRESS

WARRANTY AS TO MERCHANTABILITY OR FITNESS FOR A PARTICULAR PURPOSE. IN NO EVENT SHALL

LICENSOR BE LIABLE TO YOU OR ANY OTHER PARTY OR ANY OTHER PERSON OR FOR ANY SPECIAL,

CONSEQUENTIAL, INCIDENTAL, INDIRECT, PUNITIVE, OR EXEMPLARY DAMAGES, HOWEVER CAUSED,

ARISING OUT OF OR IN CONNECTION WITH THE DOWNLOADING, VIEWING OR USE OF THE LICENSED

MATERIAL REGARDLESS OF THE FORM OF ACTION, WHETHER FOR BREACH OF CONTRACT, BREACH OF

WARRANTY, TORT, NEGLIGENCE, INFRINGEMENT OR OTHERWISE (INCLUDING, WITHOUT LIMITATION,

DAMAGES BASED ON LOSS OF PROFITS, DATA, FILES, USE, BUSINESS OPPORTUNITY OR CLAIMS OF

THIRD PARTIES), AND WHETHER OR NOT THE PARTY HAS BEEN ADVISED OF THE POSSIBILITY OF SUCH DAMAGES. THIS LIMITATION APPLIES NOTWITHSTANDING ANY FAILURE OF ESSENTIAL PURPOSE OF ANY LIMITED REMEDY PROVIDED HEREIN.

Termination and Cancellation

10. 1. The License and all rights granted hereunder will continue until the end of the applicable period shown in Clause 5.1 above. Thereafter, this license will be terminated and all rights granted hereunder will cease.

10. 2. Licensor reserves the right to terminate the License in the event that payment is not received in full or if you breach the terms of this License.

General

11. 1. The License and the rights and obligations of the parties hereto shall be construed, interpreted and determined in accordance with the laws of the Federal Republic of Germany without reference to the stipulations of the CISG (United Nations Convention on Contracts for the International Sale of Goods) or to Germany´s choice-oflaw principle.

11. 2. The parties acknowledge and agree that any controversies and disputes arising out of this License shall be decided exclusively by the courts of or having jurisdiction for Heidelberg, Germany, as far as legally permissible.

11. 3. This License is solely for Licensor's and Licensee's benefit. It is not for the benefit of any other person or entity.

Questions? For questions on Copyright Clearance Center accounts or website issues please contact springernaturesupport@copyright.com or +1-855-239-3415 (toll free in the US) or +1-978-646-2777. For questions on Springer Nature licensing please visit https://www.springernature.com/gp/partners/rights-permissions-third-partydistribution

Other Conditions:

Version 1.4 - Dec 2022

Questions? E-mail us at customercare@copyright.com.

RightsLink

View Orders

Displayed below are the orders associated with: The FIAT transcriptional repressor as a drug target for bone regeneration

Date	Order No	Type of Use	Fee	Publication	Title
May 10, 2024	5785560044328	Thesis/Dissertation	0.00 USD	Nature Reviews Molecular Cell Biology	Mechanisms of bone development and repair
Feb 21, 2024	5733760465516	Dissertation/Thesis	0.00 CAD	British Journal of Pharmacology	Principles of early drug discovery

Back

JOHN WILEY AND SONS LICENSE

TERMS AND CONDITIONS

Feb 21, 2024

This Agreement between McGill University -- Caitlin Anderson ("You") and John Wiley and Sons ("John Wiley and Sons") consists of your license details and the terms and conditions provided by John Wiley and Sons and Copyright Clearance Center.

License Number	5733760465516
License date	Feb 21, 2024
Licensed Content Publisher	John Wiley and Sons
Licensed Content Publication	British Journal of Pharmacology
Licensed Content Title	Principles of early drug discovery
Licensed Content Author	KL Philpott, SB Kalindjian, S Rees, et al
Licensed Content Date	Feb 22, 2011
Licensed Content Volume	162
Licensed Content Issue	6
Licensed Content Pages	11
Type of use	Dissertation/Thesis
Requestor type	University/Academic
Format	Print and electronic
Portion	Figure/table
Number of figures/tables	1

Will you be translating?	No
Title of new work	The FIAT transcriptional repressor as a drug target for bone regeneration
Institution name	McGill University
Expected presentation date	Jun 2024
Portions	Figure 2
Requestor Location	McGill University 1003 Bd Décarie Montreal, QC H4A 0A9 Canada Attn: McGill University
Publisher Tax ID	EU826007151
Total	0.00 CAD
Terms and Conditions	

TERMS AND CONDITIONS

This copyrighted material is owned by or exclusively licensed to John Wiley & Sons, Inc. or one of its group companies (each a"Wiley Company") or handled on behalf of a society with which a Wiley Company has exclusive publishing rights in relation to a particular work (collectively "WILEY"). By clicking "accept" in connection with completing this licensing transaction, you agree that the following terms and conditions apply to this transaction (along with the billing and payment terms and conditions established by the Copyright Clearance Center Inc., ("CCC's Billing and Payment terms and conditions"), at the time that you opened your RightsLink account (these are available at any time at http://myaccount.copyright.com).

Terms and Conditions

!"The materials you have requested permission to reproduce or reuse (the "Wiley Materials") are protected by copyright.

!"You are hereby granted a personal, non-exclusive, non-sub licensable (on a stand-alone basis), nontransferable, worldwide, limited license to reproduce the Wiley Materials for the purpose specified in the licensing process. This license, **and any CONTENT (PDF or image file) purchased as part of your order,** is for a one-time use only and limited to any maximum

distribution number specified in the license. The first instance of republication or reuse granted by this license must be completed within two years of the date of the grant of this license (although copies prepared before the end date may be distributed thereafter). The Wiley Materials shall not be used in any other manner or for any other purpose, beyond what is granted in the license. Permission is granted subject to an appropriate acknowledgement given to the author, title of the material/book/journal and the publisher. You shall also duplicate the copyright notice that appears in the Wiley publication in your use of the Wiley Material. Permission is also granted on the understanding that nowhere in the text is a previously published source acknowledged for all or part of this Wiley Material. Any third party content is expressly excluded from this permission.

!"With respect to the Wiley Materials, all rights are reserved. Except as expressly granted by the terms of the license, no part of the Wiley Materials may be copied, modified, adapted (except for minor reformatting required by the new Publication), translated, reproduced, transferred or distributed, in any form or by any means, and no derivative works may be made based on the Wiley Materials without the prior permission of the respective copyright owner.**For STM Signatory Publishers clearing permission under the terms of the STM Permissions Guidelines only, the terms of the license are extended to include subsequent editions and for editions in other languages, provided such editions are for the work as a whole in situ and does not involve the separate exploitation of the permitted figures or extracts,** You may not alter, remove or suppress in any manner any copyright, trademark or other notices displayed by the Wiley Materials. You may not license, rent, sell, loan, lease, pledge, offer as security, transfer or assign the Wiley Materials on a stand-alone basis, or any of the

rights granted to you hereunder to any other person.

!"The Wiley Materials and all of the intellectual property rights therein shall at all times remain the exclusive property of John Wiley & Sons Inc, the Wiley Companies, or their respective licensors, and your interest therein is only that of having possession of and the right to reproduce the Wiley Materials pursuant to Section 2 herein during the continuance of this Agreement. You agree that you own no right, title or interest in or to the Wiley Materials or any of the intellectual property rights therein. You shall have no rights hereunder other than the license as provided for above in Section 2. No right, license or interest to any trademark, trade name, service mark or other branding ("Marks") of WILEY or its licensors is granted hereunder, and you agree that you shall not assert any such right, license or interest with respect thereto

!"NEITHER WILEY NOR ITS LICENSORS MAKES ANY WARRANTY OR REPRESENTATION OF ANY KIND TO YOU OR ANY THIRD PARTY, EXPRESS, IMPLIED OR STATUTORY, WITH

RESPECT TO THE MATERIALS OR THE ACCURACY OF ANY INFORMATION CONTAINED

IN THE MATERIALS, INCLUDING, WITHOUT LIMITATION, ANY IMPLIED WARRANTY OF

MERCHANTABILITY, ACCURACY, SATISFACTORY QUALITY, FITNESS FOR A PARTICULAR

PURPOSE, USABILITY, INTEGRATION OR NON-INFRINGEMENT AND ALL SUCH WARRANTIES ARE HEREBY EXCLUDED BY WILEY AND ITS LICENSORS AND WAIVED BY YOU.

!"WILEY shall have the right to terminate this Agreement immediately upon breach of this Agreement by you.

!"You shall indemnify, defend and hold harmless WILEY, its Licensors and their respective directors, officers, agents and employees, from and against any actual or threatened claims, demands, causes of action or proceedings arising from any breach of this Agreement by you.

!"IN NO EVENT SHALL WILEY OR ITS LICENSORS BE LIABLE TO YOU OR ANY OTHER PARTY OR ANY OTHER PERSON OR ENTITY FOR ANY SPECIAL, CONSEQUENTIAL,

INCIDENTAL, INDIRECT, EXEMPLARY OR PUNITIVE DAMAGES, HOWEVER CAUSED,

ARISING OUT OF OR IN CONNECTION WITH THE DOWNLOADING, PROVISIONING,

VIEWING OR USE OF THE MATERIALS REGARDLESS OF THE FORM OF ACTION,

WHETHER FOR BREACH OF CONTRACT, BREACH OF WARRANTY, TORT, NEGLIGENCE,

INFRINGEMENT OR OTHERWISE (INCLUDING, WITHOUT LIMITATION, DAMAGES BASED

ON LOSS OF PROFITS, DATA, FILES, USE, BUSINESS OPPORTUNITY OR CLAIMS OF THIRD

PARTIES), AND WHETHER OR NOT THE PARTY HAS BEEN ADVISED OF THE POSSIBILITY OF SUCH DAMAGES. THIS LIMITATION SHALL APPLY NOTWITHSTANDING ANY FAILURE OF ESSENTIAL PURPOSE OF ANY LIMITED REMEDY PROVIDED HEREIN.

!"Should any provision of this Agreement be held by a court of competent jurisdiction to be illegal, invalid, or unenforceable, that provision shall be deemed amended to achieve as nearly as possible the same economic effect as the original provision, and the legality, validity and enforceability of the remaining provisions of this Agreement shall not be affected or impaired thereby.

!"The failure of either party to enforce any term or condition of this Agreement shall not constitute a waiver of either party's right to enforce each and every term and condition of this Agreement. No breach under this agreement shall be deemed waived or excused by either party unless such waiver or consent is in writing signed by the party granting such waiver or consent. The waiver by or consent of a party to a breach of any provision of this Agreement shall not operate or be construed as a waiver of or consent to any other or subsequent breach by such other party.

!"This Agreement may not be assigned (including by operation of law or otherwise) by you without WILEY's prior written consent.

!"Any fee required for this permission shall be non-refundable after thirty (30) days from receipt by the

CCC.

!"These terms and conditions together with CCC's Billing and Payment terms and conditions (which are incorporated herein) form the entire agreement between you and WILEY concerning this licensing transaction and (in the absence of fraud) supersedes all prior

agreements and representations of the parties, oral or written. This Agreement may not be amended except in writing signed by both parties. This Agreement shall be binding upon and inure to the benefit of the parties' successors, legal representatives, and authorized assigns.

!"In the event of any conflict between your obligations established by these terms and conditions and those established by CCC's Billing and Payment terms and conditions, these terms and conditions shall prevail.

!"WILEY expressly reserves all rights not specifically granted in the combination of (i) the license details provided by you and accepted in the course of this licensing transaction, (ii) these terms and conditions and (iii) CCC's Billing and Payment terms and conditions.

!"This Agreement will be void if the Type of Use, Format, Circulation, or Requestor Type was misrepresented during the licensing process.

!"This Agreement shall be governed by and construed in accordance with the laws of the State of New York, USA, without regards to such state's conflict of law rules. Any legal action, suit or proceeding arising out of or relating to these Terms and Conditions or the breach thereof shall be instituted in a court of competent jurisdiction in New York County in the State of New York in the United States of America and each party hereby consents and submits to the personal jurisdiction of such court, waives any objection to venue in such court and consents to service of process by registered or certified mail, return receipt requested, at the last known address of such party.

WILEY OPEN ACCESS TERMS AND CONDITIONS

Wiley Publishes Open Access Articles in fully Open Access Journals and in Subscription journals offering Online Open. Although most of the fully Open Access journals publish open access articles under the terms of the Creative Commons Attribution (CC BY) License only, the subscription journals and a few of the Open Access Journals offer a choice of Creative Commons Licenses. The license type is clearly identified on the article.

The Creative Commons Attribution License

The Creative Commons Attribution License (CC-BY) allows users to copy, distribute and transmit an article, adapt the article and make commercial use of the article. The CC-BY license permits commercial and non-

Creative Commons Attribution Non-Commercial License

The Creative Commons Attribution Non-Commercial (CC-BY-NC)License permits use, distribution and reproduction in any medium, provided the original work is properly cited and is not used for commercial purposes.(see below)

Creative Commons Attribution-Non-Commercial-NoDerivs License

The Creative Commons Attribution Non-Commercial-NoDerivs License (CC-BY-NC-ND) permits use, distribution and reproduction in any medium, provided the original work is properly cited, is not used for commercial purposes and no modifications or adaptations are made. (see below)

Use by commercial "for-profit" organizations

Use of Wiley Open Access articles for commercial, promotional, or marketing purposes requires further explicit permission from Wiley and will be subject to a fee.

Further details can be found on Wiley Online Library http://olabout.wiley.com/WileyCDA/Section/id-410895.html

Other Terms and Conditions:

v1.10 Last updated September 2015

Questions? customercare@copyright.com.

McGill

December 12, 2023

Animal Certificate

This is to certify that **Dr René St-Arnaud, Shriners Hospitals for Children,** currently holds an approved **Animal Use Protocol # SHRN-4491** with McGill University and its Affiliated Hospital's Research Institutes for the following project:

Animal Use Protocol Title: Role of NFIL3 in the osteoanabolic response to PTH / Compounds blocking FIAT activity increase osteogenesis.

Start date: December 1, 2023

Expiration date: November 30, 2024

McGill University and Affiliated Hospitals Research Institutes recognize the importance of animal research in our efforts to further our knowledge of natural processes, diseases and conservation. Research, educational and testing projects are conducted with full commitment to the wellbeing of the animal subjects. In order to limit animal use to meritorious research or educational projects, the institution relies on stringent peer review processes, along with assessment of ethical issues by the Animal Care Committee. McGill University recognizes that the use of animals in research, teaching and testing carries significant responsibilities. The institution will continue to develop and maintain guidelines and regulations, following the high standards established by the Canadian Council on Animal Care. It is committed to conducting the highest-quality research and to providing animals with the best care.

Cynthia Lavoie
Animal Ethics and Compliance Administrator
Animal Compliance Office
Office of Vice-Principal (Research and Innovation)
Suite 325, James Administration Building, McGill University 845
Sherbrooke Street West, Montreal, Quebec, Canada H3A 0G4
animal.approvals@mcgill.ca